Demonstrating functional crosstalk between DNA base excision repair and cellular bioenergetics: A strategy for the treatment of chemotherapy resistant glioblastoma

by

Eva Marie Goellner

B.S Chemical Engineering and Biomedical Engineering, Carnegie Mellon University, 2006

Submitted to the Graduate Faculty of

University of Pittsburgh School of Medicine in partial fulfillment

of the requirements for the degree of

Doctor of Philosophy

University of Pittsburgh

2011

UNIVERSITY OF PITTSBURGH

SCHOOL OF MEDICINE-MOLECULAR PHARMACOLOGY

This dissertation was presented

by

Eva Marie Goellner

It was defended on

July 29th, 2011

and approved by

Chairperson: Guillermo Romero, Ph.D., Associate Professor, Department of Pharmacology & Chemical Biology

Bennett Van Houten, Ph.D., Professor, Department of Pharmacology & Chemical Biology

Christopher Bakkenist, Ph.D., Assistant Professor, Department of Radiation Oncology

Jian Yu, Ph.D., Associate Professor, Department of Pathology

Dissertation Advisor: Robert W. Sobol, Ph.D., Assistant Professor, Department of Pharmacology & Chemical Biology

Demonstrating functional crosstalk between DNA base excision repair and cellular bioenergetics: A strategy for the treatment of chemotherapy resistant glioblastoma

Eva Marie Goellner, PhD

University of Pittsburgh, 2011

DNA damaging agents are commonly used in the clinic for the treatment of cancer. In particular, the DNA alkylating agent, temozolomide, is the primary chemotherapeutic option for the treatment of glioblastoma, a particularly aggressive form of brain cancer. Temozolomide produces three main DNA lesions: O^6-methylguanine, N7-methylguanine and N3-methyladenine. Most of the clinical toxicity is a result of the O^6-methylguanine lesion, which activates the mismatch repair pathway and results in apoptosis. The N7-methylguanine and N3-methyladenine lesions are effectively repaired by the base excision repair pathway (BER) and hence the toxicity of these lesions is minimal. Resistance to O^6-methylguanine mediated cell death is prevalent, particularly in recurrent glioblastomas, at which point treatment options are limited. We have previously shown that targeting of the BER pathway through genetic means or small molecules (resulting in BER failure) can produce tumor cell death independent of the O^6-methylguanine lesion. This dissertation addresses the critical questions of the mechanisms by which BER failure results in tumor cell death and investigates new combinational therapy options to enhance tumor cell death by BER failure. Cell death after BER failure results from accumulation of repair intermediates and hyperactivation of PARP1. I have shown PARP1 hyperactivation results in cellular loss of NAD^+ and ATP. In particular, nuclear PARP activation results in a severe block to glycolysis and a defect in mitochondrial respiratory capacity. These metabolic defects result in subcellular ATP loss from the mitochondria as well as from the

nuclear and cytosolic compartments. This suggests that targeting both BER and cellular energetic pathways would enhance N7-methylguanine and N3-methyladenine mediated toxicity. To this end I have shown that dual targeting of BER (inhibition by methoxyamine) and NAD^+ biosynthesis (inhibition by FK866) in combination with TMZ results in enhanced tumor cell death and is capable of overcoming resistance to the O^6-methylguanine lesion. This opens the possibility for further pre-clinical testing using xenograft models, as well as, potential synthetic lethal interactions for the treatment of glioblastomas deficient in an alternate arm of NAD^+ biosynthesis.

TABLE OF CONTENTS

LIST OF TABLES

LIST OF FIGURES

PREFACE

Abbreviations

5'dRP	5'deoxyribose phosphate
AIF	apoptosis inducing factor
AMPK	AMP kinase
APE1	AP endonuclease 1
BER	base excision repair
BRCA	breast cancer, early onset
DSB	double strand break
ECAR	extracellular acidification rate
ELISA	enzyme-linked immunosorbent assay
FRET	Förster resonance energy transfer
GBM	glioblastoma multiforme
HMGB1	high-mobility group box 1
HR	homologous recombination
KO	knockout
LKB1	Serine/threonine kinase 11
MEF	mouse embryonic fibroblast

MGMT	O^6-methylguanine-DNA methyltransferase
MMR	mismatch repair
MMS	methyl methanesulfonate
MNNG	methyl-N'-nitro-N-nitrosoguanidine
MPG	methylpurine glycosylase
MX	methoxyamine
NA	nicotinic acid
NAD	nicotinamide adenine dinucleotide
NADH	nicotinamide adenine dinucleotide hydride
NAMPT	nicotinamide phosphoribosyltransferase
NAPRT	nicotinate phosphoribosyltransferase
NMN	nicotinamide mononucleotide
NMNAT	nicotinamide mononucleotide adenylyltransferase
OCR	oxygen consumption rate
PAR	poly(ADP-ribose)
PARG	poly(ADP-ribose) glycohydrolase
PARP	poly(ADP-ribose) polymerase
Polß	polymerase ß
ROS	reactive oxygen species
SER	sensitizer enhancement ratio
SIRT	silent mating type information regulation 2 homolog
TMZ	temozolomide
WT	wildtype

XRCC1	X-ray repair complementing defective repair in Chinese hamster cells 1

Acknowledgements

I would like to take a moment to thank all the people who have helped me along this journey. First and foremost I would like to thank my mentor, Dr. Robert Sobol. He has been a constant source of inspiration and motivation, and has pushed me not only to be successful in completing my graduate degree but has fostered my love of science through example. Some of my happiest times in the last five years have been discussing a new piece of data and hypothesizing about the next experiments to be done. His excitement for the work has inspired me to keep moving forward in science and to never lose the love for what I do.

The Sobol lab past and present has been a wonderful group of companions over the years. I thank you all for your friendship and help. I especially want to thank Dr. Jiang-bo Tang for his guidance when I first joined the lab and for being an example of a wonderful collaborator on our co-first author paper.

I am extremely grateful to my committee members: Ben Van Houten, Chris Bakkenist, Guillermo Romero and Jian Yu for being willing to serve on my committee and for the guidance through my time in the program. I could not have asked for a better group of people to help shape my career. They have gone above and beyond what I think is expected from a committee and have not only been instrumental in bettering my publications and planned experiments but have offered critical advice on surviving in this field. I am especially grateful for all the advice and support in my post-doctoral search.

A special thanks to the DNA repair group and pharmacology department including students, post docs and faculty. I am lucky to be a part of both communities. I have benefited so much from the support and activities from these groups. I am incredibly thankful to the

department of pharmacology for their support in the form of fellowship support. Without this funding I would not have been able to do any of this research.

Finally I do not have words to express my gratitude and love for my family and fiancé, Sam. Thank you for always listening to me in the bad times and celebrating with me in the good times. My parents have never faltered in their support of my dreams, even when that dream was a private university across the country, promptly followed by pursuing a graduate degree unrelated to that expensive undergraduate degree. I love you all and I could never have made it through this without you.

Finally this dissertation is dedicated to Kathy Arno. The first person to really challenge my scientific thinking in her AP chemistry class, and who solidified my desire to pursue a scientific career. I can't thank you enough for the push to leave behind what was safe and to go after my dreams.

Chapter 3 has been published:

Tang, J. B.*, **Goellner, E. M.***, Wang, X. H., Trivedi, R. N., St Croix, C. M., Jelezcova, E., Svilar, D., Brown, A. R., and Sobol, R. W. (2010) Bioenergetic metabolites regulate base excision repair-dependent cell death in response to DNA damage. *Mol Cancer Res* **8**, 67-79

***These author's contributed equally to the work**

Chapter 4 is in preparation as part of a publication:

Goellner, E.M., Johnson, A.L., Barbi, M., Wheeler, D.S., Feinstein, T., Brown, A.R., St Croix, C.M., Romero, G., Van Houten, B., and Sobol R.W. Utilizing real-time techniques to determine temporal and spatial dynamics of cellular energy loss after DNA damage. ***In preparation***

Chapter 5 has been published:

Goellner, E. M., Grimme, B., Brown, A. R., Lin, Y. C., Wang, X. H., Sugrue, K. F., Mitchell, L., Trivedi, R. N., Tang, J. B., and Sobol, R. W. (2011) Overcoming Temozolomide Resistance in Glioblastoma via Dual Inhibition of NAD^+ Biosynthesis and Base Excision Repair. *Cancer research* **71**, 2308-2317

1.0 INTRODUCTION

1.1 GLIOBLASTOMA

1.1.1 Glioblastoma physical and genetic characteristics

Malignant glioma is a particularly devastating disease with limited treatment options. While rare, occurring in 5/100,000 people, malignant glioma is the most commonly occuring primary brain tumor (1, 2). Research into the pathophysiology of the disease is particularly intense due to the poor prognosis of these tumors. Malignant gliomas occur most frequently in white males and are typically diagnosed in middle age to old age (1). The majority of malignant gliomas are not inherited. Only 5% of cases have a family history, and these patients are generally from families with genetic cancer predisposition syndromes such as Li-Fraumeni syndrome (1). Malignant gliomas can be categorized into glioblastomas (70%), anaplastic astrocytomas (15%) and anaplastic oligodenrogliomas/anaplastic oligoastrocytomas (10%) (1). Of these, glioblastomas are considered WHO grade IV and have by far the worst prognosis with a median survival time of 14.6 months under optimal treatment and a 2-year survival rate of 26.5%. Anaplastic glioma patients have a better outcome with a median survival of 2 to 5 years (1). Glioblastomas can either be primary glioblastomas or secondary tumors that progress from lower grade anaplastic astrocytomas to glioblastomas over a period of years. These two sub-types present different

genetic profiles, and while primary glioblastomas occur in older patients (median age of diagnosis is 64 years), secondary glioblastomas generally present at a younger age (median age of 45) after progression from a lower grade tumor to a glioblastoma over a period of 4-5 years (1, 4).

The most common mutation in primary glioblastomas (occurring in 60-80% of tumors) is loss of heterozygozity in chromosome 10 resulting in inactivation of phosphatase and tensin homolog (PTEN) (4). Another genetic marker of primary glioblastoma is amplification of epidermal growth factor receptor (EGFR) (occurring in 40-50% of tumors), and of this subset, 50% express a constitutively active variant of EGFR (1, 4). Targeting of receptor tyrosine kinase signaling cascades in tumors overexpressing EGFR has been aggressively pursued as a potential treatment option for primary glioblastomas as has targeting of the AKT and mTOR pathways, however inhibitors of tyrosine kinase signaling have had little success to date (4).

Secondary glioblastomas commonly have p53 mutations and abnormal platelet derived growth factor receptor (PDGFR) expression (1, 4). Very recently, large-scale analysis of malignant gliomas has identified mutations in isocytrate dehyrogenase 1 and 2 (IDH1/2) that are largely seen in secondary glioblastomas versus primary glioblastomas (5, 6). IDH1 and IDH2 under normal conditions generate α-ketogluterate. The IDH1 and IDH2 mutations result in an altered active site and generation of an alternative tumor specific product, 2-hydroxy-gluterate (2-HG), generated from α-ketogluterate (7). 2-HG seems to have an impact on tumor cell epigenetics, and the discovery of a tumor specific metabolite has sparked an intense interest in studying and manipulating 2-HG and IDH mutations for the treatment of glioblastoma (7).

1.1.2 Treatment of GBM

Current standard treatment for GBM includes maximal debulking surgery whenever possible. GBMs are diffuse tumors and infiltrate into normal tissue, making surgery difficult or in some cases impossible. Surgical reduction is followed by fractionated radiation up to 60 Gy and concurrent and adjuvant chemotherapy with the DNA alkylating drug, temozolomide (Temodar) (1, 8). Radiation therapy has been used in the treatment of glioblastoma for the last 30 years and increases median survival from 3-4 months without radiation to 7-12 months with radiation treatment (1). Prior to adding temozolomide to the treatment regimen the most common chemotherapy for glioblastoma were nitrosoureas (e.g., carmustine). However, they provided only a small survival benefit of a 5% increase in two-year survival based on meta-analysis of 12 randomized trials (8). The monofunctional alkylating agent, temozolomide, showed promise as a monotherapy in malignant gliomas and malignant metastatic melanoma (2). A multicenter randomized phase III trial involving 573 patients published by Strupp et. al. in 2005 showed radiotherapy with concomitant and adjuvant temozolomide provided significant improvement in patient outcome for newly diagnosed glioblastomas. Temozolomide, in addition to standard treatment of surgery and radiation, enhanced median survival from 12.1 months to 14.6 months and two-year survival from 10.4% to 26.5% adding an additional 1.9 months of progression-free survival (8). The survival benefit extended to the 5-year follow up and provided critical information about which patients might most benefit from temozolomide treatment (9). Current standard chemotherapy for glioblastoma is now either temozolomide or carmustine wafers implanted into the resected tumor bed (1). Carmustine wafers are polymer wafers allowing delivery of chemotherapy directly to the site of the tumor without systemic treatment (1).

The most difficult aspect in the treatment of glioblastoma is the eventual recurrence of the tumor, even in cases of optimal treatment. 80-90% of tumors recur within 2 cm of the original tumor, and almost all recurrent glioblastomas no longer respond to chemotherapy (1, 4). The benefits of surgery and radiation for recurrent tumors remains controversial (1). Recurrent tumors are largely temozolomide resistant, with only a 5.4% response rate (10). There are currently very few alternate chemotherapy treatment options for patients with recurrent disease.

1.2 DNA ALKYLATING AGENTS AS CHEMOTHERAPY

1.2.1 Temozolomide

Temozolomide is a 194 dalton monofunctional alkylating agent of the imidazotetrazine class generated in a laboratory at Aston University in 1984 (11). Temozolomide, unlike the other clinically useful imidazotetrazine, 5-(3,3-dimethyltriazeno)imidazol-4-carboxamide (DTIC), does not require metabolism by the liver or any enzyme for activation, but rather breaks down spontaneously at biological pH to form 5-(3-metyltriazene-1-yl)-imidazole-4-carboxamide (MTIC). MTIC breaks down spontaneously into 5-aminoimidazole-4-carboxamide (AIC) and the reactive methyldiazonium cation responsible for DNA methylation (2, 11). Temozolomide has 100% bioavailability after oral dosing; the low pH of the stomach prevents the spontaneous breakdown to MTIC, and temozolomide is easily absorbed by the intestinal tract (11). This results in peak plasma concentration within 30-90 minutes of administration (11). The lipophilic characteristic of the drug allows it to easily cross the blood-brain barrier where it accumulates to 30-40% of the peak plasma concentration (11). Temozolomide (TMZ) and other monofunctional

alkylating agents such as the commonly used laboratory agents methyl methanesulfonate (MMS) and methyl-N'-nitro-N-nitrosoguanidine (MNNG), create a spectrum of DNA base lesions: primarily O^6-methylguanine, N7-methylguanine and N3-methyladenine (2, 12). The percentage of each lesion formed is in Table 1 below for comparison (2, 12).

Table 1. Breakdown of methyl adducts formed by monofunctional alkylating agents

	O^6-methylguanine	N7-methylguanine	N3-methyladenine
TMZ	5%	70%	9.2%
MMS	10.4%	81%	0.3%
MNNG	12%	67%	7%

The N7-methylguanine and N3-methyladenine adducts are substrates for the base excision repair pathway (BER) via methylpurine DNA glycosylase recognition of the lesion and subsequent removal and repair (11, 13). This rapid repair of adducts by BER limits any potential toxicity of the adducts, specifically the N3-methyladenine, which is believed to act as a toxic block to replication (14). The O^6-methylguanine lesion produces most of the TMZ, MMS and MNNG associated toxicity in the presence of an intact BER pathway (11). O^{6-}methylguanine, if not removed by the suicide repair protein O^6-methylguanine-DNA methyltransferase (MGMT), is either paired correctly with cytosine or can be mispaired with thymine, creating a mispair recognized by the mismatch repair (MMR) complex. However, MMR does not remove the damaged base but rather the mispaired thymine, resulting in multiple futile cycles of MMR (11). This can induce apoptosis through two separate proposed mechanisms: 1) repeated rounds of futile repair result in persistent strand breaks that become double strand breaks upon multiple rounds of replication. 2) hMutsα (heterodimer of MSH6 and MSH2) recruits

hMutLα (heterodimer of MLH1 and PMS1), ATRIP and ATR resulting in DNA damage signaling, cell cycle arrest and apoptosis (15, 16). Temozolomide's dose limiting toxicity is mediated by thrombocytopenia (2).

1.2.2 Modes of O^6-methylguanine resistance

The other significant challenge in the treatment of glioblastoma is either endogenous or acquired resistance to O^6-methylguanine induced cell death. While BER function results in tolerance of 80% of the lesions induced by TMZ, MGMT expression can confer resistance to the O^6-methylguanine lesion through direct repair of the lesion (17). Forty-five percent of glioblastomas have a methylated MGMT promoter, resulting in repression of MGMT expression and sensitivity to TMZ, leaving 55% of glioblastomas at least partially resistant to O^6-methyguanine mediated cell death (1). The data generated by the 5-year follow up of the multi-site phase III trial for radiotherapy with concomitant and adjuvant temozolomide revealed that patients with MGMT methylation did significantly better in terms of survival in both groups treated with radiotherapy alone or combination treatment (9). In patients receiving combined radiotherapy and TMZ, those with unmethylated MGMT survived a median of 12.6 months versus those with methylated MGMT who survived a median of 23.4 months. Of all the subgroups in the study (degree of resection, age, MGMT methylation status), MGMT gene methylation was the strongest predictor of outcome (9).

In addition to MGMT promoter methylation and expression, the functionality of the MMR pathway represents another possible mechanism for TMZ resistance. Mutations in mismatch repair genes result in failure to recognize the O^6-methylguanine lesion and to signal for apoptosis (18). Recent studies performing large scale sequencing of tumor genomes have

identified mutations in MMR genes in recurrent tumors specifically after temozolomide treatment. In particular, they identified mutations in MSH6 (19, 20). Since the MMR pathway is further down in the cell death pathway initiated by O^6-methylguanine than MGMT-mediated repair of the lesion, MMR mutations can confer TMZ resistance independent of MGMT status (2). Even patients with favorable MGMT promoter methylation may still present as TMZ resistant due to MMR mutations.

1.2.3 MGMT inhibition in combination with TMZ

Given the strong negative correlation between MGMT expression and extended survival after TMZ treatment, there was a strong effort put into developing ways to prevent MGMT activity in combination with TMZ and other DNA alkylators such as carmustine. O^6-benzylguanine (O^6-BG) and O^6-(4-bromothenyl) guanine (PaTrin) are small molecules that compete for MGMT binding with the O^6-methylguanine lesion (11). While O^6-BG and PaTrin were effective in promoting TMZ and carmustine sensitivity in pre-clinical studies, their efficacy was limited by dose limiting myelosuppression, and they ultimately yielded no advantageous effect over TMZ treatment alone (21). Another strategy for overcoming TMZ resistance by MGMT expression is to deplete MGMT by combining alkylating agents or using an alternate dosing schedule of TMZ, in which TMZ dosing was either extended or compressed to deliver cumulatively higher amounts of TMZ than the standard dosing schedule of 200 mg/m^2/d for 5 days. The compressed schedule, in which patients with metastatic melanoma received 200mg/m^2 every 4 hours for 16 hours, resulted in no significant enhancement in TMZ antitumor activity but significant hematological side effects (17). A number of extended schedules are being tested for ways to minimize hematological side effects and maximize MGMT depletion.

1.3 BASE EXCISION REPAIR AND TEMOZOLOMIDE

1.3.1 Base excision repair of alkylated bases

Base excision repair is the pathway responsible for removing and repairing small single base lesions such as oxidized bases, methylated bases, uracil, 8-oxoG and spontaneous abasic sites (22). BER can proceed through short patch repair, removing a single base or through long patch repair, in which a larger section of DNA is removed (22). Repair of N7-methylguanine and N3-methyladenine generated by TMZ proceeds primarily through short patch repair. BER can be broken down into the steps of: lesion recognition and removal, strand scission, gap tailoring, DNA synthesis and ligation (22). Damage specific glycosylases facilitate the detection and removal of DNA base lesions. Alkylated bases are recognized and removed by the monofunctional glycosylase, methylpurine DNA glycosylase (MPG), which utilizes a base flipping mechanism to interrogate DNA for alkylation lesions (23). The abasic site formed by MPG removal of the damaged base is recognized by APE1, which cleaves the DNA backbone to produce a 3'OH end and a 5'dexoyribose phosphate (5'dRP) repair intermediate (22). It is widely accepted that PARP1 plays a critical role in BER by recognizing the single strand DNA break and generating poly(ADP)ribose that recruits the rest of the BER complex, such as XRCC1/LigIII and DNA Polymerase ß (Polß) (24). The 5'dRP repair intermediate must be removed for further repair of the DNA. This is executed by the 5'dRP lyase activity of the X family polymerase, Polß (22, 25). Polß is primarily a dedicated BER polymerase, and while other DNA polymerases such as Pol lambda and Pol iota have 5'dRP lyase activity, they are unable to complement phenotypes generated by Polß deficiency, such as alkylation hypersensitivity (13,

26, 27). Polß polymerase activity fills in the now tailored DNA gap, and XRCC1/LigIII ligates the DNA nick to complete repair (22). A summary of the BER pathway is presented in Figure 1.

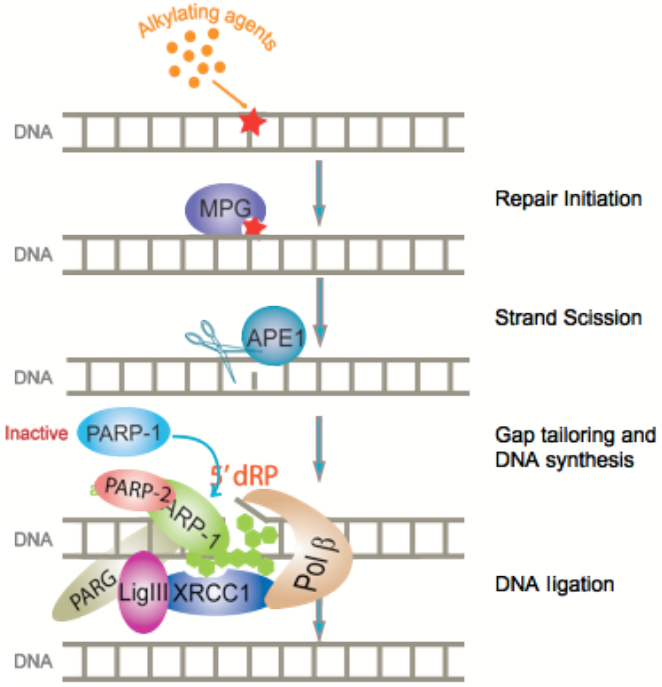

Figure 1. Model of the BER Pathway

1.3.2 BER inhibitors

Given that over 80% of the lesions formed by TMZ and other monofunctional alkylating agents such as MMS or MNNG are repaired by BER, inhibiting the BER pathway is another potential strategy for enhancing TMZ toxicity and overcoming O^6-methylguanine resistance due to either MGMT expression or MMR defects. Inhibitors to several proteins critical to BER have been developed. Inhibitors of APE1 such as lucanthone and CRT0044867, can sensitize cells to TMZ (28, 29). The rationale and development of inhibitors to Polß or PARP1 will be explored further below. Another BER inhibitor of note is Methoxyamine (TRC102), which does not inhibit a BER protein directly but binds to the aldehydic form of the abasic site formed by the

glycosylase-mediated removal of the damaged base and blocks further processing of the lesion by APE1. Methoxyamine has been investigated in combination with alkylating agents in pre-clinical settings for the treatment of cancer with promising results (30-32). Currently Dr. Gerson at Case Western Reserve is conducting a phase I clinical trial to determine the pharmacokinetic profile and safety of methoxyamine in combination with temozolomide in a variety of cancers (lung, breast, pancreatic skin adnexal) (33). The preliminary report shows the combinations are well tolerated, and that a one hour intravenous infusion results in reduction in detectable AP sites (as predicted by MX binding) and an increase in DNA strand breaks (33).

1.3.3 Role of Polß and BER failure

The protein Polß is of particular interest in attempts to inhibit BER and enhance toxicity to TMZ. Polß is a 39 kDa protein with an 8 kDa 5'dRP lyase domain and a 31 kDa polymerase domain (34, 35). Polß plays two critical roles, the removal of the 5'dRP repair intermediate via its 5'dRP lyase activity and DNA synthesis via its polymerase activity (26). Polß knockout in mice results in death shortly after birth making *in vivo* studies of Polß function difficult, but Polß knockout mice can be used to generate Polß knockout MEFs (36). Polß knockout MEFS exhibited hypersensitivity to the alkylating agent MMS, confirming the critical role of Polß in repair of alkylated bases (36). Interestingly, it is not the lack of polymerase function of Polß that results in this hypersensitivity. Complementation of the KO MEFs with polymerase domain mutants R283A and D256A, affecting nucleotide incorporation and discrimination or polymerase activity, respectively, were able to completely recover the Polß KO phenotype similar to WT Polß, indicating no role of polymerase activity in the hypersensitivity to alkylating agents (26). Alternatively, mutations in the 8kDa 5'dRP lyase domain, K35A, K68A and K72A, all resulting

in loss of 5'dRP lyase activity, were not able to complement the Polß KO phenotype, indicating that inability to perform removal of the 5'dRP lesion results in hypersensitivity to alkylating agents (26). To further strengthen this report, complementation with the 31kDa domain of Polß, lacking the 5'dRP lyase domain, did not rescue the Polß KO MEF sensitivity to MMS, whereas complementation with the 8 kDa 5'dRP lyase domain alone completely reverted Polß KO cells to the WT phenotype (26).

The ability of repair intermediates to elicit sensitivity to alkylating agents is dependent on initiation of repair by MPG (37). The unrepaired alkylated bases appear to be non-toxic, whereas incomplete repair results in cell death. Sensitivity to MMS in Polß KO cells is independent of p53 signaling, but repair intermediates may be shuttled into the alternate repair pathway of homologous recombination (HR) (38). Polß KO cells treated with MMS showed an increase in sister chromatid exchange suggesting repair intermediates eventually form double strand breaks that can be repaired by HR (38). This ability of MPG expression and Polß 5'dRP lyase activity to generate toxic repair intermediates and enhance sensitivity to alkylating agents has profound implications on inhibiting BER to enhance toxicity of the TMZ lesions N7-methylguanine and N3-methyladinine and strongly suggests that Polß inhibitors could be effective in combination with TMZ. Polß inhibitors that prevent Polß lyase activity would be especially desirable for enhancing accumulation of toxic 5'dRP repair intermediates. There are a number of reported Polß inhibitors that exhibit inhibition of 5'dRP lyase activity; although in many cases the specificity and selectivity of these for Polß versus other polymerases or other cellular enzymes is largely untested (39). Wilson and Hecht have begun to address this through targeted NMR, biochemical and cell biology approaches and have determined a number of lead compounds that are 5'dRP lyase inhibitors. They tested each inhibitor in combination with MMS in WT and Polß

KO MEFs in order to rule out off target effects. From these efforts pamoic acid has been identified as the most promising lead compound, and studies with this class of inhibitors are ongoing (39, 40).

1.4 ROLE OF PARP IN DNA DAMAGE

1.4.1 PARP in DNA damage response

The poly(ADP-ribose) polymerase (PARP) or ADP-ribosyltransferase (ART) family of proteins catalyze the formation of mono (ADP-ribose) or poly(ADP-ribose) (PAR) from NAD^+ onto the glutamine and aspartate residues of proteins (41). PAR is formed by the glycosidic linkage of ADP-ribose monomers and can form linear or branched chains up to 200 units long (41). Whether chain length or branching determines the specific functions and consequences of PAR polymers as either free polymer or protein modification is yet to be determined. PARP1, PARP2 and PARP3 are among the poly(ADP-ribose) polymerases. PARP1 and PARP2 have been implicated in response to DNA damage through participation in BER. PARP1 is the primary PARP family member implicated in repair. PARP1 is the most abundant of the PARP family members with approximately $1x10^6$ molecules per cell (41). Its involvement in the DNA damage response was first documented in 1980 when Durkacz et. al. found that PARP inhibition resulted in delayed rate of repair and increased cell death following treatment with DNA damaging agent dimethyl sulphate (DMS). PARP1 is activated up to 500 fold higher than basal levels by DNA strand breaks (41). Activation occurs when PARP1 zinc finger motifs recognize the altered DNA structure of a DNA nick or break. PARP1 binds to the strand break as a homodimer, stimulating

PARP1 catalytic activity (41). Once activated, PARP1 then poly(ADP) ribosylates a number of proteins including histones, topoisomerases, transcription factors and other nuclear proteins (42). However, the primary target of poly(ADP) ribosylation is PARP1 itself on glutamine residues in its BCRT domain (the primary domain associated with PARP protein- protein interaction) (41, 42). PARP1 activity has been linked to BER repair capacity through a number of studies. PARP1 binds to repair proteins, such as XRCC1, and auto-modification enhances XRCC1 recruitment to damage sites (24,43). Inhibition of PARP in conjunction with DNA damage increases cytotoxicity *in vivo* and in clonogenic cell culture assays, presumably through an increase in unrepaired single strand breaks being converted into double strand breaks. PARP1 knockout mice are viable with no visible phenotype, but show increased sensitivity to whole body irradiation or high dose DNA damaging agents such as MNU or MNNG (44).

While PARP1 plays a critical role in facilitating DNA repair by BER, PARP1 activity can also mediate cell death following excessive DNA damage. PARP1 hyperactivation has been observed after high doses of alkylation damage or excitoxicity by NMDA receptors after ischemic stroke, traumatic brain injury or MPTP induced Parkinson's disease (41). PARP family members utilize NAD^+ to catalyze poly(ADP-ribose) polymer formation. Excessive activation of PARP after ischemia or alkylation damage has been shown to reduce NAD^+ levels to 10-20% of original levels. NAD^+ and NADH are required cofactors for ATP generating processes, and resynthesis of NAD^+ consumed by PARP requires between 2-4 molecules of ATP depending on which arm of the NAD^+ salvage pathway is used (45). ATP depletion follows NAD^+ depletion resulting in eventual necrotic cell death. Alternatively, the Dawson's have set forth a model in which PARP hyperactivation induced cell death after ischemia or MNNG treatment is dependent on the PAR polymer itself, with long complex PAR polymers causing the most toxicity (42).

PAR mediated cell death activates a signaling cascade resulting in apoptosis inducing factor (AIF) release from the mitochondria to the nucleus and an AIF dependent caspase independent form of cell death, termed "Parthanatos" (46, 47). Inhibition of PARP1 after ischemic stroke or mycocardial infarction is protective of the necrotic cell death typically seen after insult (48).

PARP2 has been linked to DNA damage repair more recently. Ame et. al. demonstrated PARP2 can also be stimulated by DNA damage (49); although PARP2 activation only accounts for 10% of PARP activity in the cell, whereas PARP1 accounts for 85% of PARP activity. PARP2 binds to XRCC1, Polß and DNA ligaseIII (50). PARP2 knockout mice are also viable with no phenotype except for increased sensitivity to high levels of DNA damage, although to a lesser degree than PARP1 knockout mice (49).

PARP3, whos function was previously unknown, has recently been implicated in two separate reports as a double strand break repair protein. Rulten et. al. reported that PARP3 has ADP-ribosylation activity that is stimulated by DNA double strand breaks versus the single strand break stimulation of PARP1 or PARP2. PARP3 modifies histone H1 and PARP3 itself resulting in the recruitment of aprataxin-and-PNK-like factor 1 (APLF1). APLF1 then recruits and retains XRCC4-ligaseIV that is responsible for the final step of non-homologous end joining (51). While PARP3 influences the kinetics of DSB repair, it is not essential since simply overexpressing XRCC4-ligaseIV can overcome a depletion of PARP3 (51). Boehler et. al. simultaneously reported that PARP3 played an important role not only in double strand break repair, but also in maintenance of the mitotic spindle and telomeres, through association with NuMA and tankyrase1 respectively (52).

PAR polymers formed by PARP family members are catabolized primarily by the protein poly(ADP-ribose) glycohydrolase (PARG). PARG breaks the glycosidic bond between PAR

monomers resulting in release of free ADP-ribose (45). PARG expression has been linked to both repair capacity and PARP1 hyperactivation induced cell death. PARG knockout in mice results in embryonic lethality and the accumulation of PAR polymers during development and apoptosis (41). Lower levels of PARG worsen cell death after ischemic brain injury (42). Interestingly overexpression of a cytosolic version of PARG can rescue ischemic cell death and prevent AIF release, supporting a cytosolic role of PAR, despite most studies showing primarily nuclear localization of PARP and PAR after DNA damage (42). PARG has also been shown to associate with XRCC1 (53). After auto-ribosylation, the highly negative charge of the PAR polymers forces PARP1 off of the DNA. Removal of the PAR from PARP1 by PARG allows PARP1 to be recycled back onto sites of DNA damage, thus making PARG a critical member of the BER repair complex (41).

1.4.2 PARP inhibitors

There are currently a large number of clinical and experimental PARP inhibitors being used within the clinic and laboratory. Most PARP inhibitors are specific for PARP1 and PARP2, although some effect on PARP3 has also been seen at higher doses (54). Inhibition of PARP has been shown to rescue necrosis after PARP hyperactivation, and PARP inhibitors have shown to be potentially beneficial for the treatment of ischemia reperfusion injury after stroke or mycocardial infarction (37, 55, 56). Perhaps PARP inhibitors are most exciting at the moment for their ability to treat BRCA1 or BRCA2 deficient breast cancers as a monotherapy. BRCA1 and BRCA2 are critical proteins in homologous recombination. Mutation of BRCA1 and BRCA2 are hereditary and lead to genomic instability and a greatly increased risk for breast and ovarian cancers (57). It was shown that inhibition of PARP is synthetically lethal with BRCA1/2

mutations resulting in apoptotic cell death, presumably through inhibition of the BER pathway resulting in increased double strand breaks that can no longer be repaired by homologous recombination due to the cancer specific defect in BRAC1/2 (57-59).

Given the critical role of PARP1 and PARP2 in BER, there is intense interest in combining TMZ with PARP inhibitors in the clinic. The Abbott Labs PARP inhibitor, ABT-888, has been shown to enhance the efficacy of multiple DNA damaging agents, including TMZ, in a number of xenograft and preclinical models, including lung, pancreatic, breast, ovarian and prostate (60). A note of particular interest was that the PARP inhibitor-TMZ combination was able to overcome TMZ resistance due to tolerance of the O^6-methylguanine lesion. This supports the idea of enhancing the toxicity of BER substrates, N7-methylguanine and N3-methyladenine, through BER inhibition (60). In this case BER inhibition via PARP inhibition results in unrepaired single strand breaks, conversion of those single strand breaks to double strand breaks upon replication and apoptosis.

1.5 HYPOTHESIS

Over 80% of the lesions created by TMZ are BER substrates, which are efficiently repaired by tumor cells. Previous studies by the Sobol lab and others have identified Polß as a critical step in BER repair of TMZ induced lesions. It has been shown that genetic depletion of Polß results in BER failure, accumulation of 5'dRP repair intermediates and hypersensitivity of tumor cells to TMZ. However, the mechanism of 5'dRP cell death is still unknown.

Hypothesis: The base excision repair pathway functionally interacts with cellular energetic pathways such as NAD^+ biosynthesis, glycolysis and oxidative phosphorylation through PARP activation. A drug combination that targets both BER and NAD^+ biosynthesis would enhance response to TMZ in resistant glioblastoma tumors.

This thesis addresses the mechanism behind 5'dRP mediated cell death, linking BER to cellular energetic pathways. These studies further expand the mechanistic link between BER failure and PARP hyperactivation to investigate the subcellular kinetics of energy depletion and the effects on cellular metabolic processes. Based on the mechanistic studies, this thesis puts forth a novel dual targeting strategy, inhibiting both BER and NAD^+ biosynthetic pathways, for the treatment of glioblastomas with multiple modes of O^6-methylguanine resistance.

2.0 MATERIALS AND METHODS

2.1.1 Chemicals and reagents

Alpha EMEM was from MediaTech (Manassas, VA). MEM, heat-inactivated fetal bovine serum (FBS), L-glutamine, antibiotic/antimycotic, and geneticin were from InVitrogen (Carlsbad, CA). Gentamycin was from Sigma (St. Louis, MO). Temozolomide (NSC# 362856; IUPAC name: 3-methyl-2-oxo-1, 3, 4, 5, 8-pentazabicyclo[4.3.0]nona-4,6,8-triene-7-carboxamide; CAS number: 856622-93-1) (61) was obtained from the National Cancer Institute Developmental Therapeutics Program and Sigma (St. Louis, MO). A temozolomide (TMZ) stock solution was prepared in DMSO at 100 mM. FK866 (NIMH #F-901; IUPAC name: (E)-[4-(1-Benzyoylpiperidin-4-yl)butly]-3-(pyridin-3-yl)acrylamide; CAS number: 201034-75-5) was obtained from the National Institute of Mental Health Chemical Synthesis and Drug Supply Program (Bethesda, MD). FK866 was dissolved in DMSO to prepare a stock solution at a concentration of 1mM and stored at -20˚C. Methyl methanesulfonate (MMS) and methoxyamine hydrochloride (MX) were from Sigma (St. Louis, MO). Puromycin, Gentamicin and Neomycin were purchased from Clontech Laboratories, Irvine Scientific and InVitrogen, respectively. PJ34 was purchased from Calbiochem. ß-nicotinamide mononucleotide (NMN) was obtained from Sigma (cat# N3501) and Nicotinic Acid (NA) was obtained from Fisher (cat# AC12829).

2.1.2 Cell culture and cell line development

All cells were cultured at 5% CO_2 and 37°C. LN428 glioblastoma cells (a generous gift from Dr. Ian Pollock, University of Pittsburgh) and derived cell lines were cultured in Alpha EMEM supplemented with 10% heat inactivated FBS, L-glutamine, antibiotic/antimytotic and gentamycin (62, 63). The LN428/MPG cells (over-expressing methylpurine DNA glycosylase; MPG) were supplemented with 6 mg/mL G418. LN428/MPG cell lines with stable knockdown of PARP1, PARP2, MLH1, MSH2 and MSH6 were generated via lentiviral transduction of shRNA as previously described (37) and cultured in growth media with 6 mg/mL G418 and 1.0 μg/mL puromycin. Knockdown of the target gene was assessed by reverse transcription PCR (RT-PCR). The T98G glioblasoma cell line was purchased from American Type Culture Collection and cultured in MEM supplemented with 10% heat inactivated FBS, non-essential amino acids, sodium pyruvate and antibiotic/antimytotic (64). Both cell lines were tested for cross species contamination and authenticated by RADIL cell check services as of 11/16/2010. The genetic profiles provided by RADIL were checked against the ATCC STR loci database to confirm the identity of the T98G cell line, and to ensure that the LN428 genetic profile was unique from any ATCC banked cell line.

2.1.3 Short term cytotoxicity assay

Glioma cells were seeded 24 hours prior to treatment at 2000 cells/well in 96-well plates. For FK866 pre-treatment experiments, cells were treated with the indicated dose of FK866 or media control for 24 hours. Media was then removed and cells were treated with the indicated dose of MMS for 1 hour. Cells were then washed with media and allowed to recover for 48 hours, at

which point cell survival was assayed utilizing the MTS assay (Promega). For PJ34, cells were pre-exposed to the inhibitor for 30 minutes and were then treated with TMZ in the presence of the inhibitor for 48 hours. For NA and NMN, cells were pre-exposed to each for 24 hours (concentrations as indicated in the legend) and were then treated with TMZ (1.0 mM) in the presence of NA or NMN for 48 hours prior to assaying for cell survival. Results shown are the average of three independent experiments and reported as percent survival of MMS treated cells compared to control wells.

2.1.4 PAR lysate collection, Western blot and PAR ELISA

For whole cell extracts used in poly(ADP-ribose) (PAR) formation assays, 3×10^6 cells were seeded into a 100 mm cell culture dish 24 hours before drug treatment. Cells were either treated with TMZ only or pre-exposed to a PARP inhibitor (PJ34) followed by PARP inhibitor plus TMZ treatment. For the FK866 experiments cells were seeded at 1.5×10^6 24 hours prior to treatment, cells were then incubated in the presence of FK866 (10 nM) or DMSO for 24 hours followed by treatment with MMS. After treatment, cells were washed twice with cold PBS, collected and lysed with 400 µL of 2 × Laemmli buffer (2% SDS, 20% Glycerol, 62.5 mM Tris-HCl pH6.8, 0.01% Bromophenol Blue). Samples were boiled for 8 min and extract from approximately 1.5×10^5 cells were loaded each lane on a 4-12% pre-cast NuPAGE Tris-Glycine gel (InVitrogen) for immunoblot assay (used in Chapter 3). Alternatively, cells were treated as above and lysed in modified Laemmli buffer containing 1% SDS in the absence of bromophenol blue. Protein content was quantified using the DC protein assay (Bio-Rad). 30 micrograms of protein was loaded for analysis (used in Chapter 5).

The following primary antibodies were used for immunoblot analysis: anti-PCNA (Santa Cruz); anti-poly(ADP-ribse) (PAR) (Clone 10H, kindly provided by M. Ziegler) and anti-poly(ADP-ribose) polymerase-1 (PARP1) (BD Pharmingen).

Quantitative PAR assay

Cells were seeded at 3 x 10^6 cells per 100 mm dish 24 hours prior to treatment. Cells were then treated with media (control) or MMS for the indicated time. Cells were immediately lysed in modified Laemmli buffer containing 1% SDS in the absence of bromophenol blue. Protein content was quantified using the DC protein assay (Bio-Rad). PAR content was quantified using a colorimetric PAR ELISA kit (Trevigen). Briefly, strip wells were coated with PAR capture antibody 24 hours prior to assay. PAR lyastes, generated as specified above, were incubated with 5μg total protein per well at room temperature (2 hr), followed by washing and incubation with PAR detection antibody. A secondary antibody to the PAR detection antibody was incubated for 1 hour at room temperature, and signal was generated using horseradish peroxidase to generate a luminescent signal. Signal was determined using a Molecular Devices VersaMax™ tuneable plate reader.

2.1.5 AIF immunofluorescence and confocal microscopy

Cells were cultured on glass coverslips for 24 hours prior to treatment with MMS or media control. One-hour post treatment cells were washed and allowed to recover in media for 5 hours. Cells were then fixed with 4% paraformaldehyde for 20 minutes, permeabilized with 0.5% Triton X-100 for 15 minutes, and blocked with 2% BSA for 1 hour, all at room temperature. AIF was detected by incubating 1 hour at room temperature with an anti-AIF antibody (Santa Cruz)

at 1:100 dilution, followed by goat anti-mouse Alexa 488 secondary antibody (Molecular Probes) at 1:500, Alexa 647 phalloidin actin stain at 1:250 (Molecular Probes), and 5 μM DRAQ5 nuclear stain for 1 hour at room temperature. Slides were mounted and imaged on the Olympus fluoview 500 confocal microscope.

2.1.6 NAD^+ and ATP measurement

NAD^+ Measurement

Cells were seeded 24 hours prior to treatment. One-hour post treatment with MMS or 24 hours post FK866 treatment cells were trypsinized, counted and $1x10^5$ cells were pelleted. NAD^+ lysates were prepared and NAD^+ measurements obtained using the Enzychrom™ NAD^+/NADH assay kit (BioAssay Systems). Absorbance was determined using a Molecular Devices VersaMax™ tuneable plate reader.

ATP measurements

Cells were seeded in black 96-well plates (Perkin Elmer) 24 hours prior to treatment. One-hour post treatment with MMS cells were washed and allowed to recover in normal media for one hour before analysis. For experiments with methoxyamine or FK866, treatments were performed as described in the short-term cyototoxicity experiments. Cells were then lysed and ATP content measured by luminescent output using the ATP-lite assay kit (PerkinElmer). Luminescent readings were performed using a BioTek Synergy™ 2 Multi-Mode microplate reader.

2.1.7 Long term cytotoxicity Assay

Long-term cytotoxicity assay in modified LN428 cell lines

For long-term survival assays with FK866 pre-treatment, cells were seeded at 80,000 cells/well in 6-well plates 24 hours prior to treatment. Cells were treated with FK866 or media control for 24 hours. Cells were then trypsinized and plated into 60 mm dishes with or without FK866 and were allowed to attach for 6 hours prior to replacing media with TMZ containing media. All doses were done in triplicate 60 mm dishes. Cells were allowed to grow for 10-12 days in the presence of TMZ. Cells were then trypsinized and counted using a CASY automated cell counter. All experiments were performed in triplicate. Long-term survival experiments combining FK866 with MX pre-treatment were performed as above, but after the 6-hour attachment, cells were treated for 30 minutes with 10 mM MX that was diluted to 5 mM upon addition of TMZ. Cells were allowed to grow for 10-12 days in the presence of MX and TMZ prior to counting.

Long-term cytotoxicity assay in T98G cells

T98G cells (1,150) were seeded in 60mm dishes and allowed to adhere for 24 hours. Cells were then treated with FK866 or media control for 24 hours, followed by MX pre-treatment or media control as described above. Cells were treated with TMZ either alone or as a co-treatment with MX for 6 hours, at which time the drug treatments were removed and replaced with normal culture media. Cells were allowed to grow for an additional 7 days and were assayed for cell survival as described above. All doses were performed in triplicate.

2.1.8 Subcellular ATP analysis

ATeam FRET probes were designed by Hiromi Imamura et. al. to measure subcellular ATP through FRET by linking mVenus and mseCFP to the ε subunit of the *Bacillus subtilis* F_0F_1-ATP synthase (65). ATeam version 1.03 targeted to the mitochondria, cytoplasm or nucleus were obtained from Hiromi Imamura at the Institute of Scientific and Industrial Research, Osaka University Japan. ATeam 1.03 has a K_d for ATP of 3.3mM, has no change in fluorescence between pH 7.1-8.5 and has a K_{on} and K_{off} of $1.7x10^{-2}$ and $9.8x10^{-2}$ s^{-1}. Subcellular FRET probes were able to detect differential depletion of ATP in the cytoplasm and mitochondria after treatment with 2-DG and potassium cyanide respectively (65).

For experiments determining loss of subcellular ATP after alkylation damage, cells were seeded in 35mm glass bottom MatTek dishes 24 hours prior to transfection. Cells were transfected with Fugene transfection reagent according to the manufacturer. After culturing the cells for 48-72 hours, media was replaced with phenol red free imaging media and analyzed by epifluorescent microscopy with measurements taken every minute with 400ms to 800ms exposure and 2x2 binning. A ten-minute baseline was taken before adding MNNG to a final concentration of 5μM. Change in FRET ratio was measured for one hour until a change in the FRET ratio in LN428/MPG cells had plateaued. FRET ratio was calculated by subtracting background values from CFP and mVenus signals. FRET ratios were generated by dividing background corrected CFP/YFP. Ratios for each subcellular measurement were normalized by dividing by the ratio at time point 0. Traces are the average of all normalized FRET traces +/- standard error.

2.1.9 Metabolic flux measurement

To measure metabolic flux in real time the Seahorse Extracellular Flux Analyzer (Seahorse biosciences) was utilized. Cells were plated at a density of 40,000 cells per well in the specialized Seahorse plates (well area is equivalent to that of a 96 well plate) in normal culture media. Pretreatment with PJ34 or FK866 was performed as described in the short-term cytotoxicity experiments. One hour prior to the experiment media was replaced with un-buffered DMEM, un-buffered DMEM with MNNG or un-buffered DMEM with inhibitor alone or inhibitor plus MNNG. Cells were incubated in un-buffered media and drug combinations for 1 hour at 37°C and 0% CO_2. The Seahorse cartridge containing probes for oxygen and pH was loaded with the metabolic inhibitors oligomycin, carbonyl cyanide-p-trifluoromethoxyphenylhydrazone (FCCP), 2-deoxyglucose and rotenone into injection ports A-D respectively to inject at final concentrations of 1 μM oligomycin, 300 nM FCCP, 100 mM 2-DG and 1 μM rotenone. The protocol was set up as illustrated below, with a baseline measurement of 4 points, followed by injection of port A, 3 measurements, injection of port B, etc. to produce a general metabolic profile for oxygen consumption rate (OCR) and extracellular acidification rate (ECAR).

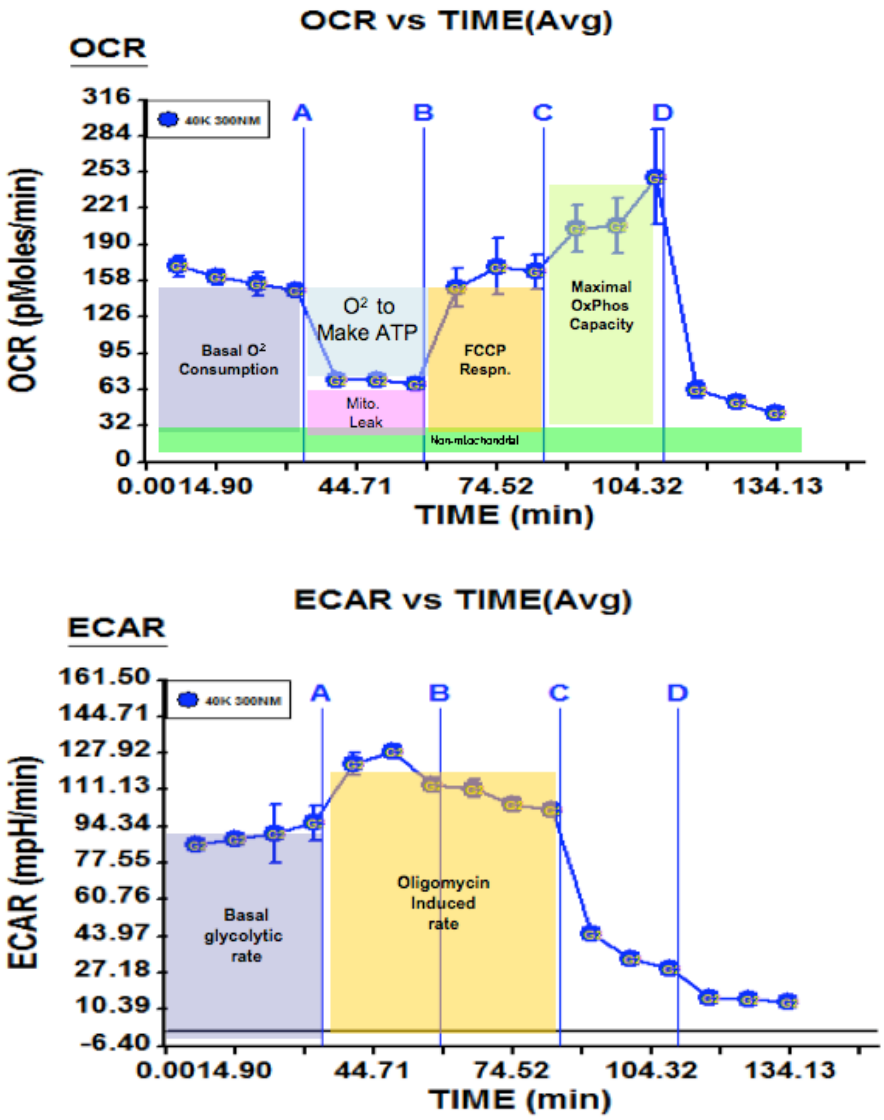

Figure 2. Illustration of metabolic profiles generated by Seahorse Extracellular Flux Analyzer

General metabolic profile for T98G glioblastoma cell line seeded at 40,000 cells per well.

Each data point is from the average of 5 separate wells to form technical replicates for each treatment group. Each experiment was run in independent duplicates. The OCR and ECAR metabolic profiles of the two independent trials were averaged and the standard error of the mean for each measurement was calculated. The following measurements were calculated from OCR and ECAR profiles.

Table 2. Calculation of metabolic parameters from Seahorse data

Non-mitochondrial respiration	Average of OCR points 14-16 (post rotenone measurements)
Basal OCR	Average of OCR points 1-4 (baseline OCR) minus Non-mitochondrial respiration
Proton Leak	Average of OCR points 5-6 (post oligomycin measurements) minus non-mitochondrial respiration
ATP-coupled OCR	Basal OCR minus Proton leak
Total mitochondrial reserve capacity	Average of OCR points 11-13 (post 2-DG measurement) minus non-mitochondrial respiration
Basal glycolytic rate	Average of ECAR points 1-4 (baseline ECAR)
Oligomycin induced glycolytic rate	Average of ECAR points 5-6 (post oligomycin measurement)

2.1.10 Statistical Analysis

All data is shown as a mean +/- standard error from 3 independent experiments unless otherwise indicated. Student's t-test was used for comparisons between two groups. For multiple comparisons, one-way ANOVA followed by post-hoc test with Bonferroni correction was used. Statistical analysis was performed using GraphPad PRISM.

3.0 BIOENERGETIC METABOLITES REGULATE BASE EXCISION REPAIR DEPENDENT CELL DEATH IN RESPONSE TO DNA DAMAGE

3.1 INTRODUCTION

Efficacy of chemotherapy or radiation treatment is intimately dependent on DNA repair capacity (18). Robust repair of therapeutically induced DNA damage can provide significant resistance whereas tumor-specific defects in DNA repair or inhibition of specific DNA repair proteins can provide therapeutic advantage (66). In particular, inhibiting base excision repair (BER) can be an effective means to improve response to temozolomide (TMZ), radiation, bleomycin and cisplatin, among other treatments (22, 36, 67-72). As with most DNA repair pathways, BER is a multi-step mechanism comprised of more than 20 proteins, depending on the initial base lesion (22). However, inhibiting each step in the BER pathway will have different outcomes. DNA glycosylase inhibition or loss blocks BER initiation, leading to the accumulation of both cytotoxic (67) and mutagenic base lesions (68), the latter contributing to cellular dysfunction. In this regard, the preferred option is the inhibition of BER after repair initiation, promoting the accumulation of cytotoxic BER intermediates such as abasic sites and DNA single-strand breaks by inhibiting abasic site repair with methoxyamine, inhibiting the BER enzyme poly(ADP-ribose)polymerase-1 (PARP1) or by loss or inhibition of DNA polymerase ß

(Polß) (36, 66, 69). We refer to inhibition of the intermediate steps in BER as the induction of "***BER failure***", since repair is initiated yet is unable to be completed.

Importantly, understanding the mechanisms that are responsible for the increase in cell death due to BER inhibition or BER failure is critical in tailoring treatment, as well as designing rational adjuvant or combination treatments that may further increase overall response. For example, inhibiting PARP1 has proven effective in improving TMZ induced cell death (70). Inhibition of PARP1 results in the accumulation of replication-mediated DNA double-strand breaks (DSBs) and the onset of apoptosis (71, 72). This detailed understanding of the mechanism of cell death induced by combining a DNA damaging agent (TMZ) and a PARP1 inhibitor suggests that PARP1 inhibition would be effective against many tumors but may be ineffective against tumors that are resistant to apoptosis (73). Further, cell death induced by PARP1 inhibition suggested a requirement for homologous recombination (HR) in the cellular response to the accumulated DSBs, prompting pre-clinical and clinical trials of PARP1 inhibitors in the treatment of HR defective tumors (66).

There are several BER proteins essential for the repair of TMZ-induced DNA lesions. Using a mouse embryonic fibroblast (MEF) cell model, we have shown that loss of Polß can significantly improve the cytotoxic effect of TMZ (13), suggesting that inhibition of Polß may improve response to TMZ in human tumor cells. TMZ is currently used in the treatment of glioblastoma (17) and it is therefore critical to evaluate the role of Polß in glioma cell response to TMZ treatment. No previous studies have investigated the role of Polß in the response of human glioma tumor cells to TMZ. Further, there is no mechanistic explanation for the increase in alkylation-induced cell death observed in cells that are deficient in Polß beyond the evidence that cell death in mouse cells is the result of accumulation of un-repaired BER intermediates (13, 36).

Acute alkylation damage has been suggested to induce cell death by multiple mechanisms, including necrosis (74), caspase-3 and caspase-9 activation and the onset of apoptosis (75), apoptosis inducing factor (AIF) translocation from the mitochondria to the nucleus (46, 76, 77), ADP-ribose induced activation of the Ca^{2+} channel TRPM2 or AMP-mediated inhibition of ATP transport (78-80). In most, if not all cases, cell death has been attributed to the direct action of either poly(ADP-ribose) (PAR) formed by PARP1 activation or PAR catabolites that accumulate after PAR degradation by the catabolic enzyme poly(ADP-ribose) glycohydrolase (PARG). Polß deficient mouse cells are hypersensitive to the cell killing effects of alkylating agents due to failure to repair the 5'dRP BER intermediate (26). However, the exact downstream signaling events and mechanism of cytotoxicity specifically induced by the un-repaired 5'dRP lesion remains unclear. Previous studies in mouse cells have not been conclusive. One report suggested that the absence of Polß led to damage-induced cell death via apoptosis (81) whereas a later study proposed a necrotic form of cell death for both wild-type and Polß deficient cells (82), similar to what has been proposed as a general mechanism of alkylation-induced cell death in mouse fibroblasts (74). However, this latter study required the use of apoptosis-deficient cells to observe necrotic cell death (74). None of these previous studies have identified a mechanism of cell death specific to Polβ deficiency and BER failure or a failure to repair the cytotoxic BER intermediate 5'dRP.

The studies described herein were designed to specifically define the mechanism of cell death in human tumor cells resulting from failure to repair the BER intermediate 5'dRP due to 'inhibition of' or a 'deficiency in' Polß (***BER failure***). We have hypothesized that PARP1 functions in BER as both a complex coordinator and as a molecular repair sensor. As a BER molecular sensor, we suggest that PARP1 facilitates cell death in response to incomplete BER or

BER failure. In support of this hypothesis, we show that a specific BER intermediate, a single-strand DNA strand break containing a 3'OH and 5'dRP, is an *in vivo* substrate in human cells that activates PARP1 in the context of BER and that elevated cytotoxicity observed in Polß deficient human cells is controlled by the activation of PARP1. Further, we provide clear evidence that following "BER failure" human cells die independent of RIP1 activation or AIF translocation, thus ruling out PAR as the cell death signal that is initiated upon BER failure. Further, we show that the observed cell death in Polß deficient cells is un-related to the accumulation of PAR catabolites such as ADP-ribose or AMP yet is dependent on NAD^+ metabolite bioavailability or the bioenergetic capacity of the cell.

This study provides mechanistic insight into why Polß deficiency leads to cell death, defines the mode of death and offers a mechanistic link between BER failure and energy metabolism - the novel finding that DNA damage-induced cytotoxicity mediated via BER inhibition is primarily dependent on cellular metabolite bioavailability. Finally, we offer a mechanistic justification for the elevated alkylation-induced cytotoxicity of Polß deficient cells, suggesting a linkage between DNA repair, cell survival and cellular bioenergetics.

3.2 RESULTS

Hyperactivation of PARP due to Polß deficiency and failure to repair the base excision repair intermediate 5'deoxyribose phosphate

BER is a finely tuned process that requires balanced expression of several proteins to avoid accumulation of mutatgenic or cytotoxic repair intermediates (22). To understand how alterations in BER enzyme activity in human tumor cells leads to DNA damage-induced cell

sensitivity, we developed human glioma (LN428) cell lines with a functional deficiency in Polß by increasing expression of MPG and depleting the cell of Polß by stable, lentiviral-mediated expression of shRNA. As we have reported, human cells with elevated expression of MPG are sensitive to alkylation damage due to a deficiency in Polß (83), a phenotype that is enhanced by Polß knockdown (Polß-KD). Conversely, re-expression of Polß eliminated the alkylation hypersensitive phenotype (**Appendix A; Supplementary Fig S1 and S2**). These cells (LN428/MPG and LN428/MPG/Polß-KD cells) are therefore functionally deficient in Polß and were utilized to determine the mechanism that mediates the enhanced DNA damage-induced cell death resulting from Polß deficiency. This allows for a model system in which events related to incomplete BER can be dissected from other alkylation damage events such as effects on translation (84). In addition, by utilizing relatively low doses of alkylating agent that produce an effect only in the LN428/MPG or LN428/MPG/Polß-KD cell line we can eliminate effects from other alkylation events such as the formation of DNA double-strand breaks or protein alkylation (85). For example, LN428/MPG cells are hypersensitive to the alkylating agent MMS at doses as low as 0.5 mM, a dose that has no cytotoxic effect on the parental LN428 cell line (**Figure 3A**).

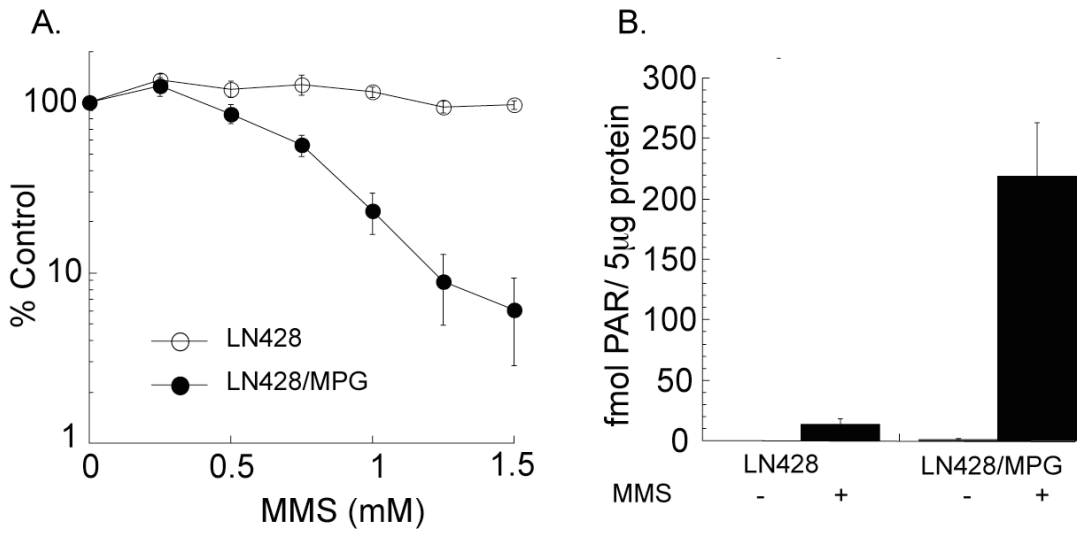

Figure 3. Functional Polß deficiency results in sensitivity to alkylating agents and PARP activation

(A) Cell viability of LN428 or LN428/MPG cells after 1 h MMS treatment, as measured by an MTS assay 48 hours after exposure. Plots show the % viable cells as compared to untreated (control) cells. Means are calculated from quadruplicate values in each experiment. Results indicate the mean ± S.E. of three independent experiments.
(B) PAR generation in LN428 or LN428/MPG cells before or after 15 minute MMS exposure (1.5 mM), as measured by quantitative ELISA (see Materials & Methods). Results indicate the mean ± S.E. of three independent experiments

The DNA binding and signaling molecules PARP1 and PARP2 have each been implicated in BER (22). PARP1 facilitates BER complex formation and it has been postulated that local, strand-break induced activation of PARP1 and the resultant synthesis of PAR mediates recruitment of the BER proteins XRCC1 and Polß to stimulate DNA repair (86). We therefore have hypothesized that in cells that fail to complete BER (e.g., when 5'dRP lesions are not repaired; herein referred to as '**BER Failure**'), PARP1 is hyper-activated and functions as a DNA damage signaling protein that triggers cell death. To determine whether PARP is activated by the BER intermediate (5'dRP) *in vivo*, we exposed the control (LN428) and corresponding BER defective cells (Polß deficient LN428/MPG and LN428/MPG/Polß-KD cells) to TMZ for up to 90 minutes. Whole cell extracts were probed by immunoblot for PAR accumulation following TMZ exposure (**Appendix A; Fig 1A**). The level of PAR accumulation was shown to correlate with the extent of the BER defect. PARP activation was elevated in the LN428/MPG

cells (an intermediate level of sensitivity), with the highest level of PAR observed 30 minutes following exposure to TMZ whereas essentially no PARP activation was observed in the LN428 cells. In the more sensitive cell line (LN428/MPG/Polß-KD), PARP activation was more robust and rapid as compared to that of the LN428/MPG cell line, as PAR reached its highest level at 15 minutes after exposure to TMZ (**Appendix A; Fig 1A)**. This is further demonstrated utilizing a quantitative ELISA method, where we find that PAR generation is 10-fold higher in LN428/MPG cells treated with an MMS dose of 1.5 mM at the 15 minute time point compared to LN428 cells under the same conditions (**Figure 3B**). Comparable results were also observed in a Polß defective breast cancer cell line where elevated TMZ-induced PARP activation is restricted to the cells with Polß deficiency (**Appendix A; Supplementary Fig. S2B and C**) (37). Conversely, exposure to etoposide resulted in a low level of PARP activation at all time points for all three cell lines LN428, LN428/MPG and LN428/MPG/Polß-KD (**Appendix A; Supplementary Fig S2D**). Thus, PARP activation is elevated in BER defective (Polß deficient) cells following alkylation damage.

Since the combination of alkylating agent treatment and Polß deficiency triggers PARP activation, we next validated the significance and specificity of this finding by re-expression of Polß in the LN428/MPG and LN428/MPG/Polß-KD cells. We find that the BER deficient phenotype (increased cellular sensitivity to alkylating agents) observed in both the LN428/MPG and LN428/MPG/ Polß-KD cells was reversed by complementation (expression) of FLAG- Polß (WT) (**Appendix A; Fig. 1B, Supplementary Fig S1E**) (37). Similarly, we find that complementation with FLAG- Polß (WT) but not with the Polß 5'dRP lyase mutant eliminated the TMZ-induced activation of PARP observed in BER defective cells (**Appendix A; Fig. 1B**

and C) (37). These data therefore suggests that the Polß specific BER intermediate (5'dRP lesion) triggers rapid and robust PARP1 activation *in vivo*, triggering the onset of cytotoxicity.

The correlation between PARP activation and alkylation sensitivity prompted us to determine if inhibition of PARP reverses the cellular hypersensitivity of Polß deficient human tumor cells. We inhibited activation of PARP by pre- and co-treatment with the PARP1/PARP2 inhibitors PJ34 or DR2313. Inhibition of PARP by PJ34 significantly reduced the level of TMZ-induced PARP activation in the Polß deficient cells (LN428/MPG) (**Appendix A; Fig 2A**) (37). We next assayed if PARP inhibition can rescue the alkylation-sensitive phenotype of LN428/MPG cells, as determined by an MTS assay 48 hours after TMZ exposure. Most importantly, we find that PARP inhibition by either PJ34 or DR2313 treatment converted the LN428/MPG cells from a sensitive phenotype to a resistant phenotype (**Appendix A; Fig. 2B, Supplementary Fig. S3A**) (37). Rescue by PARP inhibition was also observed in Polß deficient MDA-MB-231 cells (**Appendix A; Supplementary Fig. S3B**) (37). This resistant phenotype is confined to short-term survival assays. Upon several rounds of replication PARP inhibition potentiates TMZ cell killing measured by a long-term survival assay, presumably through BER failure induced single-strand breaks leading to the formation of DNA double-strand breaks and the onset of apoptosis (87). Regardless, these studies support our hypothesis that PARP hyperactivation mediates the alkylation sensitive phenotype of Polß deficient cells.

Un-repaired base excision repair intermediates (5'dRP lesions) trigger cell death via energy depletion in the absence of PAR or PAR-catabolite mediated signaling

A number of different mechanisms have been attributed to PARP1 activation-induced cell death. We first evaluated the involvement of caspase-dependent cell death in control cells as

compared to the corresponding Polß deficient cells following TMZ treatment (**Appendix A; Supplementary Fig. S4A and B**) (37). These experiments rule out a caspase-dependent response due to BER failure, in-line with our previous report (83). Although it has been demonstrated that an autophagic-response contributes to TMZ-induced cell death in some cells (88), TMZ hypersensitivity of Polß deficient cells is not affected by the autophagy inhibitor 3-MA (**Appendix A; Supplementary Fig S4C**) (37). In support of this observation, we did not observe increased LC3 puncta in BER defective cells following TMZ exposure (83).

A major mechanism that has been attributed to PARP-activation induced cell death is direct PAR signaling to the mitochondria where PAR mediates translocation of apoptosis inducing factor (AIF) from the mitochondria to the nucleus to induce caspase-independent cell death (46, 76, 89) via a mechanism that requires receptor (TNFRSF)-interacting serine-threonine kinase 1 (RIP1) activation (90) (**Figure 4**).

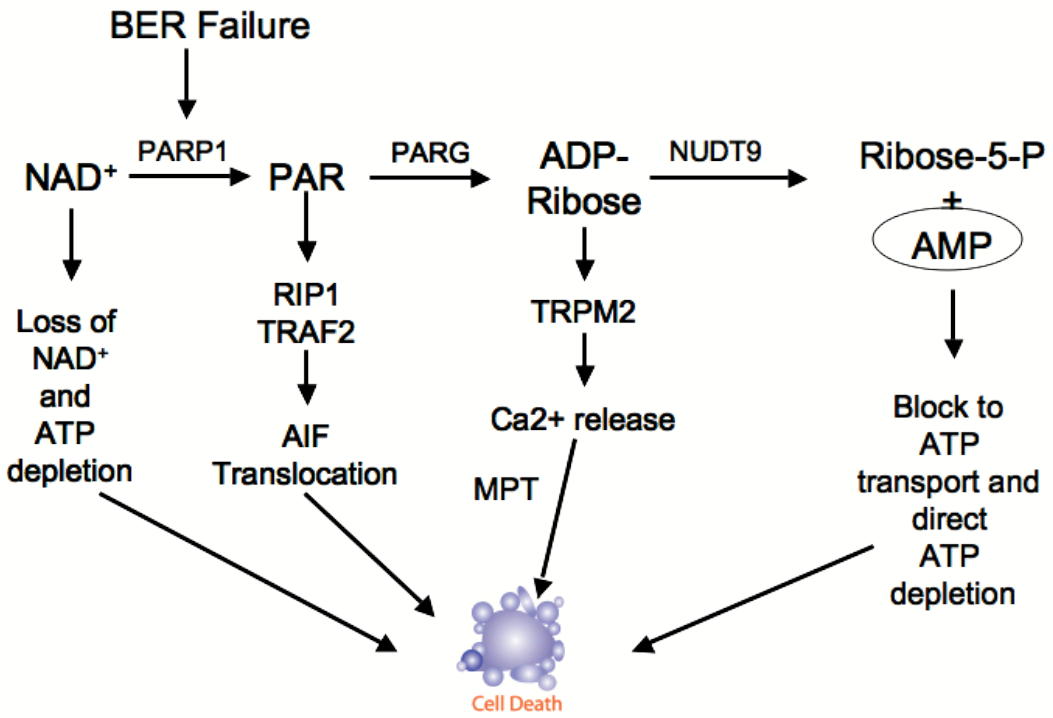

Figure 4. Model of possible mechanisms of cell death after PARP hyperactivation.

RIP1 can be inhibited by necrostatins, small molecule inhibitors shown to inhibit cell death (91, 92). Therefore, we investigated the role of RIP1 in the PARP-mediated cell death we observed by inhibiting RIP1 with Necrostatin-1 (92) and evaluating the impact of RIP1 inhibition on DNA damage-induced cell survival in both control and Polß deficient cells (**Appendix A; Supplementary Fig. S5**) (37). However, inhibition of RIP1 did not prevent cell death in either the parental or Polß deficient cells, suggesting but not proving that AIF translocation may not be related to the observed cell death.

We therefore next evaluated the sub-cellular localization of AIF in control and Polß deficient cells following exposure to the alkylating agents MMS or TMZ as compared to vehicle (media) by immunoflourescent staining and confocal microscopy (**Figure 5**) or by sub-cellular fractionation and immunoblot analysis (**Appendix A; Supplementary Fig. S6**). In-line with the

RIP1 inhibition data above, alkylating agent treatment of Polß deficient cells did not alter the sub-cellular localization of AIF (**Figure 5**).

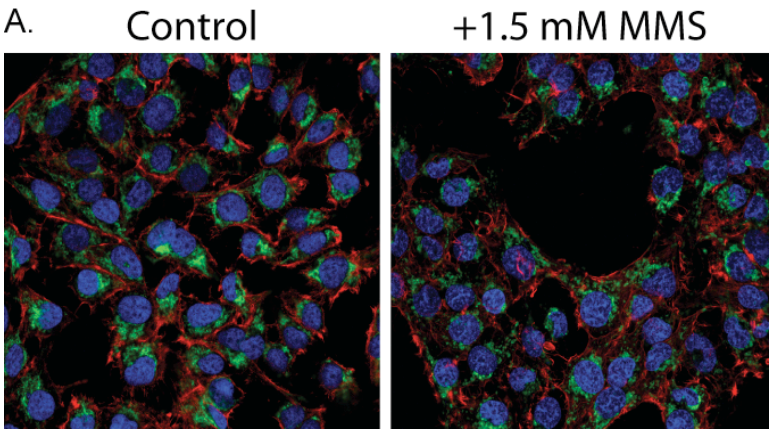

Figure 5. Subcellular localization of AIF before and after alkylation treatment.

Absence of mitochondria to nucleus translocation of AIF due to BER failure as determined by confocal microscopy. BER deficient cells (LN428/MPG) were treated with media (left panel) or 1.5 mM MMS (right panel) for 1 hour and then washed and allowed to recover in media for 5 hours prior to fixation and staining for AIF (green), actin (red) and nucleus (blue).

All the detectable AIF was localized to the mitochondria in both cell lines regardless of agent or time of exposure (up to 12 hours), thus ruling out PAR as a cell death signal upon BER failure.

In the absence of a PAR-mediated cell death process (AIF translocation), it is possible that cell death is initiated via the rapid breakdown of PAR (**Appendix A; Fig. 1A**) by the catabolic enzyme PARG and the accumulation of the PAR catabolites ADP-ribose, ribose-5-phosphate and/or AMP (**Figure 4**) (84). ADP-ribose acts as a second messenger to activate the cation channel TRPM2 to trigger Ca^{2+} influx, resulting in cell death (78, 79) or inhibits ABC transporters (93) whereas elevated AMP can block ATP transport, leading to ATP depletion and cell death (80). To investigate the possibility that PAR catabolites contribute to PARP-mediated cell death in Polß deficient cells, we first blocked Ca^{2+} influx with BAPTA-AM, shown recently by Boothman and colleagues to abrogate PARP1-activation induced cell death (94, 95). Unlike

that observed following DNA damage from reactive oxygen species (ROS) or oxidative stress, BAPTA-AM did not prevent the elevated damage-induced cell death in Polß deficient cells (**Appendix A; Supplementary Fig. S7**) (37). However, as there may be multiple mechanisms of PAR-catabolite-induced cell death, we next knocked-down expression of PARG by stable-transduction of both cell lines with a lentivirus expressing shRNA specific to PARG. Expression of PARG mRNA is reduced to 35% as compared to the GFP-control cells when determined by qRT-PCR. Importantly, we found no evidence for PAR degrading activity in the cells with stable depletion of PARG (**Figure 6; left panel**). When exposed to an alkylating agent, BER deficient PARG-KD cells accumulate significant levels of PAR with no evidence for PAR degradation (**Figure 6; left panel lanes 2-4**). This is in contrast to the presence of PARG, when the PAR molecule is degraded within 60-90 minutes (**Appendix A; Fig.1, lanes 7-12**). These data demonstrate that these PARG-KD cells do not degrade PAR and hence do not accumulate PAR-catabolites, providing an opportunity to determine if PAR catabolites contribute to cell death in these cells. As shown in Figure 6 (right panel), PARG-KD did not rescue or reverse the enhanced damage-induced cell death phenotype of Polß deficient (LN428/MPG) cells. In fact, PARG-KD cells (black bars) were more sensitive to the cell killing effect of the alkylating agent TMZ as compared to the PARG expressing cells (open bars) **(Figure 6, right panel**).

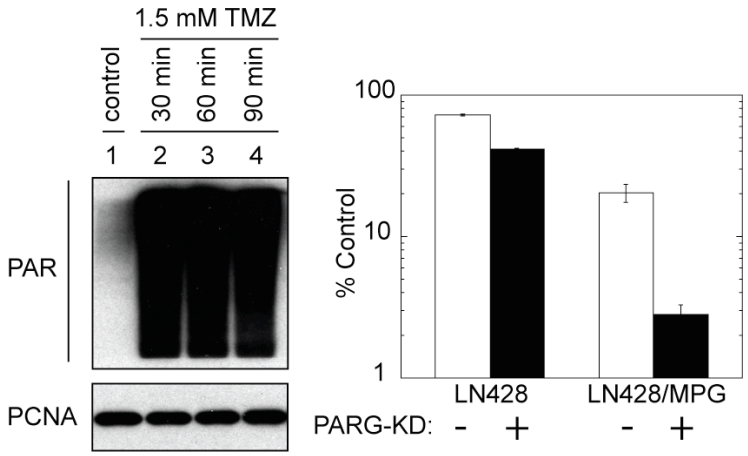

Figure 6. PARG knockdown does not rescue BER failure induced cell death.

PARG KD prevented degradation of DNA damage-induced PAR. (Left Panel) Immunoblot of PAR to determine the degradation of PAR in LN428/MPG/PARG-KD cells following treatment with 1.5 mM TMZ. Compare to Appendix A Figure 1A lanes 7-12. PCNA protein expression level was shown as a loading control. (Right Panel) Preventing generation of PAR catabolites from degradation of PAR via PARG KD enhances TMZ-induced cytotoxicity. LN428 and LN428/MPG cells with (black solid bars) or without (white empty bars) PARG KD were exposed to TMZ (1 mM) or vehicle control (DMSO) for 48 hours. Viable cells are reported as percentage relative to vehicle control treated cells (% control). Results indicate the mean ± S.E. of three independent experiments.
***This figure contributed by Dr. Jiang-bo Tang as part of co-author manuscript (37)**

The inability of necrostatins to abrogate the response and the lack of PAR-mediated AIF translocation strongly suggests that PAR is not acting as a signaling molecule to induce cell death, as has been suggested (42, 96). Further, the inability of BAPTA-AM and most importantly, PARG-KD, to reverse the alkylation-sensitive phenotype of Polß deficient cells also suggests that the observed cell death is un-related to the accumulation of PAR catabolites such as ADP-ribose or AMP. Finally, one of the hallmarks of caspase-independent cell death is secretion of HMGB1 into the extracellular space (97, 98). A significant level of HMGB1 was secreted into the culture media following exposure of the BER defective cells (LN428/MPG) to TMZ as compared to that of the control LN428 cells (**Appendix A; Fig. 3D**). HMGB1 release was mediated through PARP activation, likely due to PARP1 modification (98), as PARP inhibition greatly reduced the release of HMGB1 (**Appendix A; Fig. 3D)**. It is unclear how or if HMGB1 release due to failed BER is related to the recently reported role of HMGB1 in BER (99).

An alternate process of cell death due to PARP1 activation was originally proposed by Berger to involve energy (NAD^+ and ATP) depletion (100, 101), in support of an earlier observation by Jacobson and colleagues demonstrating a decrease in NAD^+ concurrent with an increase in PAR synthesis (102). We therefore measured NAD^+ and ATP levels in the control (LN428) and Polß deficient (LN428/MPG and LN428/MPG/Polß-KD) cells before and after exposure to MMS or TMZ. In line with the cytotoxicity and PARP1 activation results described above, exposure of Polß deficient cells to MMS or TMZ led to a rapid and drastic depletion of both NAD^+ and ATP whereas the NAD^+ and ATP levels in the control cells were not affected (**Figure 7A**). We next measured the impact of alkylation damage on the corresponding cells depleted of PARG (PARG-KD). If PAR catabolites trigger cell death, we would expect that NAD^+ and ATP loss would be attenuated in PARG-KD cells. However, exposure of Polß deficient PARG-KD cells to TMZ led to enhanced depletion of both NAD^+ and ATP (**Figure 7B**). The absence of PAR or PAR-catabolite mediated cell death together with the specific loss of NAD^+ and ATP even when the formation of PAR-catabolites are prevented, suggests that the BER failure response is linked to the cellular bioenergetic capacity of the cell.

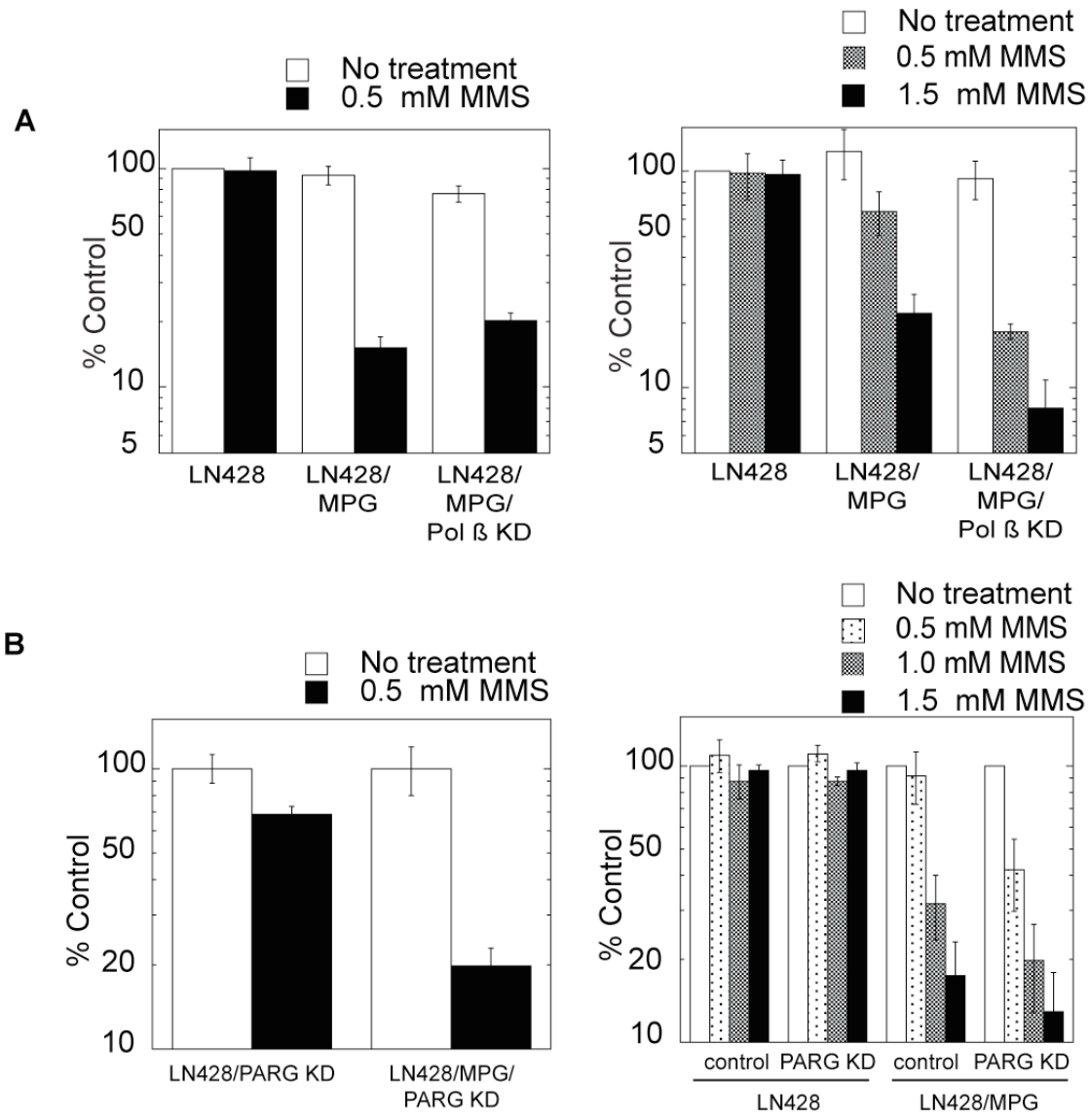

Figure 7. BER failure results in energetic depletion that is not rescued by PARG knockdown.

(A) Alkylation damage promotes NAD^+ and ATP depletion in BER defective cells. NAD^+ content (*left panel*): Cells were treated with media (white bars) or 0.5 mM MMS (black bars) for 1 hour prior to collection for NAD^+ content analysis via enzymatic assay as described in the Materials and Methods section. ATP content (*right panel*): Cells were treated with media (white bars), 0.5 mM MMS (grey bars) or 1.5 mM MMS (black bars) for one hour. ATP content was measured after 1-hour recovery in normal media via the luminescence ATP assay described in the Materials and Methods section. NAD^+ levels or ATP levels shown are the average of three independent experiments and are reported as percent control of the untreated control cell line.
(B) PARG-KD does not rescue alkylation damage induced NAD^+ and ATP depletion in BER defective cells. NAD^+ content (left panel): PARG-KD cell lines were treated with media (white bars) or 0.5 TMZ (black bars) for one hour prior to collection for NAD^+ content analysis as described in the Materials and Methods section. ATP content (*right panel*): PARG-KD cells were treated with media (white bars), 0.5 mM TMZ (dotted bars), 1.0 mM TMZ (grey bars) or 1.5 mM TMZ (black bars) for one hour. ATP content was measured after 1-hour recovery in normal media via the luminescence ATP assay described in the Materials and Methods section. NAD^+ levels or ATP levels shown are the average of three independent experiments and are reported as percent control of the untreated control cell line.

For this paradigm to hold, we hypothesized that the availability of bioenergetic metabolites would impact the survival of Polß deficient cells exposed to an alkylating agent. In-line with this hypothesis, we find that supplementation of the cells with either ß-nicotinamide mononucleotide (NMN) (103) or nicotinic acid (NA) reversed the DNA damage-induced phenotype, rendering the Polß deficient cells (black bars) completely (NMN) or 80% (NA) resistant to the cell killing effects of the alkylating agent, as compared to the BER proficient cells (open bars) (**Figure 8**).

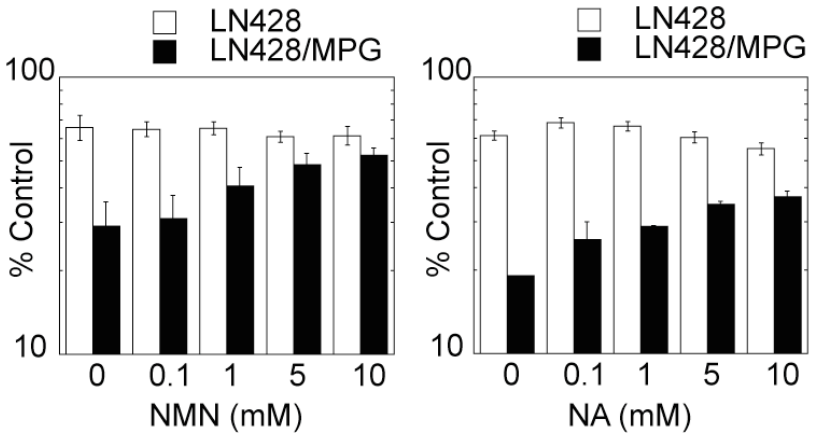

Figure 8. NAD$^+$ precursors rescue BER failure induced cell death.

Bioenergetic metabolites rescue Polß deficient cells from DNA damage-induced cell death. LN428 and LN428/MPG cells were pre-treated with NMN, NA or vehicle control (media) for 24 hours and were then exposed to TMZ (1 mM) in the presence or absence of NMN or NA for 48 hours. Viable cells were measured as in Figure 1B and were reported as percentage relative to vehicle control treated cells (% control). Results indicate the mean ± S.E. of three independent experiments.

***This figure contributed by Dr. Jiang-bo Tang as part of co-author manuscript (37)**

Conversely, we anticipated that the hypersensitive phenotype of Polß deficient cells would be exacerbated by a reduction in the cellular level of NAD$^+$ and related bioenergetic metabolites. We therefore evaluated the impact of transient NAD$^+$ depletion on the observed "**BER Failure**" response by pre-treating cells with FK866, a highly specific non-competitive small molecule inhibitor of nicotinamide phosphoribosyltransferase (NAMPT), a critical enzyme in the NAD$^+$

biosynthetic salvage pathway that catalyzes the synthesis of NMN (104). Most importantly, the sensitivity of control cells to alkylation damage was not altered by FK866 treatment. However, the BER deficient cells are 9-fold more sensitive to MMS following a non-toxic (10 nM) treatment with FK866, as compared to the untreated cells (**Figure 9A**) even though PAR synthesis after the combined FK866 + MMS treatment is attenuated (**Figure 9B).**

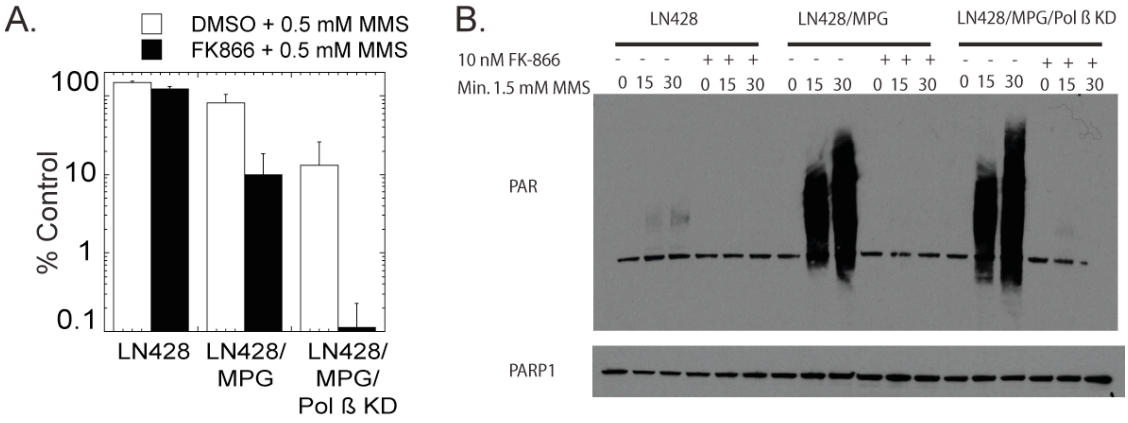

Figure 9. Enhancement of BER failure induced cell death by NAD^+ biosynthesis inhibition.

(A) NAD^+ biosynthesis inhibition augments BER failure-induced cell death. Cells were pretreated for 24 hours with a non-toxic 10nM dose of FK866 (black bars) or DMSO (white bars). Cells were then exposed to media control or MMS (0.5 mM) for 1 hour. Results indicate the mean ± S.E. of three independent experiments.
(B) FK866 prevents BER failure induced PAR synthesis. Cells were pretreated with FK866 (10nM) or DMSO control for 24 hours prior to exposure to MMS (1.5mM). PAR synthesis at multiple time points post exposure was measured via immunoblot. PARP1 immunoblot is provided as loading control.

These results support our overall hypothesis that the BER failure phenotype of Polß deficient cells is mediated by BER intermediate (5'dRP) induced PARP1 activation and induction of caspase-independent cell death that is uniquely dependent on the availability of bioenergetic metabolites such as NMN and NAD^+.

3.3 DISCUSSION

The requirement for BER in general and Polß more specifically in the repair of genomic DNA base damage, (13, 36), elevates the significance of characterizing the mechanism responsible for Polß deficiency-induced cell death [e.g., a failure to complete repair of the BER intermediate 5'dRP in the absence of Polß]. As evidenced recently by the development of clinically significant PARP1 inhibitors, identifying BER proteins critical for response to DNA damaging agents (e.g., chemotherapy) can have broad human health implications. Equally important is a clear understanding of the mechanism(s) that contribute to the enhanced cell death observed upon DNA repair inhibition. For example, PARP1 inhibition triggers apoptosis via the accumulation of DSBs (71, 72) and a requirement for homologous recombination proteins such as BRCA1 and BRCA2 (66). To this end, we have developed a unique series of genetically modified human tumor cell lines as models of Polß deficiency that accumulate the cytotoxic BER intermediate 5'dRP following exposure to alkylating agents (TMZ, MMS and MNNG). By directly comparing BER (Polß deficient) defective and BER competent isogenic human cell lines, the cellular, biochemical and signaling responses to DNA base damage can be defined as either global (non-specific) or BER (Polß) specific effects, the latter resulting from a cellular response to the inability to complete BER, referred to herein as "**BER Failure**". We have then utilized this system to define the mechanism of cell death resulting from Polß loss/inhibition or BER failure and propose and test paradigms to enhance the cell death response.

From these studies, we find that the un-repaired BER intermediates that accumulate upon DNA damaging agent exposure when Polß is deficient will activate PARP1, leading to a rapid onset of PARP1-dependent, caspase-independent cell death with little or no role for a caspase-dependent or autophagy-dependent process in the response. It remains to be determined if the

BER failure-induced cell death observed herein is dependent on ERK1/2–mediated PARP1 phosphorylation (105), SIRT1-regulated deacetylation of PARP1 (106) or if the observed PARP1-induced cell death requires BAX, Calpain and JNK activation (107). Coincident with damage-induced necrosis in Polß deficient cells is PARP1-dependent HMGB1 secretion (98), a hallmark of caspase-independent cell death and inflammation signaling. HMGB1 functions in the extra-cellular space as a robust RAGE ligand and inflammatory cytokine or damage-associated molecular pattern molecule (97), suggesting that BER failure and the resulting PARP1 activation may trigger an inflammatory response in tissues with a BER imbalance such as ulcerative colitis (108).

There are multiple PARP1-activation induced cell death mechanisms, as outlined in the diagram shown in Figure 4. In one, it is suggested that PAR, the product of PARP1 activation, is a cell death molecule. In this process, PAR initiates the translocation of AIF from the mitochondria to the nucleus by a RIP1-dependent mechanism (46, 76, 89, 90). Uniquely, PAR generated due to BER failure does not appear to trigger cell death via RIP1 activation nor does PAR function as a signal to initiate AIF translocation. PARP1 is involved in many DNA repair processes including homologous recombination (HR) and non-homologous end joining (NHEJ) in response to DSBs and has a role in telomere maintenance (45, 109). The question remains if PAR generated via BER failure is of a unique chemical make-up as compared to PAR generated from DSB-induced PARP1 activation. One possible explanation for the absence of a role for AIF in this study is the concentration of DNA damaging agents used. In this report, we have used TMZ or MMS at a maximum concentration of 1.5 mM or MNNG at a concentration of 5 μM, resulting in 90-95% cell death in the BER deficient cells with little or no cell death in the control cells. Many reports of PAR-induced AIF translocation include MNNG concentrations of 100 and

500 μM (107, 110, 111). Such high concentrations of DNA damaging gents (e.g., MNNG at 20x and 100x that used herein) have the potential to directly induce DNA DSBs, create overwhelming levels of both nuclear and mitochondrial genome damage (112) as well as the possibility of direct protein alkylation. Regardless, it is clear that the cell death initiated by BER failure is independent of RIP1 activation and AIF translocation, thus ruling out PAR as the cell death signal that is initiated upon BER failure.

One explanation for the absence of PAR-mediated cell death is the rapid catabolism of PAR by PARG (84). In this study, we find that PAR synthesized due to PARP activation is degraded within 90 minutes. As summarized in Figure 4, the breakdown products of PAR (PAR catabolites) are also likely mediators of cell death, including ADP-ribose (activator of the Ca^{2+} channel TRPM2) and AMP (inhibitor of ATP transport) (78-80). However, PARG knockdown did not reverse the DNA damage-sensitive phenotype of Polß deficient cells (**Figure 6**), suggesting that damage-dependent cell death in Polß deficient cells is not initiated by PAR catabolites. Conversely, it was suggested that the PAR catabolite AMP may provide a protective phenotype by activation of AMPK, induction of autophagy and enhanced ATP synthesis following ROS-induced DNA damage and PARP1 activation (113). However, this report has since been withdrawn. Although loss of AMPK activation and induction of autophagy upon PARG-KD could explain, in part, the enhanced cell death observed in the PARG-KD cells (**Figure 6**), we suggest this is unlikely, since in this study, autophagy is not involved and the activation of AMPK, if any, does not appear to overcome the damage-induced cell death phenotype resulting from BER failure in the PARG proficient cells. In all, these studies imply that the alkylation-sensitive phenotype of Polß deficient cells is un-related to the accumulation of

PAR catabolites such as ADP-ribose or AMP and is likely wholly dependent on the metabolite bioavailability or bioenergetic capacity of the cell.

The over-riding response to the loss of Polß and an inability to complete BER (BER failure) is energy failure or depletion of bioenergetic metabolites with no evidence for cell death triggered by PAR or the PAR catabolites ADP-ribose or AMP. The energy collapse or depletion of NAD^+ and ATP due to BER failure is offset by elevated levels of NMN (103) and is negatively affected by NAD^+ biosynthesis inhibition (FK866). This suggest FK866 (APO866) and related NAD^+ biosynthesis inhibitors might be combined with TMZ and BER inhibitors to improve TMZ response. This also suggests any stress on or defects in the NAD^+ biosynthesis pathway such as over-activation of SIRT1 (114) or attenuating defects in NAMPT, NMNAT1 or related NAD^+ biosynthetic enzymes (115) may have significant effects on cell survival following BER failure.

Similar phenotypes (stress-induced PARP1 activation and cell survival dependent on NAD^+ metabolites) have been observed in diverse human cell types and mammalian organ systems, stressing the significance of these findings. PARP1 activation and the resulting "NAD^+ depletion"-mediated or ATP-depletion mediated cell death plays a critical role in tissue injury from cerebral and myocardial ischemia (116-119). Analogous to the studies described herein, cellular protection from cerebral ischemia is provided by NAD^+ metabolite supplementation (120, 121). Similarly, streptozotocin-induced diabetes results from PARP1 activation, energy imbalance and cell death dependent on the BER enzyme MPG (122-125). Most importantly, cellular NAD^+ metabolism plays an essential role in pancreatic ß-cell viability and insulin secretion (126). With the observation that BER failure triggers NAD^+ depletion, it is interesting to speculate if overall BER capacity controls susceptibility to ischemia or streptozotocin-induced

and age-related diabetes onset via neuronal or ß-cell death from loss of bioenergetic metabolites subsequent to BER failure. The onset of these physiologically significant outcomes (stroke, neurodegeneration, ischemia, diabetes) involves PARP1 activation, NAD^+ depletion and cell death, similar to that reported here. Although a portion of the environmental and endogenous stressors that induce these phenotypes via PARP1 activation will directly induce DNA single-strand breaks, it is reasonable to presume that a significant proportion of cell death related to stroke, retinal degeneration, ischemia and diabetes may initiate from genomic DNA base damage, requiring repair by the BER machinery. As such, the failure to repair the DNA damage and the resulting accumulation of DNA repair intermediates (BER failure) may be the trigger of PARP1 activation and cell death.

In summary, these studies suggest that PARP1 functions as a BER molecular sensor protein to induce caspase-independent cell death following BER failure and provides mechanistic insight into why Polß deficiency leads to cell death. Further, we show that the observed DNA damage dependent cell death in Polß deficient cells is un-related to the accumulation of PAR catabolites such as ADP-ribose or AMP yet is dependent on NAD^+ metabolite bioavailability or bioenergetic capacity of the cell, suggesting a linkage between DNA repair capacity, cell survival and cellular bioenergetic metabolites. Finally, these studies have potentially important implications for therapeutic development as it relates to a chemotherapy-induced synthetic lethality approach to cancer therapy involving the combination of a chemotherapeutic DNA damaging agent, a DNA repair inhibitor and a regulator or inhibitor of NAD^+ biosynthesis.

4.0 UTILIZING REAL-TIME TECHNIQUES TO DETERMINE SPATIAL AND TEMPORAL RESOLUTION OF PARP MEDIATED ENERGY DEPLETION

4.1 INTRODUCTION

Given the prevalent use of DNA damaging agents in the treatment of tumors, it is critical to not only understand the mechanisms of DNA repair pathways that may confer resistance to chemotherapy by removal or repair of DNA lesions but to also understand the cellular consequences of incomplete or inhibited DNA repair. Inhibition of DNA repair pathways is a common strategy for enhancing the chemotherapeutic effect of DNA damaging agents. This is exemplified by the attempts of combining O^6-benzyguanine with TMZ to enhance O^6-methylguanine mediated apoptosis and the current use of PARP inhibitors to inhibit BER in homologous recombination deficient tumors (11, 58, 59).

We have previously reported that the BER substrates generated by TMZ can enhance glioblastoma and breast cancer tumor cell death in an O^6-methylguanine independent manner when BER is targeted through genetic manipulation. Targeting of the BER pathway is achieved through either overexpressing MPG or combining MPG overexpression with Polß knockdown, resulting in a functional Polß defect (37). The ability to initiate repair, but not complete it results in the accumulation of repair intermediates and is termed ***BER failure***. We have shown that BER failure results in PARP hyperactivation, the depletion of cellular NAD^+ and ATP and eventual

necrotic cell death, independent of AIF translocation to the nucleus or ADP-ribose and AMP mediated cell death pathways (37). This mechanistic insight has highlighted the BER pathway as an attractive target for inhibition in combination with TMZ or other DNA alkylating or oxidizing agents, and also suggests that cellular energetic pathways may prove to be valuable targets for inhibition in combination with alkylating agents or BER inhibitors. While the basic mechanism of BER failure induced cell death has been elucidated (37), the details of the PARP mediated energy depletion and cell death are still unclear. Understanding the metabolic pathways influenced by PARP hyperactivation, as well as the temporal and spatial resolution of cellular energy loss, will provide critical insight into not only the consequences of BER failure, providing potential additional targets for therapy, but could give general mechanistic clarity to any process resulting in PARP hyperactivation and NAD^+ depletion, such as ischemia reperfusion injury after stroke or myocardial infarction, Parkinson's disease or cisplatin treatment (56, 127).

The effects on subcellular energy pools after PARP hyperactivation are controversial. Multiple reports suggest that the mitochondrial NAD^+ pool is insensitive to depletion by PARP hyperactivation, suggesting that the ability to retain oxidative phosphorylation for the production of ATP is sufficient to promote cell survival (128, 129). David Sinclair has alternately argued that depletion of the mitochondrial NAD^+ pool is responsible for cell death after alkylation damage, and protection of this subcellular pool results in rescue of PARP-mediated cell death (130). PARP hyperactivation and cytosolic NAD^+ loss has been considered a block to glycolysis (131), and in fact Craig Thompson has shown that only cells relying on glycolysis are sensitive to alkylation mediated PARP hyperactivation and necrotic cell death (74). These conflicting reports highlight the need to be able to directly measure the subcellular energy pools. While measurement of subcellular NAD^+ is difficult, ATP sensors have recently been developed that

are specific for subcellular pools (65). We used these ATP probes here to dissect energetic depletion of the mitochondria, cytosol and nucleus in live cells after DNA damage.

The effect of PARP hyperactivation on metabolic processes such as glycolysis and oxidative phosphorylation is also unclear. Cytosolic NAD^+ depletion has been argued to be a glycolytic block, and repletion of NAD^+ or glycolytic products that serve as TCA cycle substrates, such as α-ketogluterate and pyruvate, have been shown to rescue PARP mediated cell death (131, 132). Other reports describe mitochondrial dysfunction that results in defective oxidative phosphorylation, enhanced production of reactive oxygen species and eventual loss of membrane potential (133). It has been proposed that PARP hyperactivation results in complex I dysfunction in mouse mycocardium, potentially via depletion of NADH, a required cofactor for complex I function (134). Despite multiple metabolic processes being potentially affected by PARP hyperactivation and NAD^+ depletion, it is unknown which of these metabolic defects is responsible for PARP mediated ATP depletion or if ATP depletion is simply a result of an effort to resynthesize NAD^+ (100, 101). Further, it is unclear if loss of ATP from specific subcellular compartments after PARP hyperactivation results from defective energy production in that compartment, such as direct mitochondrial ATP loss via PARP mediated oxidative phosphorylation defects.

Finally, it is unresolved whether NAD^+ depletion alone is sufficient for the observed metabolic defects and ATP depletion or if there is an alternate more direct role for PARP in necrotic cell death, such as signaling of the PAR polymers themselves or the ADP ribosylation of metabolic or signaling proteins. Some studies have suggested that long complex PAR polymers themselves result in AIF release and caspase independent cell death after DNA damage (42); however, it is unclear if PAR polymers play a direct role in the ***BER failure*** phenotype given the

lack of observed AIF translocation. This study aims to clarify the mechanisms of PARP mediated energetic depletion and necrosis utilizing novel real-time live cell techniques to measure subcellular ATP loss and metabolic dysfunction. Here we show that mitochondrial ATP is lost in a similar time frame as cytosolic and nuclear ATP, within 15 minutes of the peak of PAR accumulation. It demonstrates that BER failure results in a PARP mediated block to glycolysis and identifies a novel PARP dependent, but NAD^+ independent defect in mitochondrial respiratory capacity.

4.2 RESULTS

Alkylation damage results in loss of mitochondrial ATP followed by loss of cytosolic and nuclear ATP.

As previously described, we have engineered a model cell line to study alkylation-induced events utilizing low doses of alkylating agent. The LN428 glioblastoma cells overexpressing MPG (LN428/MPG) preferentially accumulate base excision repair intermediates leading to robust PARP hyperactivation and enhanced sensitivity to alkylating agents, whereas the LN428 parental cell line has endogenously low levels of MPG with no observable PARP activation after alkylation and no alkylation induced toxicity at the doses under study (**Figure 3, see chapter 3)**. This allows for the use of alkylation doses 50-100 fold less than commonly used to study the effects of PARP activation. We have previously reported that alkylation induced PARP hyperactivation leads to NAD^+ depletion within an hour of exposure and ATP depletion within 2 hours of exposure, eventually resulting in necrotic cell death within 48 hours (37). Using a whole cell measure of cellular ATP levels, we find that ATP levels are stable 15

minutes after exposure, but begin to drop 30 minutes after treatment with MNNG (**Figure 10**). This loss of ATP is approximately 15 minutes after the peak of PARP activation.

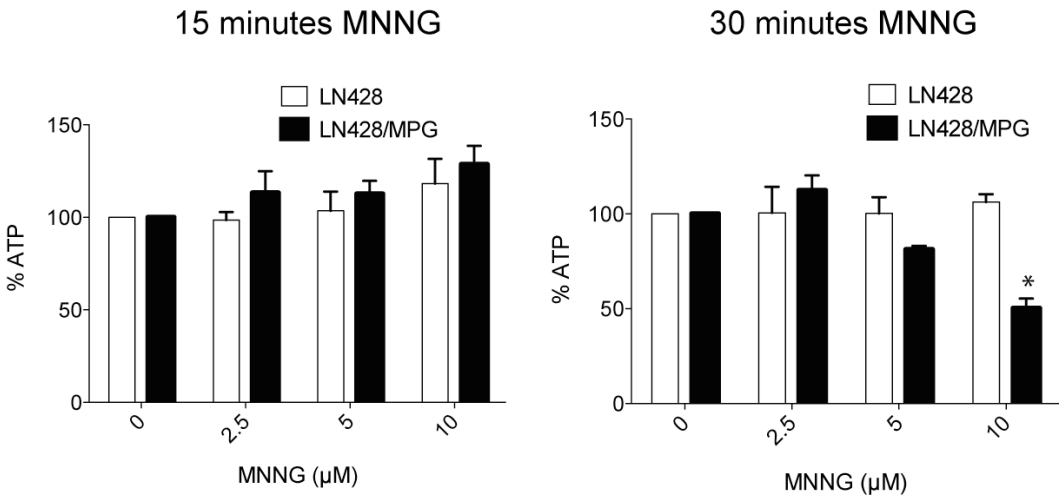

Figure 10. Time course of global depletion of ATP after PARP hyperactivation

Global ATP levels begin to decrease 30 minutes after DNA damage. Global ATP levels were measured by ATPlite assay 15 minutes after MNNG treatment at the indicated MNNG doses (left panel) or 30 minutes after MNNG treatment at the indicated MNNG doses (right panel) in both parental LN428 cells and LN428/MPG cells. ATP levels shown are the average of three independent experiments ± S.E and are reported as percent control of the untreated control cell line.
*Represents statistical significance with a $p < 0.05$ compared to the LN428 cell line treated at the same dose.

Despite reports attempting to determine which NAD^+ compartments are critical for PARP mediated cell death, it has not been determined in which subcellular compartments ATP is depleted after alkylation induced PARP hyperactivation. Imamura et. al. recently published the generation and validation of FRET based ATP sensors with subcellular targeting sequences, in which the ε subunit of the *Bacillus subtilis* F_0F_1-ATP synthase is fused with CFP and mVenus resulting in a FRET signal when ATP is bound (65). Therefore, utilizing live cell imaging, loss of ATP after treatment can be measured as a loss of FRET signal. These constructs are fused to either nuclear or mitochondrial targeting sequences, allowing the visualization of ATP depletion in specific subcellular compartments. We have used these ATP FRET sensors to answer the

questions of where in the cell ATP is lost after alkylation damage and PARP hyperactivation, and what are the kinetics of subcellular ATP loss. An increase in CFP signal indicates a loss of ATP bound to the FRET sensor, thus an increase in CFP/YFP ratio above 1 indicates loss of ATP in relation to the baseline measurement. In the LN428 and LN428/MPG glioblastoma cells the subcellular FRET plasmids were transiently transfected 48 hours prior to the experiment. A ten-minute baseline of FRET ratio was taken prior to the addition of 5μM MNNG. Surprisingly, mitochondrial ATP was lost most rapidly, with an observed loss of ATP beginning at 22 minutes, followed by the cytosolic and nuclear compartments, which both begin to lose ATP at 34 minutes after alkylation (**Figure 11 and 12**). In the LN428 cells, which show no visible PARP activation after alkylation damage, there is no change in FRET ratio at these low doses of alkylation (**Figure 11**).

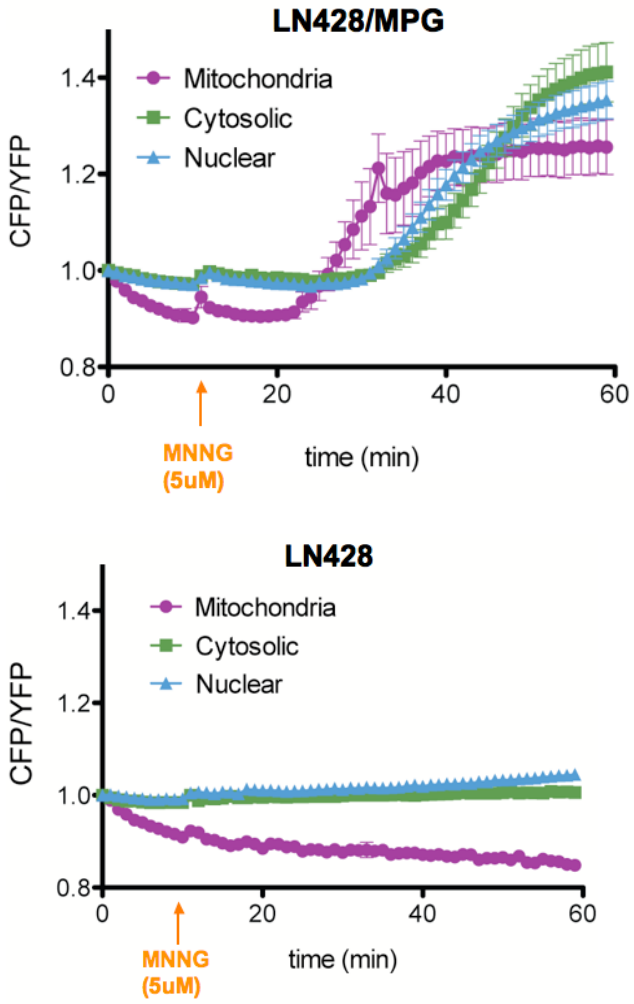

Figure 11. Measurement of subcellular ATP loss after PARP hyperactivation

Depletion of ATP occurs in all subcellular compartments after DNA damage. The FRET ratio was calculated for either LN428/MPG cells (top panel) or LN428 cells (bottom panel) transfected with the indicated subcellular FRET sensor. Images were acquired every minute. A ten-minute baseline measurement period was followed with treatment of 5μM MNNG as indicated by the orange arrow. FRET traces shown are the mean of 7-9 cells (top panel) or 5-7 cells (bottom panel) ± S.E.

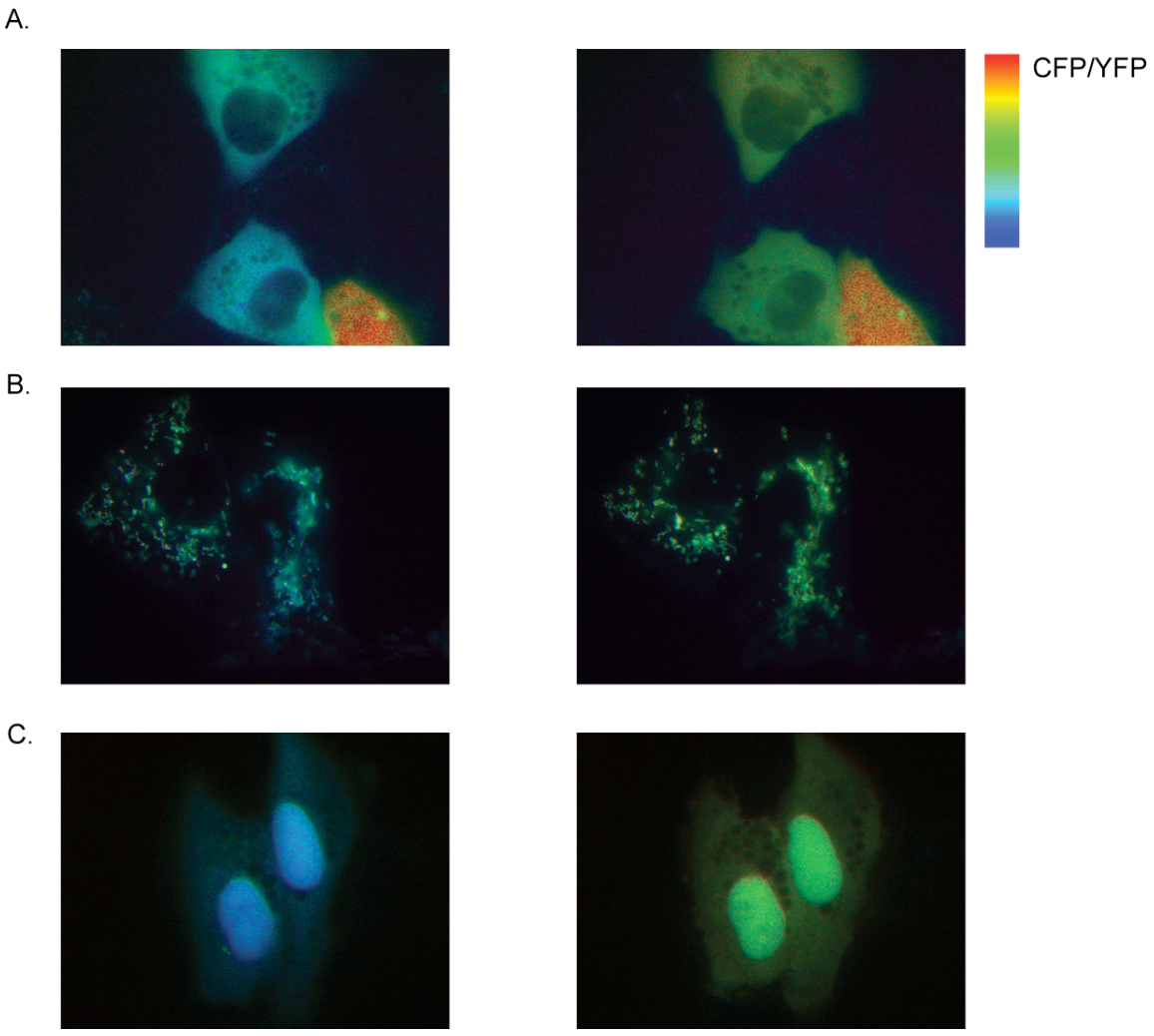

Figure 12. Images of ATP FRET before and after treatment

(A) Cytosolic ATP probe before alkylation (left) or after alkylation (right). Images shown as the ratio of CFP/YFP with high CFP (ATP loss) indicated as increasingly red.
(B) Mitochondrial ATP probe before alkylation (left) or after alkylation (right).
(C) Nuclear ATP probe before alkylation (left) or after alkylation (right).

Alkylation induced PARP activation leads to acute inhibition of glycolysis and loss of mitochondrial capacity.

The ATP generating pathways of glycolysis and mitochondrial oxidative phosphorylation require NAD^+ and NADH cofactors. Given that PARP consumes NAD^+ it serves to reason that NADH and other NAD^+ metabolite and precursor pools will also be affected. Whole cell measurement of NAD^+ and NADH show loss of both cofactors 30 minutes after alkylation (**Figure 13**).

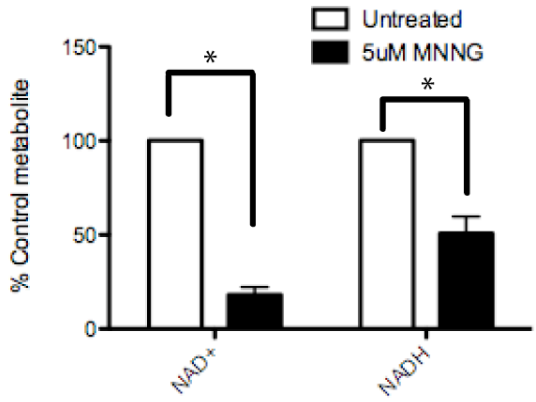

Figure 13. Loss of NAD^+ and NADH 30 minutes after PARP hyperactivation

Both global NAD^+ and NADH are depleted after DNA damage. Global NAD^+ and NADH levels were measured as described in materials and methods after 30 minutes of treatment with either media control (white bars) or 5μM MNNG (black bars). NAD^+ and NADH levels shown are the average of three independent experiments ± S.E and are reported as percent control of the untreated cell line.
*Represents statistical significance with a $p < 0.05$

This data combined with the previously observed loss of ATP in both the mitochondrial and cytosolic compartments led us to investigate to what degree glycolysis and oxidative phosphorylation are compromised after alkylation treatment. In order to measure both oxidative phosphorylation and glycolysis concurrently in live cell culture conditions we utilized the Seahorse Extracellular Flux Analyzer and the standard protocol for measurement of overall

metabolic profiles determined by the subsequent addition of the metabolic inhibitors oligomycin, FCCP, 2-deoxyglucose and rotenone. Previous studies from Swanson and colleagues have demonstrated that PARP activation acts as a glycolytic block in mouse astrocyte cultures and that repletion of NAD^+ can rescue glycolysis and PARP mediated cell death (48, 131). Consistent with these reports, one hour after alkylation treatment the LN428/MPG cell line (under conditions that lead to high levels of PARP activation) has basal levels of glycolysis 10 fold less than untreated wells, whereas the LN428 cells showed no glycolytic defect (**Figure 14**; **bottom panel**). In addition, the LN428/MPG cells retain their basal levels of OCR coupled to ATP production, but have severely reduced mitochondrial reserve capacity (calculation described in materials and methods), a novel mitochondrial defect not able to be observed in the set up of past studies that used mitochondrial extraction to measure oxidative phosphorylation (**Figure 14; top panel**). The LN428 cells (with no observable PARP activation or NAD^+ depletion) do not show reduced glycolytic levels (**Figure 14; bottom panel**); however, they do have an apparent decrease in mitochondrial reserve capacity (**Figure 14; top panel**). This latter result indicates that mitochondrial reserve capacity is either affected by alkylation directly or that very low levels of PARP activation are capable of disturbing mitochondrial reserve capacity.

(A)

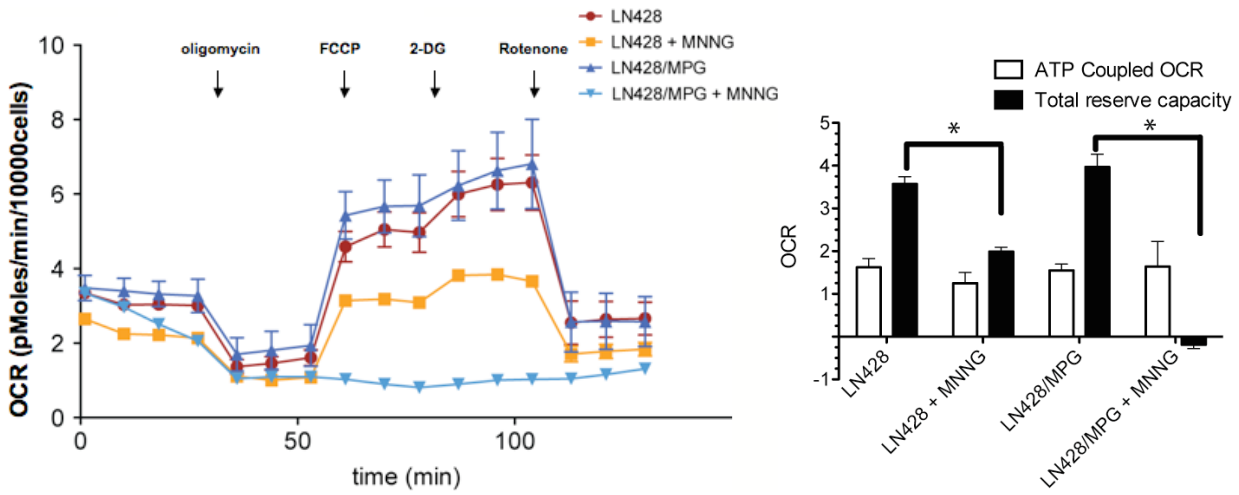

(B)

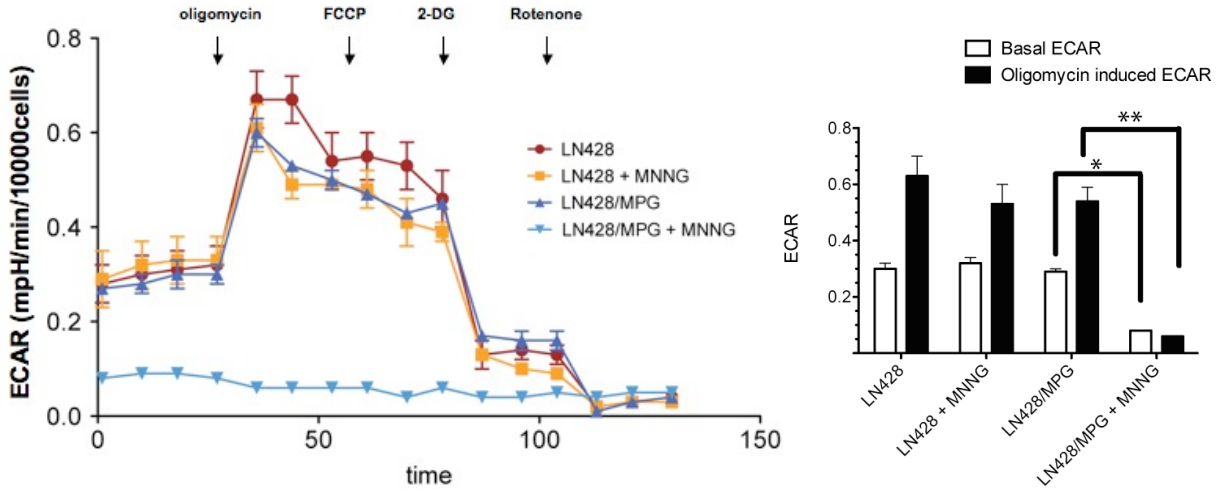

Figure 14. Measurement of MNNG induced metabolic changes

(A) MNNG induces reduction of mitochondrial reserve capacity. Seahorse measurement of the OCR metabolic profile were performed in the LN428 or LN428/MPG cells treated with either media control or 1 hour MNNG at 5 μM. Bar graphs representing ATP coupled OCR and total reserve capacity are shown to the right. Data shown is the mean of two independent experiments ± S.E for seahorse traces or ± S.D. for calculated ATP coupled OCR and reserve capacity.

*Represents statistical significance with a $p < 0.05$

(B) MNNG induces loss of glycolysis in LN428/MPG cells. Seahorse measurement of the ECAR metabolic profile were performed in the LN428 or LN428/MPG cells treated with either media control or 1 hour MNNG at 5 μM. Bar graphs representing basal ECAR and oligomycin induced ECAR is shown to the right. Data shown is the mean of two independent experiments ± S.E for seahorse traces or ± S.D. for calculated basal ECAR and oligomycin induced ECAR.

*Represents statistical significance with a $p < 0.05$ compared to media control for basal ECAR

** Represents statistical significance with a $p < 0.05$ compared to media control for oligomycin induced ECAR

To further elucidate the role of PARP hyperactivation on cellular metabolism, the PARP inhibitor, PJ34, was used. Thirty minute pretreatment and co-treatment of 2μm PJ34 with MNNG is capable of reducing PAR levels observed by immunoblotting for PAR and is capable of preventing alkylation induced cell death in a short-term cytotoxicity assay (37). The glycolytic defect in LN428/MPG cells is completely ameliorated by PARP inhibition (**Figure 15**).

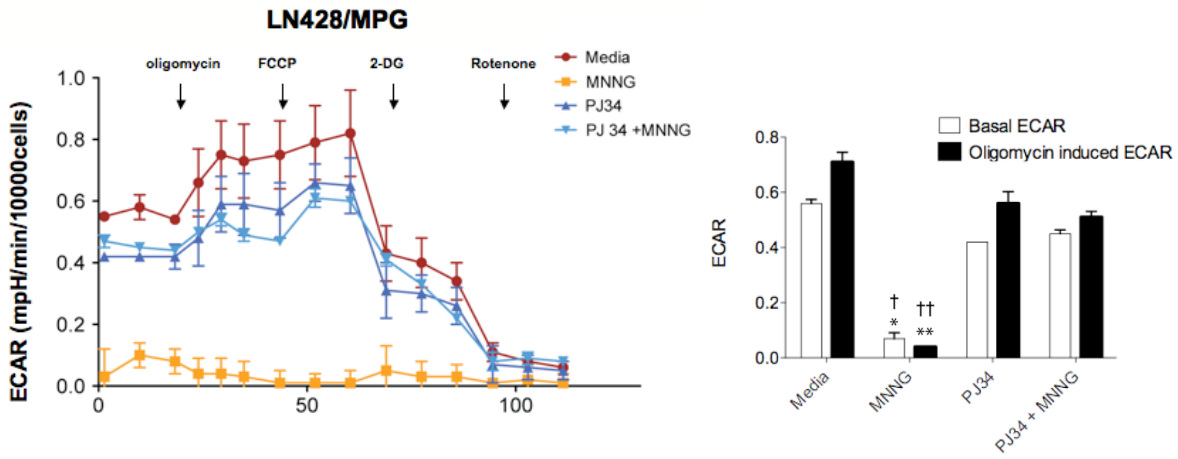

Figure 15. PARP inhibition rescues MNNG-induced glycolytic defect

Treatment with PARP inhibitor PJ34 rescues glycolytic defect. Seahorse measurement of the ECAR metabolic profile were performed in LN428/MPG cells treated with either media control or 2 μM PJ34 for 30 minutes prior to a 1 hour treatment with either media control, PJ34, MNNG or PJ34 + MNNG . MNNG was used at a dose of 5 μM. Bar graphs representing basal ECAR and oligomycin induced ECAR is shown to the right. Data shown is the mean of two independent experiments ± S.E for seahorse traces or ± S.D. for calculated basal ECAR and oligomycin induced ECAR.
*Represents statistical significance with a $p < 0.05$ compared to media control for basal ECAR
†Represents statistical significance with a $p < 0.05$ compared to PJ34 + MNNG for basal ECAR
** Represents statistical significance with a $p < 0.05$ compared to media control for oligomycin induced ECAR
††Represents statistical significance with a $p < 0.05$ compared to PJ34 + MNNG for oligomycin induced ECAR

PJ34 rescues the mitochondrial reserve defect shown in the LN428 cells, strongly suggesting that low levels of PARP activation influence mitochondrial capacity as opposed to direct alkylation damage of mitochondrial components (**Figure 16**). Interestingly, the large defect in

mitochondrial reserve capacity in LN428/MPG cells is only reversed by about 50%. Taken together with the LN428 data this suggests that PAR may act in a dose dependent manner on reserve capacity and that reserve capacity is extremely sensitive to low levels of PAR. PJ34 (2μM) completely rescues the mitochondrial defect in the LN428 cells with low levels of PAR present after damage; however, in the LN428/MPG cells with high levels of PAR, PARP inhibition results in a 50% decrease in reserve capacity, presumably from low levels of residual PAR generation.

(A)

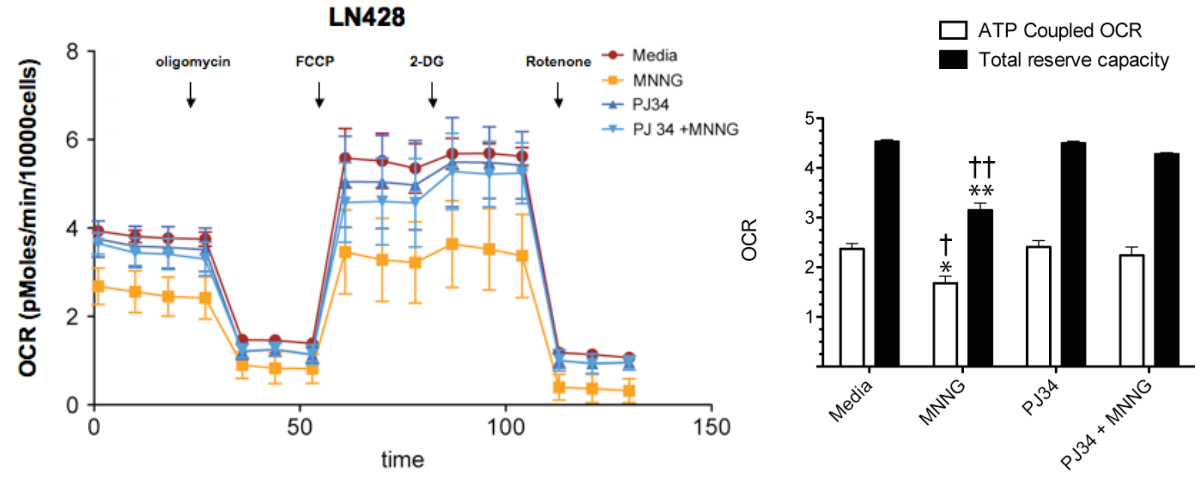

(B)

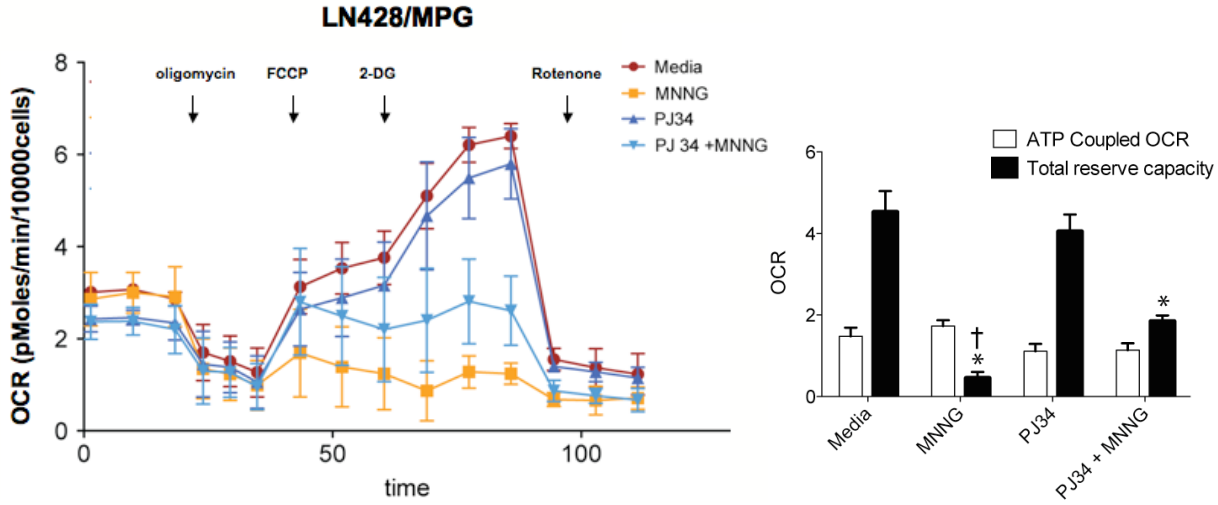

Figure 16. PARP affects mitochondrial reserve capacity in a PAR dose-dependent manner

(A) Treatment with PARP inhibitor PJ34 reverses mitochondrial reserve capacity defect in LN428 cells. Seahorse measurement of the OCR metabolic profile were performed in LN428 cells treated with either media control or 2 μM PJ34 for 30 minutes prior to treatment with either media control, PJ34, MNNG or PJ34 + MNNG for 1 hour. MNNG was used at a dose of 5 μM. Bar graphs representing ATP coupled OCR and total reserve capacity are shown to the right. Data shown is the mean of two independent experiments ± S.E for seahorse traces or ± S.D. for calculated ATP coupled OCR and reserve capacity.

*Represents statistical significance with a $p < 0.05$ compared to media control for ATP coupled OCR

†Represents statistical significance with a $p < 0.05$ compared to PJ34 + MNNG for ATP coupled OCR

** Represents statistical significance with a $p < 0.05$ compared to media control for OCR reserve capacity

††Represents statistical significance with a $p < 0.05$ compared to PJ34 + MNNG for OCR reserve capacity

(B) Treatment with PARP inhibitor PJ34 partially reverses mitochondrial reserve capacity defect in LN482/MPG cells. Seahorse measurement of the OCR metabolic profile was performed in the LN428/MPG cells treated as above. Bar graphs representing ATP coupled OCR and total reserve capacity are shown to the right. Data shown is the

mean of two independent experiments ± S.E for seahorse traces or ± S.D. for calculated ATP coupled OCR and reserve capacity.
*Represents statistical significance with a $p < 0.05$ compared to media control for OCR reserve capacity
†Represents statistical significance with a $p < 0.05$ compared to PJ34 + MNNG for OCR reserve capacity

However, this defect in reserve capacity does not have a strong impact on overall ATP levels unless reserve capacity is reduced below that of the basal level. Utilizing whole cell ATP measurements, PJ34 treatment is sufficient to rescue global ATP to control levels in LN428/MPG cells despite incomplete resolution of the spare capacity defect (**Figure 17**). This indicates that either the rescue of glycolysis is sufficient to supply 100% of the global ATP or that loss of spare capacity does not result in mitochondrial ATP loss unless it drops below basal levels (as seen in the LN428/MPG cells after MNNG treatment). Using the subcellular ATP FRET probes there is no detectable ATP loss in any subcellular compartment in LN428/MPG cells treated with PJ34 prior to MNNG, suggesting the loss of reserve capacity but maintenance of basal oxidative phosphorylation is sufficient to maintain mitochondrial ATP levels at least above the k_d of the FRET probe.

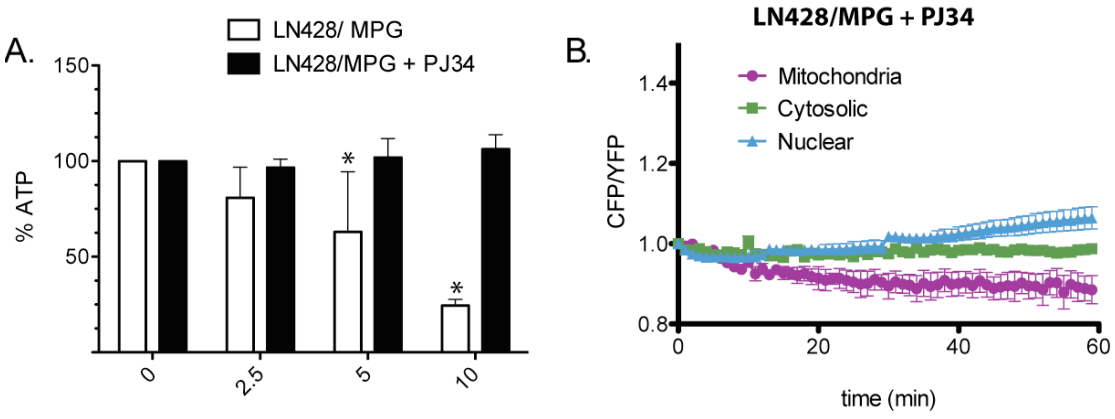

Figure 17. Incomplete rescue of mitochondrial reserve capacity does not affect ATP levels

(A) PARP inhibition rescues global ATP loss after MNNG. Global ATP was measured via ATPlite kit in LN428/MPG cells either treated with media control or 2 μM PJ34 for 30 minutes prior to treatment with either MNNG or PJ34 + MNNG for one hour. Data shown is the mean of three independent experiments ± S.E.

*Represents statistical significance with a $p < 0.05$ compared to 0 MNNG dose
(B) PARP inhibition reverses loss of ATP in all subcellular compartment. FRET ratio was calculated for FRET probes to mitochondrial, cytosolic or nuclear ATP. Cells were incubated with 2 μM PJ34 for 20 minutes prior to media change into imaging media containing PJ34. Images were acquired every minute. A ten-minute baseline measurement period was followed with treatment of MNNG to a final concentration of 5 μM . FRET traces shown are an average of 4-6 cells ± S.E.

This PARP mediated defect in mitochondrial capacity suggests an interesting separation of function between NAD^+ depletion dependent effects and PARP mediated effects. While a glycolytic block only occurs in the LN428/MPG cells with NAD^+ depletion, the loss of mitochondrial capacity, although to different extents, is present in both the LN428 and LN428/MPG cell lines. PARP inhibition can reverse the effect in both cell lines indicating that this loss of mitochondrial capacity is PARP mediated; however, LN428 cells do not exhibit NAD^+ loss at this dose or time point, suggesting a PARP or PAR driven mitochondrial defect independent of energetic depletion.

4.3 DISCUSSION

PARP1 plays a critical role in response to DNA damage events. In particular, PARP1 hyperactivation by DNA damage is a prominent factor in several human disease states, such as ischemic injury after stroke or myocardial infarction, traumatic brain injury, Parkinson's disease, meningitis and septic shock (56). In addition to its role in human disease, PARP1 hyperactivation is also of interest because of its involvement in the response to DNA damaging chemotherapeutics, such as the alkylating agent, TMZ. While PARP1 hyperactivation has been known to deplete cellular NAD^+ and ATP levels for many years, the exact mechanism of PARP hyperactivation induced cell death is still a matter of debate. We have previously shown that

BER failure results in cell death, not through PAR mediated AIF release, but through PARP mediated energetic failure (37). However, the details of energetic failure on a subcellular level are not known. Advances in technology have allowed us to analyze the spatiotemporal kinetics of PARP mediated energetic depletion in live cells and has provided information about the process that has not been uncovered in previous studies. These novel observations on the subcellular consequences of PARP hyperactivation and NAD^+ depletion not only further the field of BER inhibition and chemotherapy, but also have wide ranging implications in the above diseases where PARP activation plays a prominent role.

We have seen that PARP hyperactivation rapidly lowers global ATP levels within 30 minutes of MNNG treatment in glioblastoma cells that preferentially accumulate repair intermediates. Contrary to the popular hypothesis, this ATP depletion occurs in all subcellular ATP pools. It has been proposed that nuclear PARP activation results in cytosolic but not mitochondrial NAD^+ depletion, a block to glycolysis and only cytosolic but not mitochondrial ATP loss (48, 74). Therefore, these earlier studies would suggest that cells functioning by glycolysis, such as rapidly proliferating tumor cells, will be sensitive to PARP hyperactivation and cells utilizing oxidative phosphorylation will be resistant. The results of this study suggest that PARP hyperactivation is more complicated than suggested by this paradigm. Nuclear PARP activation results in rapid depletion of mitochondrial ATP followed closely by loss of ATP in the cytosol and nucleus. This is a novel observation, highlighting the importance of live cell subcellular measurements to provide information that is overlooked by more traditional techniques of measurement.

Utilizing live cell measurement of metabolic flux after DNA damage and PARP hyperactivation, we have been able to observe the previously reported PARP mediated glycolytic

block, but also a novel defect in mitochondria capacity. Without stress, oxygen consumption in MNNG treated and untreated cells is roughly the same after an hour; however, upon interrogation with metabolic inhibitors, it becomes clear that the MNNG treated cells have mitochondria that cannot respond to stress and lose reserve mitochondrial capacity. The control cells with only low levels of PARP activation after damage, due to reduced initiation of repair and low levels of repair intermediate accumulation, show a much milder defect in respiratory capacity incapable of changing subcellular or global ATP levels. An advantage to live cell determination of metabolic flux is the ability to modulate the system with drugs or via genetic manipulation, similar to those used in cytotoxicity assays. Cells treated with MNNG and PARP inhibitors, as analyzed with the Seahorse Extracellular Flux Analyzer, showed that both glycolytic and mitochondrial defects are PARP dependent. However, given the reduction of mitochondrial capacity in the LN428 cells, we have uncovered a novel PARP mediated but NAD^+ independent effect on mitochondrial capacity. The nature of this mitochondrial defect is yet to be discovered, but presents the possibility of PAR signaling to the mitochondria as reported by the Dawsons or a potential direct or indirect target of PARylation in the mitochondria (47). Some previous studies have indicated complex 1 dysfunction after PARP activation (134), and it would be interesting to determine which mitochondrial components are affected by PARP independent of NAD^+ depletion. One report has also shown PARylated proteins in the mitochondria after traumatic brain injury, although PARP1 is believed to be solely nuclear (135). The pattern and consequence of ADP ribosylation as a post translational modification is still very much a mystery, and understanding if these modifications can control mitochondrial function would be of critical interest in the field and might explain the significance of PARG expression in the mitochondria (136).

This study has uncovered a new level of information on the subcellular effects of PARP hyperactivaiton on metabolism and ATP pools. This data suggests that combination of metabolic inhibitors with treatments producing PARP hyperactivation, such as inhibition of BER along with TMZ, would enhance response. It also suggests that while PARP hyperactivation does affect oxidative phosphorylation, the overwhelming inhibition of glycolysis would make cells relying solely on glycolysis much more sensitive to alkylating agents than those able to use oxidative phosphorylation. While glioblastoma cells in culture seem capable of switching between energy producing sources, the hypoxic environment of the tumor may force them into glycolysis to support ATP levels, providing a level of selectivity for tumor cells over normal tissue.

Taken together this data shows subcellular and temporal resolution of PARP mediated ATP depletion. Real-time live cell techniques have uncovered the predicted glycolytic block induced by PARP hyperactivation and cytosolic ATP depletion. However, they have also uncovered a novel PARP mediated mitochondrial defect, which while more subtle than the block to glycolysis, occurs at much lower levels of PARP activation and appears to be PAR dose-dependent and independent of NAD^+ depletion. These studies have also uncovered an unpredicted rapid depletion of mitochondrial ATP. This has opened a new area of investigation into PARP mediated control of mitochondrial function through either PAR polymer signaling or ADP-ribosylation of target proteins.

5.0 OVERCOMING TEMOZOLOMIDE RESISTANCE IN GLIOBLASTOMA VIA DUAL INHIBITION OF NAD^+ BIOSYNTHESIS AND BASE EXCISION REPAIR

5.1 INTRODUCTION

Based on the previous two studies it has become apparent that BER and cellular energetics are linked through activation of the protein PARP. The mechanistic link between these two pathways opens the possibility for enhancement of BER failure through modulation of cellular energetic pathways. BER failure can be induced through treatment with chemical BER inhibitors in combination with TMZ (30, 69). This current study proposes to exploit the above mechanistic studies for the benefit of cancer patients by combining inhibition of NAD^+ biosynthesis with BER inhibition and TMZ in a proof of concept pre-clinical study.

Glioblastoma multiforme (GBM) is a devastating form of brain cancer with a dismal median survival time, a high level of resistance to current therapy and common recurrence after treatment (137). The current standard therapy for GBM includes maximum debulking surgery, radiation and treatment with the monofunctional alkylating agent temozolomide (TMZ), also referred to as Temodar® (2). Despite the current standard treatment regimen, including the addition of concomitant and adjuvant TMZ, the average survival expectancy is 14.6 months and the overall 5-year survival rate for GBM is 9.8% (8) 4). TMZ generates a spectrum of DNA lesions including O^6-methylguanine, N3-methyladenine and N7-methylguanine (**Table 1**) (61).

The O^6-methylguanine lesion is responsible for most of the TMZ associated toxicity and is a substrate for direct repair by O^6-methylguanine-DNA methyltransferase (MGMT) (138). In the absence of MGMT repair, O^6-methylguanine is suggested to initiate a futile cycle of mismatch repair (MMR) or alternately to trigger ataxia telangiectasia and Rad3 related protein kinase (ATR) activation through the action of several MMR proteins (15), leading to apoptosis and cell death (139-141). Much of the resistance to TMZ observed clinically is due to high expression of MGMT (and subsequent repair of the lesion) or loss of MMR (therefore preventing the initiation of apoptotic signalling) (3, 17, 18). Additionally, almost all patients eventually recur with the disease and the large majority of recurrent tumors are resistant to chemotherapy (19, 20). There are currently few alternate treatment options for patients with TMZ resistant tumors and adjuvant chemotherapy options are an area of intense research (137).

The N7-methylguanine and N3-methyladenine adducts make up the majority of the TMZ lesions and are base excision repair (BER) substrates. However, these DNA adducts elicit little toxicity under current therapeutic strategies due to rapid repair by BER (13, 142). Hence, small molecules targeting BER have become an attractive option for enhancing TMZ toxicity independent of the cytotoxicity related to the O^6-methylguanine DNA lesion. Repair of the alkylation induced DNA lesions N3-methyladenine and N7-methylguanine proceeds primarily through the short patch BER pathway (22). DNA polymerase ß (Polß) has been shown to be the rate-limiting step in BER and loss of Polß leads to increased sensitivity to the N3-methyladenine and N7-methylguanine lesions due to the accumulation of repair intermediates (13, 37, 83). Alternatively, blocking the abasic site formed during the BER process with the chemical inhibitor methoxyamine (MX) (also referred to as TRC102) has also been shown to enhance

alkylation sensitivity independently of the O^6-methylguanine lesion (30-32). Thus, strategic targeting of BER can enhance TMZ efficacy regardless of MGMT or MMR status.

We have recently reported that cell death due to incomplete BER is mediated through poly(ADP-ribose) polymerase (PARP) hyperactivation and subsequent NAD^+ and ATP depletion (37). The PARP1 (ARTD1) and PARP2 (ARTD2) proteins (143) act as sensors of incomplete BER and become hyperactivated, consuming NAD^+ as a substrate for poly(ADP-ribose) (PAR) synthesis (37). Consumption of NAD^+ after DNA damage leads to ATP depletion, likely due to continued resynthesis of NAD^+ as well as ongoing cellular utilization of NAD^+ and ATP for metabolic functions (45, 100). Many reports on DNA-damage induced PARP hyperactivation suggest cell death occurs via PAR signaling and apoptosis inducing factor (AIF) translocation from the mitochondria to the nucleus leading to nuclear fragmentation (42, 46). Interestingly, the caspase-independent cell death observed after incomplete BER is independent of AIF translocation or PAR catabolite signaling (37). Further, alkylation hypersensitivity observed after incomplete BER can be rescued by supplementation with the NAD^+ precursor NMN, supporting our conclusion that cell death after BER failure is an energy dependent phenotype (37).

Therefore, we hypothesized that dual targeting of the NAD^+ biosynthesis pathway and the BER pathway would greatly enhance TMZ sensitivity regardless of MGMT or MMR status. NAD^+ can be synthesized through the *de novo* pathway from L-tryptophan, but in most mammalian cells NAD^+ content is maintained through the NAD^+ salvage pathways (144). Nicotinamide phosphoribosyl transferase (NAMPT) controls the salvage-pathway rate-limiting step for the biosynthesis of NAD^+ from nicotinamide (145). The small molecule inhibitor FK866 is a specific inhibitor of NAMPT with activity in the low nanomolar range that is highly effective in reducing cellular NAD^+ levels (104). FK866 is currently in clinical trials (APO866) as a

monotherapy for the treatment of hematological cancers (146) and is reported to increase cell killing in combination with multiple cytotoxic agents (147). We report herein that combining FK866 with BER inhibition (using the small molecule BER inhibitor MX) potentiates TMZ tumor cell killing and strongly sensitizes glioma cells derived from chemotherapy resistant tumors.

5.2 RESULTS

PARP1 controls BER dependent PAR generation and cell death after alkylation exposure

There are multiple PARP family members (143), of which PARP1 (ARTD1) and PARP2 (ARTD2) have also been associated with the BER pathway (45, 49). To define the role of either PARP1 or PARP2 as the enzyme responsible for the increased generation of PAR after BER intermediate accumulation, stable PARP1 and PARP2 knockdown (KD) cell lines were generated via lentiviral shRNA expression in the LN428/MPG cells. PARP1-KD provides almost complete rescue of the MMS sensitivity and ATP depletion in the LN428/MPG/PARP1-KD cells (**Figure 18**) and reduces PAR levels as compared to the LN428/MPG cell line after 15 minutes of alkylation exposure as measured by quantitative PAR ELISA or immunoblotting for PAR (**Figure 19**). Whereas PARP2-KD had intermediate effects on rescue of cell survival and ATP levels (**Figure 18**).

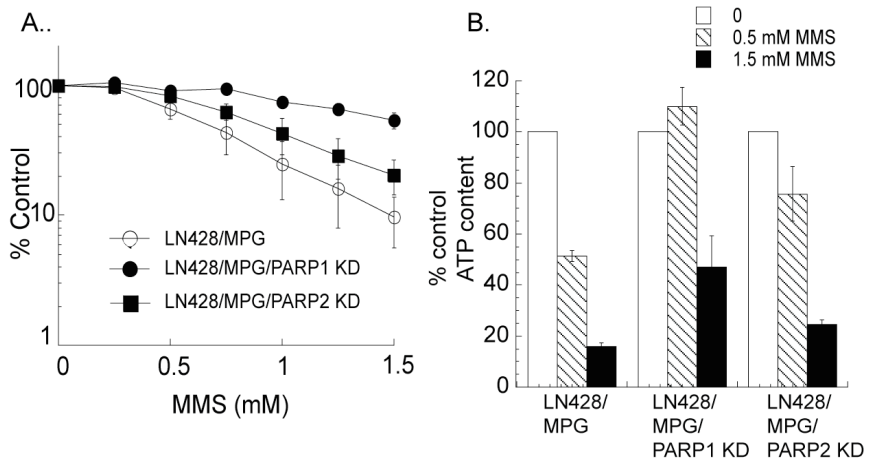

Figure 18. PARP1 and PARP2 knockdown effect on cell death and ATP

(A) Cell viability of LN428/MPG cells or LN428/MPG cells with stable knockdown of either PARP1 or PARP2 after 1 h MMS treatment, as measured by an MTS assay 48 hours after exposure. Plots show the % viable cells as compared to untreated (control) cells. Means are calculated from quadruplicate values in each experiment. Results indicate the mean ± S.E. of three independent experiments.
(B) ATP levels after 0.5 mM MMS (striped bars) or 1.5 mM MMS (black bars) in LN428/MPG, LN428/MPG/PARP1-KD and LN428/MPG/PARP2-KD cell lines.

Interestingly, PARP1-KD did not completely eliminate PAR generation, most likely representing PARP2-mediated PAR synthesis. Further, PARP1-KD had a significant effect on the kinetics of PAR catabolism, with the PAR signal remaining at the same level after 30 minutes exposure instead of the rapid PARG-mediated degradation observed in PARP1 proficient cells (**Figure 19**). This leaves open the question of whether PARP2 generated PAR has different properties and consequences compared to PAR chains generated by PARP1. Taken together, we suggest that the energy depletion-mediated cell death observed after incomplete BER (BER inhibition) is largely PARP1 mediated with only a small contribution by PARP2. Given our recent understanding that tumor cell death after BER inhibition is an energy depletion-mediated process, we sought to take advantage of this observation by targeting the intersecting pathways of BER and NAD^+ biosynthesis to enhance cell death in chemotherapy resistant tumors.

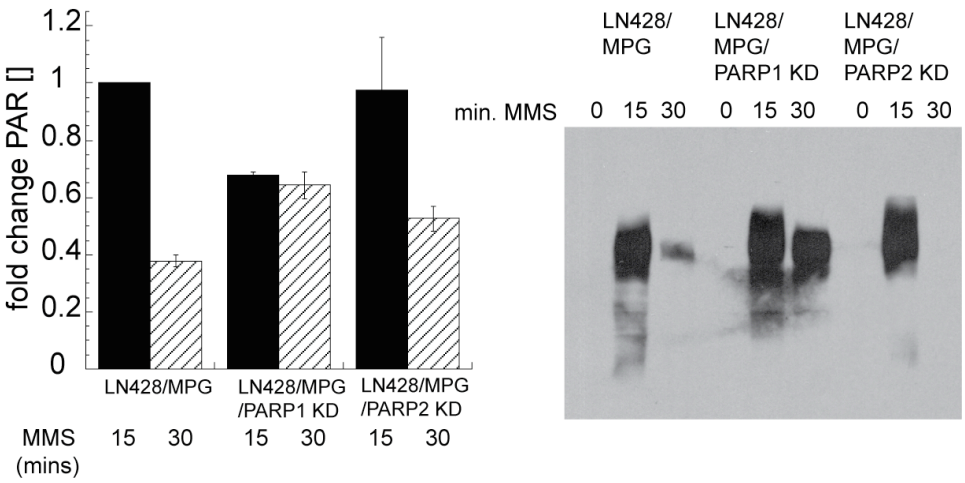

Figure 19. PARP1 and PARP2 knockdown effect on PAR generation

(A) Cells were depleted of PARP1 or PARP2 via shRNA. PAR generation in LN428/MPG, LN428/MPG/PARP1KD and LN428/MPG/PARP2KD cells is shown before or after MMS exposure (15 and 30 min.; 1.5 mM), as measured by quantitative ELISA (see Materials & Methods). All values are normalized to LN428/MPG signal at 15 min. exposure and reported as fold change PAR.
(B) Immunoblot analysis of PAR generation after 0, 15 and 30 minutes of MMS exposure at a dose of 0.5 mM in LN428/MPG, LN428/MPG/PARP1-KD and LN428/MPG/PARP2-KD cell lines. All samples were the same as utilized in the quantitative PAR ELISA. The blot shown is a representative blot (N=3).

Inhibition of NAD^+ biosynthesis enhances alkylation induced cell death after incomplete BER

Inhibition of NAD^+ biosynthesis (24 hours) with FK866 reduces cellular NAD^+ content to 25% of control levels in both parental and LN428/MPG tumor cells (**Figure 20A**). Consistent with previous reports in other cell types, this 24-hour window of NAD^+ biosynthesis inhibition is not toxic when evaluated using a short-term (48 hour) cell survival assay (**Figure 20B**), but does exhibit significant toxicity in all these cells after 72 hours of FK866 treatment independent of BER status (**Figure 20C**) (104, 147). The lack of toxicity after 24 hours of FK866 treatment is attributed to recovery of NAD^+ levels within 24 hours when cultured in normal media prior to assaying for cell survival (**Figure 20A**). Importantly, combining the non-toxic 24-hour window of NAD^+ depletion immediately followed by a minimally toxic dose of MMS (0.5 mM)

dramatically sensitized glioma cells in a BER dependent manner (**Figure 20D**). This effect was dependent on the dose of FK866.

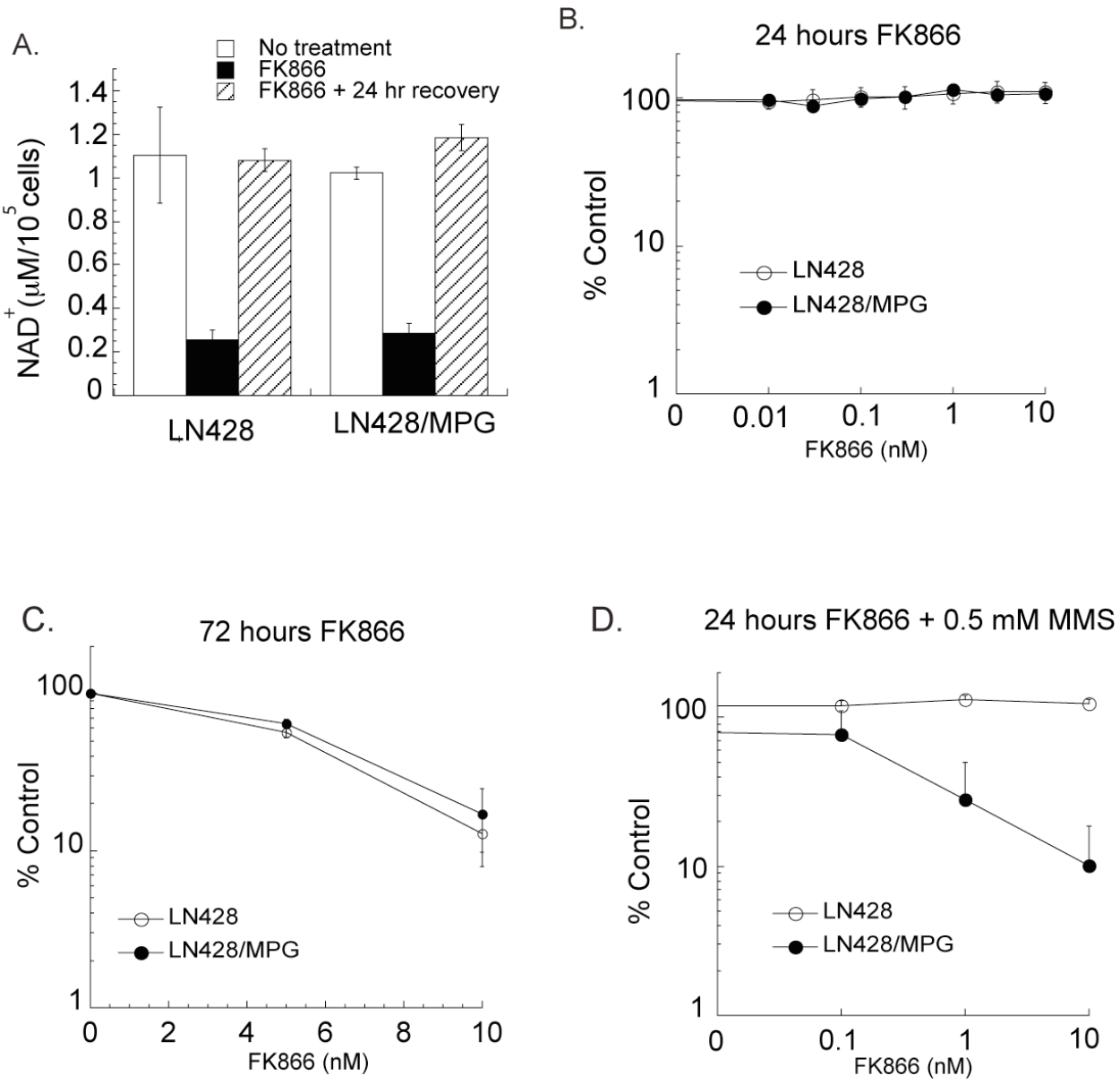

Figure 20. Inhibitor of NAD^+ biosynthesis FK866 enhances BER failure cell death

(A) Cellular NAD^+ levels in LN428 and LN428/MPG cells before exposure, after exposure to FK866 (10nM; 24 hrs) and following an additional 24 hours of recovery from FK866 treatment.
(B) Cytotoxicity profile of FK866. Viability of LN428 and LN428/MPG cells was measured by an MTS assay 48 hours after FK866 (24 hrs) treatment and reported as percentage relative to vehicle control treated cells (% Control).
(C) Cell survival assayed by MTS assay after prolonged exposure to FK866 in the LN428 (open circles) and LN428/MPG (closed circles) cell lines. Cells were treated with 10nM FK866 for 72 hours and cell survival was assayed after 48 hours of recovery.

(D) Cell viability after FK866-mediated NAD^+ depletion immediately followed by alkylation damage. LN428 and LN428/MPG cells were treated with FK866 (24 hours) at varying doses followed by 1 hour MMS treatment at 0.5 mM. Cells were allowed to recover in normal media for 48 hours prior to analysis for cell viability by the MTS assay.

Inhibition of NAD^+ biosynthesis potentiates cell death by alkylating agents after BER inhibition

To test our hypothesis that NAD^+ depletion would enhance BER inhibition-mediated cell death, we utilized methoxyamine (MX), a small molecule BER inhibitor that can potentiate alkylation damage-induced cell death (30-32) by covalently binding to the aldehydic form of the DNA abasic site formed after BER initiation (30). A 30 mM dose of MX (30 minute pre-treatment) and co-treatment with MMS potentiates cell death 10-fold, consistent with previous reports in colon and ovarian carcinomas (**Figure 21B; solid circle**) (30, 32). This potentiation is dependent on MPG expression, as the initiating DNA glycosylase is required for abasic site formation after alkylation damage (**Figure 21A; solid circle**). MX inhibition of BER, in combination with FK866 inhibition of NAD^+ biosynthesis, results in an IC_{50} for MMS of 150μM, a sensitizer enhancement ratio (SER) of 3.125. This also yields a 2-fold decrease in IC_{50} from either FK866 + MMS co-treatment or MX + MMS co-treatment (**Figure 21B**).

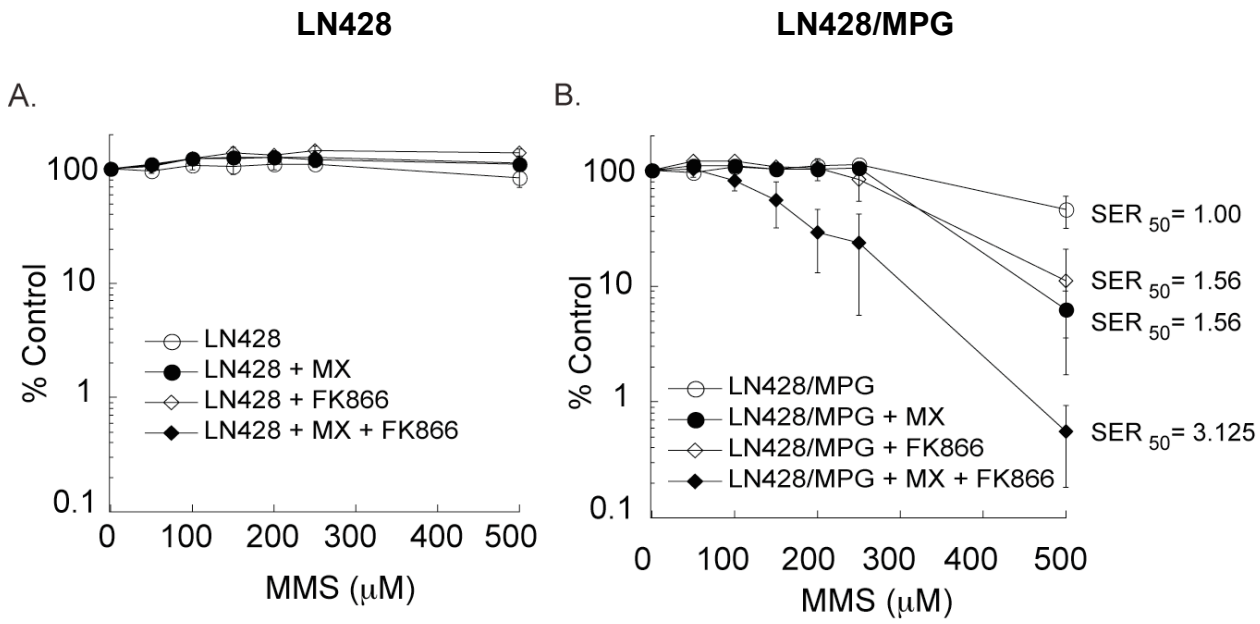

Figure 21. Dual inhibition of BER and NAD^+ biosynthesis enhances alkylation sensitivity

(A) Cell viability of LN428 cells measured by an MTS assay after treatment with MMS alone, MMS in combination with 30 mM MX, MMS in combination with 10nM FK866, or with the 3-drug combination of MX, FK866 and MMS. Drug treatments were carried out as described in the Materials and Methods section. Viable cells were determined and reported as percentage relative to vehicle control treated cells (% Control).
(B) Cell viability measured by MTS assay in the LN428/MPG cells after treatment with MMS alone, MMS in combination with 30 mM MX, MMS in combination with 10nM FK866, or with the 3-drug combination of MX, FK866 and MMS. Drug treatments were carried out as described in the Materials and Methods section. Viable cells were determined and reported as percentage relative to vehicle control treated cells (% Control). SER was calculated as IC_{50} TMZ/ IC_{50} TMZ + sensitizer.

Both FK866 and MX enhance ATP depletion after alkylation damage

To further investigate the enhanced cell death observed when MX and FK866 are combined with alkylating agents, cellular ATP levels were measured after combination treatment. As expected (37), FK866 pre-treatment prior to alkylation damage resulted in lower levels of ATP two hours after MMS treatment compared to alkylation damage alone (**Figure 22A**). However, 24 hours of NAD^+ depletion alone had no significant effect on ATP levels (**Figure 22A; striped bars**). Surprisingly, treatment with MX also induced loss of ATP beyond that observed by alkylation damage alone (**Figure 22B**). It is important to note that this enhanced ATP loss is only observed in the LN428/MPG cell line, supporting the notion that ATP loss after alkylation damage is

dependent on PARP hyperactivation (an event not seen in the LN428 cell line) (**Figure 3)**. This suggests that both inhibitors (FK866 and MX) enhance cell death when combined with alkylation by enhancing ATP loss in a BER and PARP dependent manner.

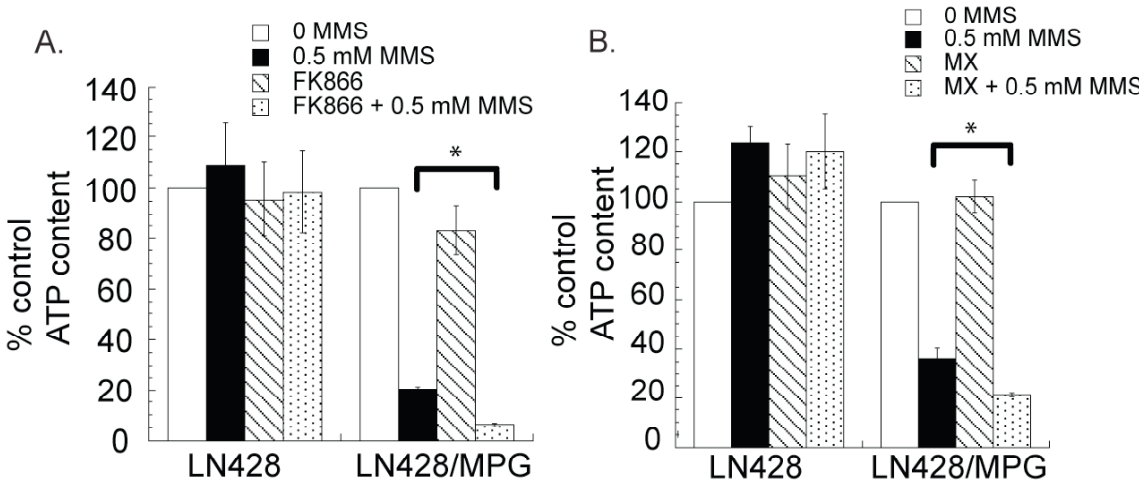

Figure 22. Effect of FK866 and methoxyamine on ATP depletion after alkylation

(A) Cellular ATP content two hours after 0.5mM MMS treatment (or media control) as measured by the ATP-lite luminescent kit. Results are reported as percent of untreated control. Cells were pre-treated for 24 hours with either 10nM FK866 or media control.
(B) Cellular ATP content two hours after 0.5mM MMS treatment (or media control) as measured by the ATP-lite luminescent kit. Results are reported as a percentage of untreated control. Cells were pre-treated for 30 minutes with MX or media control followed by co-treatment with MMS or media and post treatment as described in the Materials and Methods section.
*Represents statistical significance with a $p < 0.05$.

Dual inhibition of BER and NAD^+ biosynthesis sensitizes chemotherapy resistant glioma cells to TMZ

Given the strong potentiation of cell death with BER and NAD^+ biosynthesis inhibition combined with TMZ in a 48-hour cytotoxicity assay, we investigated whether this three-drug combination could sensitize glioma cells harbouring established TMZ-resistant genotypes. TMZ resistance can result from either over-expression of MGMT or loss of MMR (3, 17, 18). LN428 and LN428/MPG cells are both MMR positive and express low levels of MGMT. In a long-term

survival assay (allowing multiple rounds of replication required for O^6-methylguanine-mediated cell death), LN428 cells are highly sensitive to TMZ ($IC_{50} \approx 15\mu M$) (**Figure 23**).

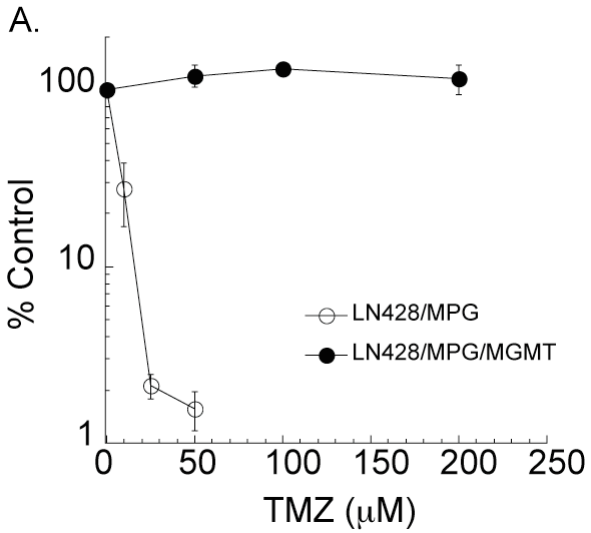

Figure 23. Sensitivity of LN428/MPG cells to TMZ in a long-term survival assay

(A) Cell survival determined by a long-term survival assay after increasing doses of TMZ in the LN428/MPG cell line (open circles) compared to the LN428/MPG/MGMT cell line (closed circles). Results indicate the mean ± S.E of three independent experiments.

To convert these cells to a TMZ-resistant phenotype, MGMT was stably over-expressed in the LN428/MPG cell line, resulting in resistance to TMZ in a long-term survival assay (**Figure 24A**). MX, in combination with TMZ, sensitizes MPG positive cells with an IC_{50} of 160 μM TMZ (**Table 3**); however, combining FK866 pre-treatment with MX and TMZ results in an IC_{50} of 17 μM, about a 10-fold decrease in IC_{50} and an sensitizer enhancement ratio (SER) value of 15.88 (**Figure 24A, Table 3**). Knockdown of the MMR proteins MSH6, MLH1 and MSH2 also renders LN428/MPG cells resistant to TMZ (**Figure 24B-D**). However, the dual inhibition of BER and NAD^+ biosynthesis can overcome the TMZ-resistance that results from MMR deficiency, yielding an increase in 75 μM TMZ response (**Figure 24B-D**).

Table 3. SER values of 3-drug combination in LN428/MPG/MGMT cell line

Treatment	IC_{50} (μM)	SER_{50}
TMZ	270	1
FK866 + TMZ	175	1.54
MX + TMZ	160	1.68
3-Drug combination	17	15.88

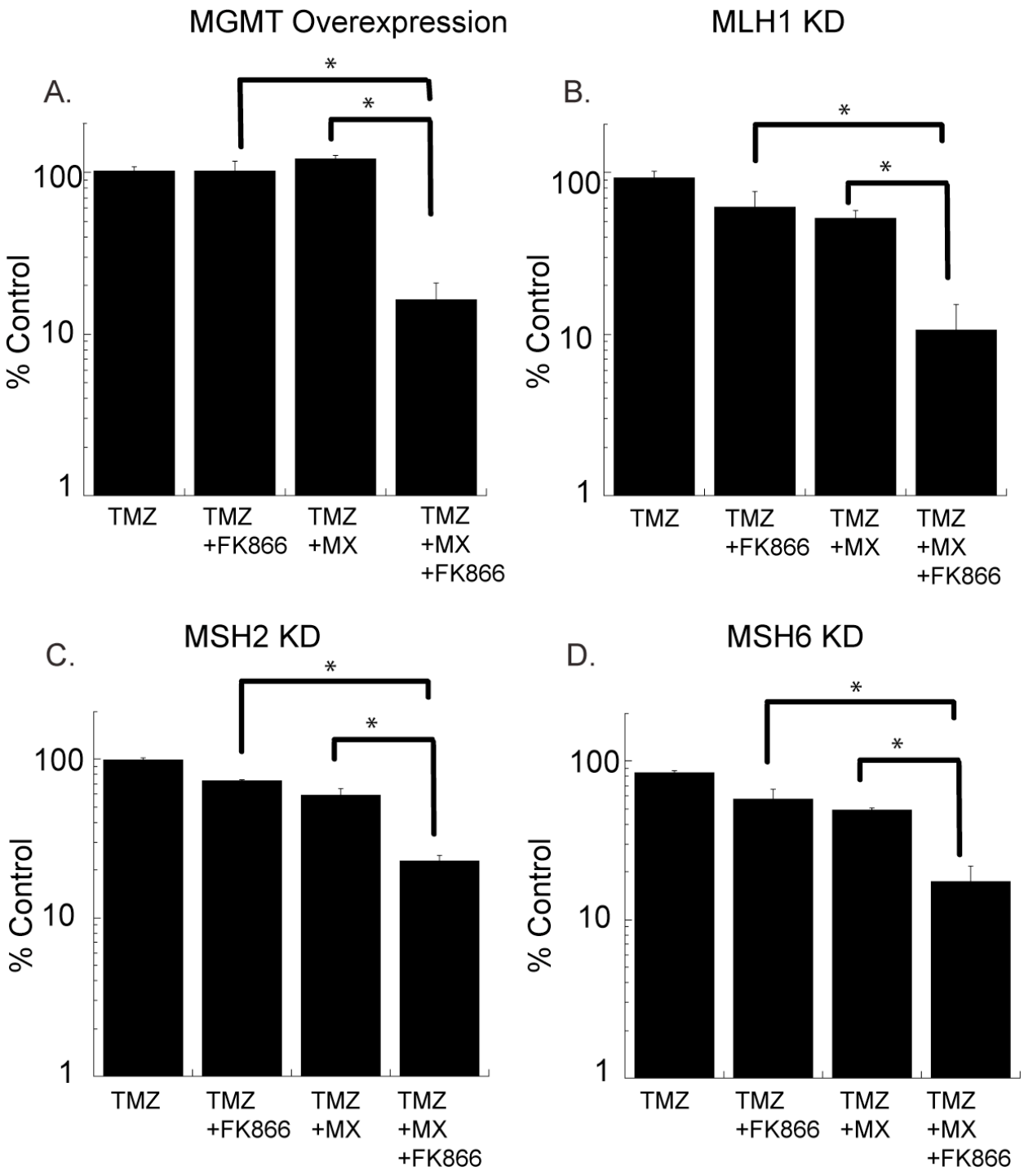

Figure 24. 3-drug combination in TMZ resistant LN428/MPG glioblastoma cells

(A) Cell survival determined by a long-term survival assay in cells modified to overexpress MGMT. LN428/MPG/MGMT cells were treated with either TMZ alone for 12 days, 24 hours of 10nM FK866 followed by 12 days of TMZ, a 30 minute pre-treatment of 10mM MX followed by MX (5mM) and TMZ co-treatment for 12 days, or the three-drug combination (a 24 hour pre-treatment of FK866, followed by a 30 minute pre-treatment with MX and a 12 day co-treatment with MX and TMZ. TMZ was used at a 75 μm dose.

(B-D) Cell survival determined by a long-term survival assay in cells stably expressing shRNA to MLH1 (B), MSH2 (C) or MSH6 (D). LN428/MPG MMR knockdown cells were treated with either TMZ alone for 12 days, 24 hours of 10nM FK866 followed by 12 days of TMZ, a 30 minute pre-treatment of 10mM MX followed by MX (5mM) and TMZ co-treatment for 12 days, or the three-drug combination (a 24 hour pre-treatment of FK866, followed by a 30 minute pre-treatment with MX and a 12 day co-treatment with MX and TMZ. TMZ was used at a 75 μm dose.
Results indicate the mean ± S.E of three independent experiments.
*Represents statistical significance with a $p < 0.05$.

To further investigate the utility of this drug combination in treating GBMs with endogenous or acquired resistance to TMZ, we utilized T98G cells, a glioma cell line with endogenous over-expression of MGMT (64) 38). T98G cells have robust expression of BER proteins as well as NAMPT and have approximately a 2-fold increase in the basal level of NAD^+ as compared to the LN428 and LN428/MPG cells (**Figure 25A**), requiring cell line specific titering of FK866 dosing. Twenty-four hour exposure to FK866 with doses up to 80nM had minimal effect on cell viability in a long-term survival assay (**Figure 25B**). FK866 enhances TMZ toxicity in a dose dependent manner (**Figure 25C**), whereas MX, in combination with TMZ, yields a slight enhancement of TMZ toxicity (**Figure 25D**). Most importantly, the combination of FK866 and MX in combination significantly enhanced cell death in an FK866 dose dependent manner beyond that of either combination alone (**Figure 25D**). All together, these results support our proposed strategy of dual BER and NAD^+ biosynthesis inhibition to overcome TMZ resistance in primary or recurrent TMZ-resistant GBM and provides proof of principle data to validate future analysis in an *in vivo* preclinical model.

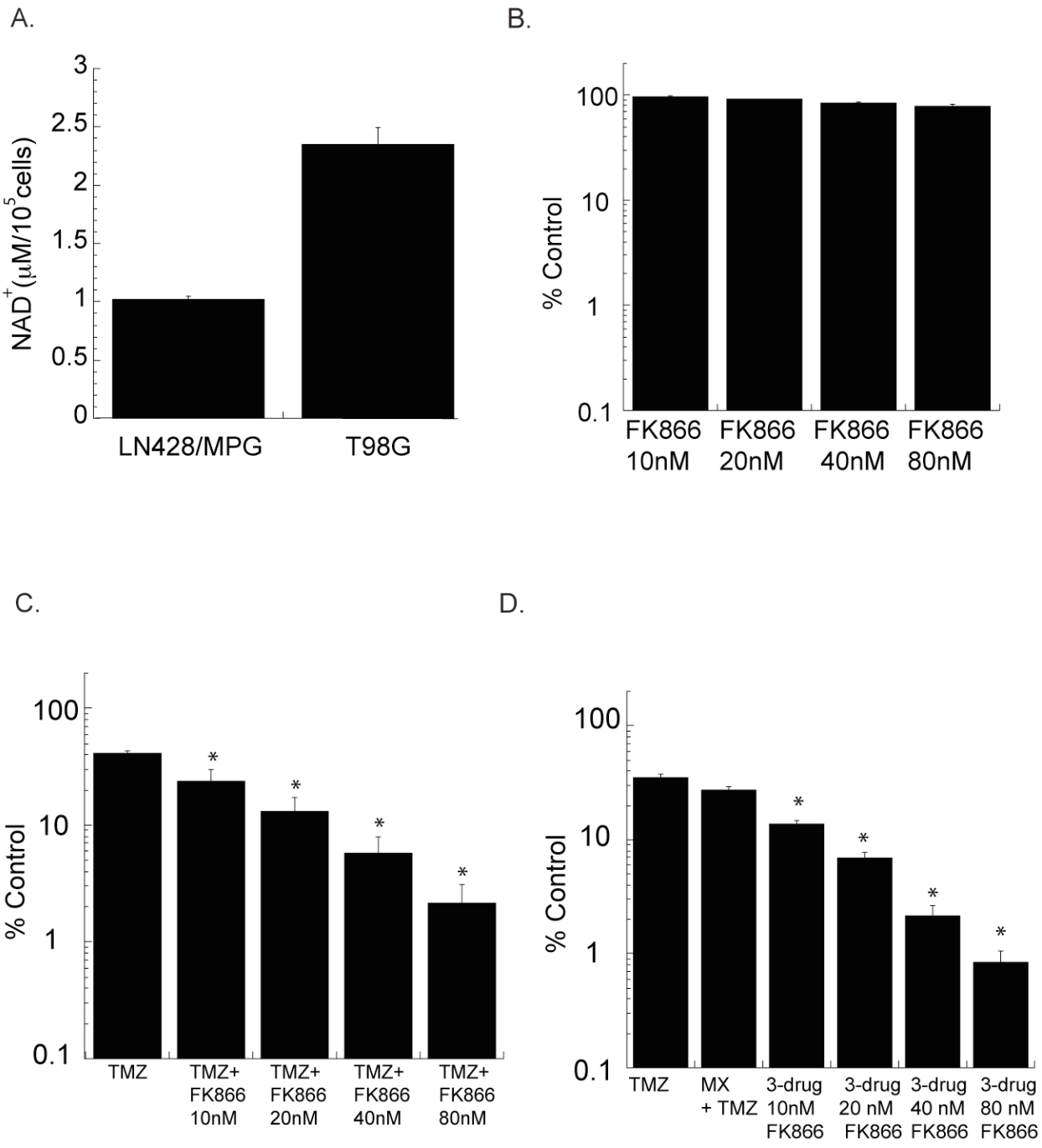

Figure 25. 3-drug combination effect on endogenously resistant T98G glioblastoma cells

(A) Basal NAD^+ content of the T98G cell line compared to basal NAD^+ content of the LN428/MPG cell line.
(B) Cell survival determined by a long-term survival assay in T98G cells after 24 hours of varying doses of FK866.
(C) Cell survival determined by a long-term survival assay in the T98G cells after a 24 hour pre-treatment with varying doses of FK866 followed by a 6 hour exposure to 500 μM TMZ.
(D) Cell survival determined by a long-term survival assay in T98G cells after treatment with either TMZ alone for 6 hours, a 30 minute pre-treatment with 10mM MX followed by 5mM MX and TMZ co-treatment for 6 hours, or the three-drug combination with varying doses of FK866 as a 24 hour pre-treatment followed by a 30 minute pre-

treatment with 10mM MX and a 6 hour co-treatment with 5mM MX and TMZ. A dose of 500μM TMZ was used in each treatment condition.
Results indicate the mean ± S.E of three independent experiments.
*Represents statistical significance with a $p < 0.05$ as compared to TMZ + MX.

5.3 DISCUSSION

This study presents a novel strategy to elicit tumor cell toxicity from the N3-methyladenine and N7-methylguanine lesions induced by TMZ by targeting two interacting pathways: the BER and NAD^+ biosynthesis pathways. The introduction of TMZ as a standard treatment for glioblastoma has resulted in a significant increase in response rate and median survival time over surgery and radiation therapy alone (4). However, 5-year survival rates still remain dismally low (8, 9), likely from inherent TMZ resistance and/or relapse with chemotherapy resistant tumors (19). Most of this resistance to TMZ is attributed to the loss of toxicity by the O^6-methylguanine lesion via elevated expression of MGMT or a defect in the MMR pathway (18). However, more than 80% of the DNA lesions produced by TMZ are BER substrates, suggesting BER modulation is a promising therapeutic option (11). The explosion of clinical trials involving TMZ combined with PARP inhibitors and ongoing clinical trials of TMZ combined with MX highlights this point (33, 60).

We have previously observed that inhibition of BER (via genetic modulation) combined with alkylation treatment leads to necrotic cell death resulting from PARP hyperactivation with concomitant NAD^+ and ATP depletion (37). Given this model, we sought to enhance TMZ response by inhibiting both BER and NAD^+ biosynthesis. This novel, combinatorial, 3-drug strategy realized a reduction of TMZ IC_{50} greater than ten fold in multiple models of TMZ resistant tumor cells as well as an endogenously resistant GBM cell line (T98G). The induction

of necrotic cell death as opposed to apoptotic cell death is a promising feature of this novel treatment combination, since a percentage of GBMs are also known to be resistant to apoptotic cell death (4), suggesting that this drug combination may be preferable over alternate chemotherapy options that induce apoptosis. While necrosis is primarily thought of as having a negative inflammatory impact on surrounding tissue, release of HMGB1 and other RAGE ligands after necrosis may aid in stimulation of the immune system and clearance of the tumor, thus potentially increasing the efficacy of this drug combination (43, 44).

MX, in combination with TMZ, is currently in Phase I clinical trials for the treatment of a variety of solid tumors and appears to be well tolerated (33). FK866 (known as APO866) is also currently in clinical trials as a monotherapy and is well tolerated (146). The concern in combining BER inhibition and NAD^+ biosynthesis inhibition is that the combination may critically lower energy levels and induce necrosis in healthy tissue. The high energy requirements and rapid NAD^+ turnover of tumor cells may allow for selectivity for the FK866/MX/TMZ drug combination over normal tissue (148). Further, it has been suggested that NAD^+ loss by PARP hyperactivation is cytotoxic by creating a glycolytic block (74, 149). Tumor selectivity may be realized from the reliance of glioblastomas on glycolysis for energy, whereas normal brain tissue exhibits higher levels of oxidative phosphorylation (150). Interestingly, in one report, up to 50% of GBMs tested were deficient in the NAPRT1-mediated NAD^+ biosynthesis pathway responsible for generating NAD^+ from nicotinic acid (NA) and in a separate report it was shown that NA supplementation can rescue the toxic effects of high dose FK866 on normal tissue (148, 151). This also suggests an opportunity for a synthetic lethal approach using our novel 3-drug combination, in which healthy tissue is supplemented with NA while selectively killing tumor cells unable to utilize the NAPRT1 arm of the pathway.

Targeted NAD^+ biosynthesis inhibition combined with BER inhibition plus TMZ gives a promising decrease in IC_{50} in resistant glioblastoma tumor cells. TMZ is also currently in clinical trials for the use with malignant melanoma, another chemotherapy resistant tumor with few treatment options (152). This drug combination may also prove to be useful in increasing efficacy of TMZ in melanoma and potentially in other tumor types that have shown little response to TMZ. For example, we have reported that genetic inhibition of BER in breast cancer cells shows similar sensitization, suggesting that this drug combination would also be useful for the treatment of triple-negative tumors (83). In conclusion, this study illustrates a novel therapeutic option for tumors resistant to the TMZ-induced O^6-methylguanine lesion, by utilizing clinically available chemical inhibitors of the interacting pathways of BER and NAD^+ biosynthesis.

6.0 CONCLUSION AND DISCUSSION

6.1 MECHANISMS OF BER FAILURE AND PARP HYPERACTIVATION

The previous chapters of this thesis have attempted to answer the question of how the inability to complete BER after alkylation damage results in hypersensitivity to alkylating agents and necrotic cell death. It had been previously shown by Sobol et. al. that Polß is the critical polymerase in repair of alkylation damage through BER and that functional loss of Polß through genetic means (and later through imbalance of the initiating glycosylase) results in alkylation hypersensitivity via accumulation of the 5'dRP BER intermediate (26, 38, 83). However, there has not been conclusive mechanistic data to determine how 5'dRP accumulation results in this cell death. We have previously determined that BER failure induced cell death is not apoptotic or autophagic (83). These studies confirm BER failure-induced cell death as necrotic. We have identified that the 5'dRP repair intermediate, if not removed by the lyase activity of Polß, leads to PARP hyperactiviation in response to failed repair and is causative of tumor cell death. Both PARP1 and PARP2 paralogues are implicated in response to DNA damage (41). These studies have confirmed that PARP1 is the primary PARP family member responsible for BER failure-induced cell death with a minor contribution by PARP2.

PARP hyperactivation in response to DNA damage has been shown to result in cell death through a number of mechanisms, and the exact mechanism of PARP-mediated cell death is still

hotly debated. We systematically tested all reported PARP mediated cell death pathways to determine which played a role in BER failure induced necrosis. Direct signaling of PAR polymers resulting in AIF release from the mitochondria to the nucleus as well as ADP ribose or AMP mediated cell death pathways were eliminated as possible BER failure modes of cell death. PARP utilizes NAD^+ as a substrate to generate PAR polymers and upon hyperactivation PAR levels can increase up to 500 fold, resulting in significant depletion of NAD^+, as previously observed by Berger et. al (41, 100, 101). After BER failure, NAD^+ and ATP levels are severely depleted within 2 hours. Supplementation of the cell culture media with NAD^+ precursors prior to treatment can rescue both alkylation-induced loss of ATP and cell viability. However, the long-term survival of these cells beyond the 48-hour assay time frame is unknown. It is possible that supplementation of NAD^+ levels simply delays cell death beyond 48 hours as opposed to complete rescue of cell viability. Regardless, the ability of NAD^+ precursor supplementation to enhance cell survival indicates that NAD^+ depletion plays a critical role in BER failure induced cell death and supports the results that other cell death signaling events are not significant in influencing necrosis.

While energetic depletion by PARP hyperactivation is a long standing observation, the detailed mechanism of how NAD^+ depletion by PARP induces ATP depletion and necrosis is largely unresolved. A prevailing hypothesis suggests that PARP mediated NAD^+ depletion occurs in the cytosol (48). Highly proliferating cells relying on glycolyisis to generate ATP can no longer utilize NAD^+ to generate ATP and therefore ATP is depleted in the cytoplasm, resulting in necrosis. Whereas non-replicating cells utilizing oxidative phosphorylation to generate ATP are less affected by NAD^+ depletion, mitochondrial ATP is not depleted and cells can undergo AIF release or apoptosis induced cell death (41). Our findings challenge this

hypothesis, at least in the context of glioblastomas, providing evidence that the glioblastoma cell lines we tested are capable of performing both oxidative phosphorylation and glycolysis and in fact are capable of up-regulating either process in the face of inhibition of the other. Importantly, we have shown that after BER failure and PARP hyperactivation, ATP is depleted from not only the cytosol, but is also rapidly depleted from the mitochondria several minutes sooner than from the cytosol or nucleus. Interestingly, not only is glycolytic function blocked by PARP hyperactivation, oxidative phosphorylation also shows a defect in oxidative capacity after an hour. Loss of capacity below the basal level of oxygen consumption seems to correlate with mitochondrial ATP loss, whereas less severe defects (seen in LN428 cells without PARP hyperactivation or in LN428/MPG cells treated with PARP inhibitor) do not influence mitochondrial or global ATP levels.

Taken together this data suggest that the while glycolysis is most strongly affected by PARP hyperactivation, oxidative phosphorylation is also affected and that the inability to produce ATP from either pathway leads to necrotic cell death. Our data in the tested glioblastoma cell lines suggest that inhibition of either pathway alone is not sufficient to deplete global ATP levels despite defects in subcellular ATP pools, and therefore rescue of either ATP producing pathway would result in cell survival after PARP hyperactivation. This has interesting implications in relation to the Warburg hypothesis (153). While glioblastoma cell lines may be metabolically flexible in culture, *in vivo* metabolism might be tilted towards glycolytic tumors and oxidative normal tissue. Tumor microenvironments are known to be hypoxic, preventing efficient oxidative phosphorylation, and *in vivo* glioblastomas perform a significant amount of glycolysis as indicated by their ability to be seen on a PET scan (154). Given that tumors *in vivo* may have impaired ability to perform oxidative phosphorylation, the stronger inhibitory effect of

PARP hyperactivation on glycolysis versus oxidative phosphorylation may provide a means of tumor selective killing.

The effect of PARP hyperactivation on mitochondrial capacity is especially interesting given that even very low levels PARP activation, as seen in cells not accumulating repair intermediates, results in a decrease in mitochondrial capacity but not basal levels of oxidative phosphorylation after treatment. Especially important is the observation that this PARP-mediated decrease in capacity is measurable even in the absence of significant NAD^+ depletion, suggesting a novel PARP dependent but NAD^+ independent defect in mitochondrial function. This defect seems to be PAR dose dependent, with high PAR levels resulting in a much more severe defect where, despite normal basal oxygen consumption, mitochondria appear to be unable to recover oxygen consumption ability after any stress (such as oligomycin injection) regardless of later uncoupling. Real-time measurement of metabolic function has shed a unique light on this process. Given that basal oxygen consumption is the same in treated and untreated cells regardless of PARP hyperactivation and mild decreases in capacity do not change ATP production, it is unlikely this phenomenon would have been observable using traditional metabolic measures.

How PARP is influencing mitochondrial function independently of NAD^+ or NADH reduction is still an open question. The possibility of alkylation damage to the mitochondria alone is ruled out by the rescue of the defect by PARP inhibition. Given the rapid appearance of the defect, within an hour of treatment, the potential of mitochondrial DNA damage resulting in mitochondrial protein dysfunction is unlikely. It is possible that PARP is PARylating a mitochondrial protein or a signaling protein upstream of mitochondrial function. Despite the well-established belief that PARP1 is solely nuclear, there have been reports of PARylated

proteins in the mitochondria after traumatic brain injury (135). Another potential scenario is that free PAR polymers themselves are resulting in a mitochondrial defect. The Dawson group has shown injection of long complex PAR polymers alone results in AIF translocation and cell death (42). However, given the lack of AIF translocation after BER failure, it is unclear if free PAR would still result in a mitochondrial defect. In line with our data, other groups have reported complex I dysfunction after PARP hyperactivation and reduced oxygen consumption in mouse cardiomyocytes after myocardial infarction (134), although it is not determined whether this is PARP dependent or NAD^+ dependent. Determining the cause of PARP mediated mitochondrial dysfunction could have important implications not only in cancer treatment but more importantly in the rescue of normal tissue either after chemotherapy or in conditions such as ischemia reperfusion, myocardial infarction or Parkinson's disease that result in PARP hyperactivation given the strong preference for oxidative phosphorylation in non-replicating cells such as neurons.

6.2 POTENTIAL ROLE OF AMPK IN BER FAILURE

One of the most intriguing and unexplained pieces of data to date in the lab is the observation that genetic manipulation resulting in BER failure (depletion of Polß or overexpression of MPG), does not always result in sensitivity to alkylating agents. This is observed in two pairs of cell lines in both the glioblastoma model cell lines and in breast cancer model cell lines. LN428 and MDA-MB-231 cells, with a functional Polß defect, are sensitive to alkylating agents via necrosis in a 48-hour toxicity assay (37, 83). T98G and MCF-7 cell lines, despite the same Polß defect, show no cell death in 48 hours (**Figure 25**). The most immediate hypothesis is a defect in PARP

activation in the latter cell lines; however, PAR generation in both T98G (data not shown) and MCF-7 (**Figure 26**) is strongly enhanced after alkylation treatment similar to the sensitive cell lines. This suggests a differential response to PARP hyperactivation on the level of cellular energetics.

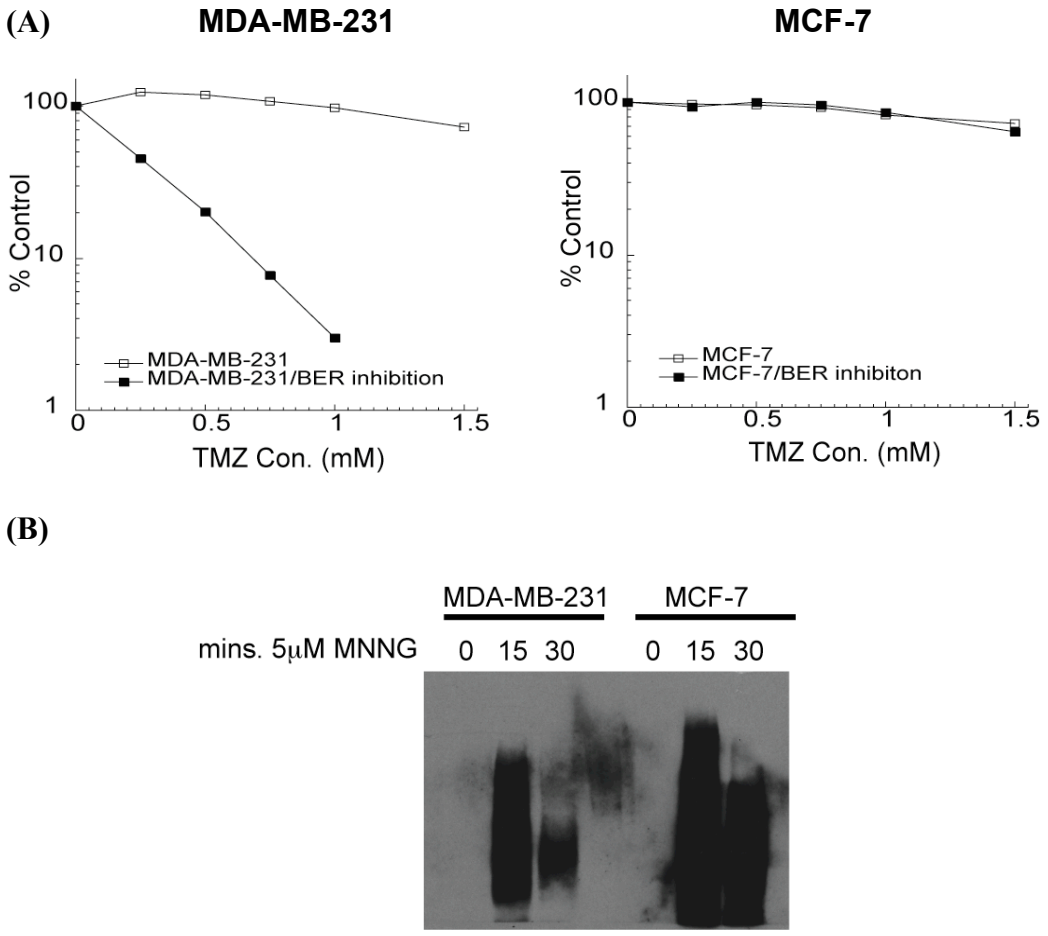

Figure 26. BER failure does not always result in sensitivity to alkylating agents

(A) Short term survival measured by MTS of MDA-MB-231 (left pane) and MCF-7 (right panel) breast cancer cells either proficient or deficient in Pol ß function.
*** Killing curve data courtesy of Dr. Ram Trivedi (MDA-MB-231 (83), MCF-7 unpublished)**
(B) Immunoblot of PAR in MDA-MB-231 and MCF-7 cells treated with 5μM MNNG for either 0, 15 or 30 minutes.

One possibility that could fit with the Warburg hypothesis (153) and Craig Thompson's report (74) is that sensitive cell lines are primarily glycolytic and therefore are more sensitive to the

PARP mediated glycolytic block, whereas resistant cell lines rely more on oxidative phosphorylation and hence survive. Previous data from our group and the Van Houten group showed no consistent trend in the amount of oxidative metabolism versus glycolysis in the two groups of sensitive versus resistant cell lines (data not shown).

Since there is no difference in basal metabolism, it is highly possible that the difference in sensitivity to PARP activation could be dependent on energetic signaling pathways. Of these, one of the most obvious possibilities is AMPK. In the presence of low ATP or elevated AMP, AMPK represses processes that utilize energy and initiates processes that restore or conserve ATP (155). Upon ATP depletion, AMP levels increase and bind to AMPK, inducing a conformational change that allows Thr-172 phosphorylation by upstream kinase LKB1 and activation of AMPK (156). There are reported differences in LKB1 status in MDA-MB-231 versus MCF-7 cells. MDA-MB-231 cells have a known LKB1 mutation resulting in non-functional LKB1, whereas MCF-7 are wild-type for LKB1 (157, 158). Overexpression of either wild-type LKB1 or dominant negative LKB1 in MDA-MB-231 cells was sufficient to reverse the BER failure induced alkylation hypersensitivity (**Figure 27**). So far this has only been shown in the breast cancer model system. While LN428 glioblastoma cells do not have a defect in LKB1 protein expression (data not shown), it is very possible that they have other defects either in upstream or downstream signaling pathways that would result in the same phenotype as seen in MDA-MB-231 cells. Showing that AMPK related defects in both tumor type model systems are responsible for sensitivity to alkylating agents would significantly strengthen the hypothesis that LKB1/AMPK regulate sensitivity to BER failure.

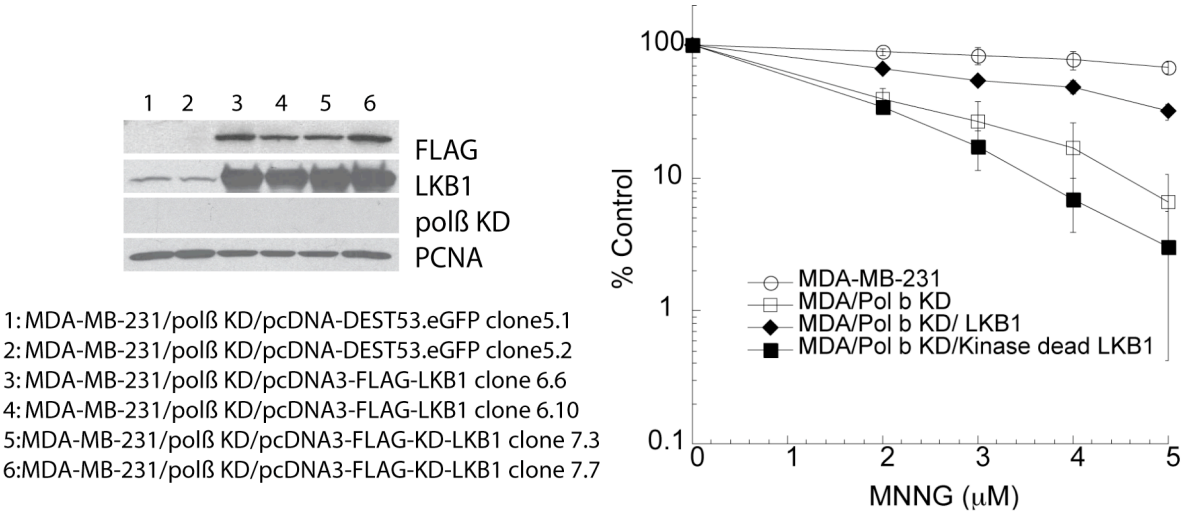

Figure 27. LKB1 expression can rescue BER failure induced MNNG sensitivity

Short term survival measured by MTS of MDA-MB-231 with either proficient or deficient BER and stable transfection of either LKB1 or LKB1 kinase dead mutant (right panel). Immunoblot of generated cell lines is shown in the left panel.
***Cell line generation and validation via immunoblot courtesy of Xiao-Hong Wang**

The mechanism behind LKB1 mediated survival of BER failure and necrotic cell death is unknown. It is also appears that LKB1 mediated survival is not maintained long term. T98G cells with BER defects or BER inhibition are sensitive to alkylating agents in the long term, and this cell death is enhanced by FK866 depletion of NAD^+. Whether LKB1 expression simply delays energetic collapse and necrosis beyond the 48-hour time point or whether it switches cells to an apoptotic mode of cell death after BER failure is unknown. Although it is yet to be confirmed whether AMPK is differentially activated between the two cell lines, there are two potential mechanisms for LKB1 mediated rescue or delay of BER failure induced necrosis based on the current literature: 1) induction of autophagy and energetic rescue or 2) modulation of energy producing pathways.

Mammalian target of rapamycin (mTOR) signaling promotes cell growth and proliferation processes and inhibits autophagy and other catabolic processes. AMPK suppresses

mTOR and results in activation of autophagy (159). Autophagy is an evolutionarily conserved process by which cellular contents and organelles are sequestered by double membrane vesicles, called autophagasomes, and delivered to the lysosome for degradation and recycling of cellular macromolecules (160). Autophagy is often activated in situations of energy starvation and can provide energy for the cell to survive by fatty acid oxidation or amino acid liberation (161). AMPK-mediated autophagy has been previously shown to rescue PARP activation induced cell death by hydrogen peroxide, reportedly through providing cell catabolites to rescue energy depletion by PARP (113,159). Although the initial papers reporting PARP mediated induction of autophagy have since been withdrawn, citing concerns on the validity of the data, another group has independently shown similar results with multiple DNA damaging agents, including alkylating agents (162). Very recently AMPK has also been shown to directly activate autophagy through phosphorylation of unc-51-like kinase 1 (ULK1) by both the Guan and Shaw groups (163, 164). Determining if autophagy induction is occurring and resulting in temporary or long-lived rescue of ATP loss in the BER failure resistant cells (MCF7 and T98G) would be of intense interest. This would link BER not only with cellular NAD^+ biosynthesis and metabolic pathways, but also with the autophagic pathway. Another interesting question is: if AMPK is indeed being activated by BER failure and PARP hyperactivation what is initiating this activation? While ATP depletion may explain activation of AMPK by changing ATP/AMP ratios, it is also possible that the breakdown of PAR itself creates the AMP needed to activate AMPK. PARG breakdown of PAR results in ADP-ribose, which can be further broken down by NUDIX enzymes to AMP and ribose 5-phosphate (165). The ability of PARG levels to dictate AMP levels after PARP hyperactivation would be a novel link between PARP and AMPK.

The other potential mechanism for LKB1 and AMPK rescue of BER failure is enhancement of energetic pathways through AMPK. AMPK is known to enhance mitochondrial biogenesis and capacity (155), although given the short time frame in which energetic depletion occurs after PARP hyperactivation, the likelihood of AMPK mediated up-regulation of mitochondria content through transcription factors is small. Resistant cell line models do not exhibit consistently higher levels of oxidative phosphorylation on the Seahorse extracellular flux analyzer, making a higher basal mitochondrial content less likely. There are some indications that LKB1 is upstream of induction of NAMPT (166, 167). NAMPT has been shown to be critical in controlling survival after PARP hyperactivation by both our group and others (130). It is interesting to speculate that cells lacking LKB1 may have lower NAMPT levels and therefore be more sensitive to BER failure induced energetic collapse compared to cells with intact LKB1 signaling.

Interestingly, recent papers have implicated PARP inhibition or knockdown of either PARP1 or PARP1 with the activation of SIRT1, potentially through increased levels of NAD^+ (168, 169). In fact SIR2 activity has been linked to NAD/NADH ratio (170). It is possible that PARP hyperactivation and reduction of NAD^+ could decrease SIRT family protein activity resulting in hyperacetylation of proteins. Pillai and colleagues have shown that SIRT3 (a mitochondrial protein) may be upstream of LKB1 and control down stream activation of AMPK. The role of SIRT family members in controlling sensitivity to BER failure would be timely and interesting research to pursue as a follow up to these studies. Potentially of the most interest would be the link between SIRT3 and complex 1 function (171). Reduction of NAD^+ resulting in a reduction of SIRT3 deacetylation of complex 1 and loss of complex 1 function could be a potential explanation for mitochondrial defects seen after PARP activation.

6.3 THERAPEUTIC IMPLICATIONS OF THIS WORK

The mechanistic data put forth in this thesis, explaining the mode of BER failure induced cell death and detailing the effects of PARP activation on metabolic processes has provided critical information on how targeting of the BER pathway in combination with alkylating agents may result in tumor cell death independent of O^6-methylguanine. It has also highlighted the usefulness of dual targeting strategies inhibiting both BER and cellular energetic pathways that control PARP-mediated necrosis. We have shown in cell culture glioblastoma models that inhibiting BER via methoxyamine and NAD^+ biosynthesis through FK866 can sensitize O^6-methylguanine resistant tumors irrespective of their mode of TMZ resistance.

Publication from Dr. Jiang-bo Tang in the Sobol laboratory has demonstrated that cytotoxicity by inhibition of BER by either MX or PARP inhibitors in combination with TMZ is enhanced by imbalanced BER (high levels of initiation and low levels of repair by Polß)(87). Despite MX trapping abasic sites prior to APE1 nuclease activity and subsequent Polß gap tailoring, Polß expression can decrease MX + TMZ induced toxicity. This suggests that the presence of Polß enhances repair and reduces residency of abasic sites for modulation by methoxyamine (87). MPG and Polß levels varied significantly among glioblastoma cell lines and glioblastoma tissue (87). MPG and Polß levels may be useful in predicting which tumors would best respond to BER failure induced by BER inhibition and TMZ combination treatment. In a similar manner high MPG and low Polß levels would also enhance dual targeting of BER and energetic pathways, as these are the tumors most likely to have high levels of PARP activation.

The use of methoxyamine also provides some interesting insights on the substrates of PARP. Genetic loss of Polß function results in generation of the 5'dRP repair intermediate that acts as a substrate for PARP resulting in PARP hyperactivation, a result confirmed by the rescue

of BER failure by WT-Polß but not K72A-Polß, the 5'dRP lyase dead mutant. Methoxyamine, however, inhibits BER several steps upstream of Polß function, at the formation of the abasic site by MPG. Unexpectedly, this inhibition also results in enhanced ATP depletion as compared to alkylation alone, suggesting enhanced PARP activation by MX trapped abasic sites. Immunoblots of PAR after MX + MMS versus MMS alone do not show a conclusive difference in PAR generation in LN428/MPG cells, although using quantitative analyses (PAR ELISA), this may now be able to be evaluated.

While MX is effective in enhancing BER inhibition induced ATP depletion and enhances cell death in combination with FK866, it may be that other BER inhibitors are better options for combination therapy. One important note is that inhibition of BER by PARP inhibitors would not be effective as a dual targeting strategy with FK866 or other inhibition of other energetic pathways given the dependence of energy depletion and BER failure induced necrosis on PARP activity. The ideal target for BER inhibition in this case would be Polß, enhancing the accumulation of the 5'dRP intermediate known to activate PARP. Generation of novel selective Polß inhibitors is an area of active research in the field (39). Of these inhibitors, those blocking Polß 5'dRP lyase activity would be of the most use in dual targeting strategies. Testing of a library of lead compounds for novel Polß 5'dRP lyase inhibitors is a project ongoing in the Sobol lab. Any potential Polß inhibitors found in this screen could be combined with FK866 and TMZ for a new dual targeting combination.

Clearly, the next step in testing the current dual targeting strategy combining TMZ, MX and FK866 or for testing future dual targeting combinations will be mouse xenograft models. While cell culture experiments indicate efficacy of the drug combination on tumor cells, they tell nothing of systemic effects (damage to rapidly proliferating tissue and bone marrow is of most

concern) or interaction with the tumor microenvironment. Although LN428 cells are not tumorogenic when injected, there are glioblastoma xenograft models that can be utilized to test the drug combination, either through subdermal implantation or stereotactic injection of tumor cells into the brain. Mouse studies showing efficacy of the drug combination in arresting glioblastoma tumor growth or showing tumor regression without unacceptable toxicity to normal tissue will be critical for moving the proof of principle experiments into the clinic.

Selective killing of tumor cells and sparing of normal tissue is a constant battle in the design of chemotherapeutic treatments. DNA damaging agents are used as chemotherapy based on the fact that tumor cells proliferate more rapidly than normal tissue, providing the first level of selectivity for the combination treatment. As previously mentioned, there appears to be a large variability in BER protein levels in tumor tissue that may enhance BER failure beyond that seen in normal tissue. The inherent differences in tumor metabolism versus normal tissue metabolism may provide a reasonable amount of tumor selectivity for the dual targeting therapy. Tumor cells have increased NAD^+ turnover due to rapid proliferation and altered metabolism, making them potentially more sensitive to NAD^+ depletion by PARP activation and FK866 (104). In fact this is the basis for the use of FK866 as a monotherapy now being tested in clinical trials against various cancers (146). The tendency of glioblastomas *in vivo* at least to rely more heavily on glycolysis may also enhance response to BER failure and energy depletion (172).

Another interesting possibility for tumor specificity with this treatment would be the potential for targeting Rb null cells. It has been shown the Rb null cells are more susceptible to DNA damage induced cell death mediated by PARP hyperactivation, due to loss of cell cycle checkpoints (173). Up to 50% of malignant gliomas have deletion of the Rb locus (1). In this case, Rb status could predict glioblastomas that may be more sensitive to dual targeting by BER

and NAD^+ biosynthesis inhibition due to checkpoint abnormalities. This genetic difference between tumor and normal tissue could give a greater therapeutic index in Rb null cells than in tumor cells without this defect.

There is however the possibility that dual targeting strategies of BER and NAD^+ biosynthesis in combination with TMZ will prove too toxic for normal tissue. In that case the dual targeting may be best suited for use in cases where it can be used to induce a synthetic lethal effect. In a recent report roughly 50% of glioblastomas tested had reduced levels of the NAD^+ biosynthetic enzyme NAPRT1 (148). The Sobol lab has independently begun to analyze NAPRT1 levels in both adult and pediatric glioblastoma tissue slides and is currently developing an antibody to NAPRT1 that can be utilized for immunohistochemistry and immunoblot analysis of cell lines and tumor tissue. NAMPT is required to catalyze the second to last step in NAD^+ biosynthesis from the nicotinamide salvage pathway catalyzing the production of NMN from nicotinamide, whereas NAPRT1 functions in an alternate route of NAD^+ synthesis by catalyzing the eventual production of NAD^+ from nicotinic acid independent from NAMPT activity (174). In this case it may be possible to supplement patients with nicotinic acid, also known as niacin and available in drug stores, in order to rescue NAD^+ levels in normal tissue but not tumor tissue during treatment with FK866, a BER inhibitor and TMZ. This strategy has been validated as able to rescue normal tissue from FK866 monotherapy (175).

A final note on the therapeutic potential of dual targeting is that this work demonstrates combination with NAD^+ biosynthesis inhibitors, such as FK866, should enhance any treatment that strongly induces PARP hyperactivation. It has recently been shown that cisplatin treatment can result in PARP hyperactivation (127). It will be interesting moving forward to see if FK866 or other metabolic inhibitors will enhance cisplatin treatment. While cisplatin is not generally

used for the treatment of glioblastoma, it is used as treatment for many other cancers such as bladder, ovarian and testicular cancers (176).

6.4 SUMMARY

In summary, this study has shown a mechanistic link between cellular energetic pathways and the BER pathway. Over 80% of the lesions generated by TMZ are BER substrates that elicit little toxicity in tumors due to robust BER repair. Given the large percentage of glioblastomas that are resistant to O^6-methylguanine mediated cell death, finding ways to enhance cell death from the BER substrates N7-methylguanine and N3-methyladenine is of great importance in advancing glioblastoma treatment. We have linked inability to complete BER (BER failure) with activation of PARP and consumption of NAD^+. Further we have shown that PARP hyperactivation depletes not only global ATP levels, but also mitochondrial, nuclear and cytosolic ATP pools. We have linked this loss of subcellular ATP with inhibition of glycolysis and disruption of mitochondrial capacity. Using the mechanistic insights gained we have established that BER inhibition induced necrosis can be enhanced by addition of inhibition of the energetic pathways that interact with it. NAD^+ biosynthesis inhibition by FK866 enhanced BER failure induced cell death by combining MX-induced BER inhibition with the alkylating agent TMZ. This dual targeting of pathways combined with alkylating agents overcame chemotherapy resistant glioblastoma cell survival regardless of their mode of O^6-methylguanine resistance, providing proof of concept for further pre-clinical and clinical studies.

BIBLIOGRAPHY

1. Wen PY, Kesari S. Malignant gliomas in adults. N Engl J Med 2008;359(5):492-507.
2. Friedman HS, Kerby T, Calvert H. Temozolomide and treatment of malignant glioma. Clinical Cancer Research 2000;6(7):2585-97.
3. Pollack IF, Hamilton RL, Sobol RW*, et al.* MGMT Expression Strongly Correlates with Outcome in Childhood Malignant Gliomas: Results from the CCG-945 Cohort. J Clin Oncol 2006;24(21):3431-7.
4. Krakstad C, Chekenya M. Survival signalling and apoptosis resistance in glioblastomas: opportunities for targeted therapeutics. Mol Cancer 2010;9:135.
5. Yan H, Parsons DW, Jin G*, et al.* IDH1 and IDH2 mutations in gliomas. N Engl J Med 2009;360(8):765-73.
6. Parsons DW, Jones S, Zhang X*, et al.* An integrated genomic analysis of human glioblastoma multiforme. Science 2008;321(5897):1807-12.
7. Prensner JR, Chinnaiyan AM. Metabolism unhinged: IDH mutations in cancer. Nat Med 2011;17(3):291-3.
8. Stupp R, Mason WP, van den Bent MJ*, et al.* Radiotherapy plus concomitant and adjuvant temozolomide for glioblastoma. New England Journal of Medicine 2005;352(10):987-96.
9. Stupp R, Hegi ME, Mason WP*, et al.* Effects of radiotherapy with concomitant and adjuvant temozolomide versus radiotherapy alone on survival in glioblastoma in a randomised phase III study: 5-year analysis of the EORTC-NCIC trial. Lancet Oncol 2009;10(5):459-66.
10. Yung WK, Albright RE, Olson J*, et al.* A phase II study of temozolomide vs. procarbazine in patients with glioblastoma multiforme at first relapse. Br J Cancer 2000;83(5):588-93.
11. Marchesi F, Turriziani M, Tortorelli G, Avvisati G, Torino F, De Vecchis L. Triazene compounds: mechanism of action and related DNA repair systems. Pharmacol Res 2007;56(4):275-87.
12. Beranek DT. Distribution of methyl and ethyl adducts following alkylation with monofunctional alkylating agents. Mutation Research 1990;231(1):11-30.
13. Trivedi RN, Almeida KH, Fornsaglio JL, Schamus S, Sobol RW. The Role of Base Excision Repair in the Sensitivity and Resistance to Temozolomide Mediated Cell Death. Cancer Res 2005;65(14):6394-400.
14. Horton JK, Wilson SH. Hypersensitivity phenotypes associated with genetic and synthetic inhibitor-induced base excision repair deficiency. DNA Repair (Amst) 2007;6(4):530-43.

15. Wang JY, Edelmann W. Mismatch repair proteins as sensors of alkylation DNA damage. Cancer Cell 2006;9(6):417-8.
16. Fishel R. Signaling mismatch repair in cancer. Nature medicine 1999;5(11):1239-41.
17. Hegi ME, Liu L, Herman JG*, et al.* Correlation of O6-methylguanine methyltransferase (MGMT) promoter methylation with clinical outcomes in glioblastoma and clinical strategies to modulate MGMT activity. J Clin Oncol 2008;26(25):4189-99.
18. Sarkaria JN, Kitange GJ, James CD*, et al.* Mechanisms of chemoresistance to alkylating agents in malignant glioma. Clin Cancer Res 2008;14(10):2900-8.
19. Cahill DP, Levine KK, Betensky RA*, et al.* Loss of the mismatch repair protein MSH6 in human glioblastomas is associated with tumor progression during temozolomide treatment. Clin Cancer Res 2007;13(7):2038-45.
20. Yip S, Miao J, Cahill DP*, et al.* MSH6 mutations arise in glioblastomas during temozolomide therapy and mediate temozolomide resistance. Clin Cancer Res 2009;15(14):4622-9.
21. Zhang J, Stevens MF, Laughton CA, Madhusudan S, Bradshaw TD. Acquired resistance to temozolomide in glioma cell lines: molecular mechanisms and potential translational applications. Oncology 2010;78(2):103-14.
22. Almeida KH, Sobol RW. A unified view of base excision repair: lesion-dependent protein complexes regulated by post-translational modification. DNA Repair 2007;6(6):695-711.
23. Hendershot JM, Wolfe AE, O'Brien PJ. Substitution of active site tyrosines with tryptophan alters the free energy for nucleotide flipping by human alkyladenine DNA glycosylase. Biochemistry;50(11):1864-74.
24. El-Khamisy SF, Masutani M, Suzuki H, Caldecott KW. A requirement for PARP-1 for the assembly or stability of XRCC1 nuclear foci at sites of oxidative DNA damage. Nucleic Acids Research 2003;31(19):5526-33.
25. Yamtich J, Sweasy JB. DNA polymerase family X: function, structure, and cellular roles. Biochim Biophys Acta 2009;1804(5):1136-50.
26. Sobol RW, Prasad R, Evenski A*, et al.* The lyase activity of the DNA repair protein ß-polymerase protects from DNA-damage-induced cytotoxicity. Nature 2000;405(6788):807-10.
27. Sobol RW. DNA polymerase ß null mouse embryonic fibroblasts harbor a homozygous null mutation in DNA polymerase iota. DNA Repair (Amst) 2007;6(1):3-7.
28. Luo M, Kelley MR. Inhibition of the human apurinic/apyrimidinic endonuclease (APE1) repair activity and sensitization of breast cancer cells to DNA alkylating agents with lucanthone. Anticancer Res 2004;24(4):2127-34.
29. Madhusudan S, Smart F, Shrimpton P*, et al.* Isolation of a small molecule inhibitor of DNA base excision repair. Nucleic Acids Res 2005;33(15):4711-24.
30. Liu L, Taverna P, Whitacre CM, Chatterjee S, Gerson SL. Pharmacologic disruption of base excision repair sensitizes mismatch repair-deficient and -proficient colon cancer cells to methylating agents. Clinical Cancer Research 1999;5(10):2908-17.
31. Taverna P, Liu L, Hwang HS, Hanson AJ, Kinsella TJ, Gerson SL. Methoxyamine potentiates DNA single strand breaks and double strand breaks induced by temozolomide in colon cancer cells. Mutat Res 2001;485(4):269-81.
32. Fishel ML, He Y, Smith ML, Kelley MR. Manipulation of base excision repair to sensitize ovarian cancer cells to alkylating agent temozolomide. Clin Cancer Res 2007;13(1):260-7.

33. Sawides P, Xu Y, Liu L, *et al.* Pharmacokinetic profile of the base-excision repair inhibitor methoxyamine-HCl (TRC102; MX) given as an one-hour intravenous infusion with temozolomide (TMZ) in the first-in-human phase I clinical trial. In: Oncology ASoC, editor 2010 ASCO Annual Meeting; 2010: Journal of Clinical Oncology 2010:p. e13662.
34. Beard WA, Wilson SH. Structure and mechanism of DNA polymerase Beta. Chem Rev 2006;106(2):361-82.
35. Abbotts J, SenGupta DN, Zmudzka B, Widen SG, Notario V, Wilson SH. Expression of human DNA polymerase beta in Escherichia coli and characterization of the recombinant enzyme. Biochemistry 1988;27(3):901-9.
36. Sobol RW, Horton JK, Kuhn R, *et al.* Requirement of mammalian DNA polymerase-ß in base-excision repair. Nature 1996;379(6561):183-6.
37. Tang J, Goellner EM, Wang XW, *et al.* Bioenergetic Metabolites Regulate Base Excision Repair-Dependent Cell Death in Response to DNA Damage. Molecular Cancer Research 2010;8(1):67-79.
38. Sobol RW, Kartalou M, Almeida KH, *et al.* Base Excision Repair Intermediates Induce p53-independent Cytotoxic and Genotoxic Responses. J Biol Chem 2003;278(41):39951-9.
39. Goellner EM, Svilar D, Almeida KH, Sobol R. Targeting DNA Polymerase ß for Therapeutic Intervention. Current Molecular Pharmacology 2012 (in press).
40. Hu HY, Horton JK, Gryk MR, *et al.* Identification of small molecule synthetic inhibitors of DNA polymerase beta by NMR chemical shift mapping. The Journal of biological chemistry 2004;279(38):39736-44.
41. Woodhouse BC, Dianov GL. Poly ADP-ribose polymerase-1: An international molecule of mystery. DNA Repair (Amst) 2008;7(7):1077-86.
42. Andrabi SA, Kim NS, Yu SW, *et al.* Poly(ADP-ribose) (PAR) polymer is a death signal. Proc Natl Acad Sci U S A 2006;103(48):18308-13.
43. Okano S, Lan L, Caldecott KW, Mori T, Yasui A. Spatial and temporal cellular responses to single-strand breaks in human cells. Mol Cell Biol 2003;23(11):3974-81.
44. de Murcia JM, Niedergang C, Trucco C, *et al.* Requirement of poly(ADP-ribose) polymerase in recovery from DNA damage in mice and in cells. Proc Natl Acad Sci U S A 1997;94(14):7303-7.
45. Hassa PO, Haenni SS, Elser M, Hottiger MO. Nuclear ADP-ribosylation reactions in mammalian cells: where are we today and where are we going? Microbiol Mol Biol Rev 2006;70(3):789-829.
46. Yu SW, Wang H, Poitras MF, *et al.* Mediation of poly(ADP-ribose) polymerase-1-dependent cell death by apoptosis-inducing factor. Science 2002;297(5579):259-63.
47. Andrabi SA, Dawson TM, Dawson VL. Mitochondrial and nuclear cross talk in cell death: parthanatos. Ann N Y Acad Sci 2008;1147:233-41.
48. Ying W, Alano CC, Garnier P, Swanson RA. NAD+ as a metabolic link between DNA damage and cell death. Journal of neuroscience research 2005;79(1-2):216-23.
49. Ame JC, Rolli V, Schreiber V, *et al.* PARP-2, A novel mammalian DNA damage-dependent poly(ADP-ribose) polymerase. J Biol Chem 1999;274(25):17860-8.
50. Schreiber V, Ame JC, Dolle P, *et al.* Poly(ADP-ribose) polymerase-2 (PARP-2) is required for efficient base excision DNA repair in association with PARP-1 and XRCC1. J Biol Chem 2002;277(25):23028-36.
51. Rulten SL, Fisher AE, Robert I, *et al.* PARP-3 and APLF function together to accelerate nonhomologous end-joining. Mol Cell 2011;41(1):33-45.

52. Boehler C, Gauthier LR, Mortusewicz O*, et al.* Poly(ADP-ribose) polymerase 3 (PARP3), a newcomer in cellular response to DNA damage and mitotic progression. Proc Natl Acad Sci U S A 2011;108(7):2783-8.
53. Keil C, Grobe T, Oei SL. MNNG-induced cell death is controlled by interactions between PARP-1, poly(ADP-ribose) glycohydrolase, and XRCC1. J Biol Chem 2006;281(45):34394-405.
54. Loseva O, Jemth AS, Bryant HE*, et al.* PARP-3 is a mono-ADP-ribosylase that activates PARP-1 in the absence of DNA. J Biol Chem 2010;285(11):8054-60.
55. Koh DW, Dawson TM, Dawson VL. Poly(ADP-ribosyl)ation regulation of life and death in the nervous system. Cell Mol Life Sci 2005;62(7-8):760-8.
56. Jagtap P, Szabo C. Poly(ADP-ribose) polymerase and the therapeutic effects of its inhibitors. Nat Rev Drug Discov 2005;4(5):421-40.
57. Lord CJ, Ashworth A. Targeted therapy for cancer using PARP inhibitors. Curr Opin Pharmacol 2008;8(4):363-9.
58. Farmer H, McCabe N, Lord CJ*, et al.* Targeting the DNA repair defect in BRCA mutant cells as a therapeutic strategy. Nature 2005;434(7035):917-21.
59. Bryant HE, Schultz N, Thomas HD*, et al.* Specific killing of BRCA2-deficient tumours with inhibitors of poly(ADP-ribose) polymerase. Nature 2005;434(7035):913-7.
60. Palma JP, Wang YC, Rodriguez LE*, et al.* ABT-888 Confers Broad In vivo Activity in Combination with Temozolomide in Diverse Tumors. Clin Cancer Res 2009.
61. Sobol RW. Temozolomide. In: Schwab M, editor. Encyclopedia of Cancer. 2nd ed. Berlin, Heidelberg, New York: Springer; 2009.
62. Park MJ, Kim MS, Park IC*, et al.* PTEN suppresses hyaluronic acid-induced matrix metalloproteinase-9 expression in U87MG glioblastoma cells through focal adhesion kinase dephosphorylation. Cancer Res 2002;62(21):6318-22.
63. Ishii N, Maier D, Merlo A*, et al.* Frequent co-alterations of TP53, p16/CDKN2A, p14ARF, PTEN tumor suppressor genes in human glioma cell lines. Brain Pathol 1999;9(3):469-79.
64. Stein GH. T98G: an anchorage-independent human tumor cell line that exhibits stationary phase G1 arrest in vitro. Journal of cellular physiology 1979;99(1):43-54.
65. Imamura H, Nhat KP, Togawa H*, et al.* Visualization of ATP levels inside single living cells with fluorescence resonance energy transfer-based genetically encoded indicators. Proc Natl Acad Sci U S A 2009;106(37):15651-6.
66. Ashworth A. A synthetic lethal therapeutic approach: poly(ADP) ribose polymerase inhibitors for the treatment of cancers deficient in DNA double-strand break repair. J Clin Oncol 2008;26(22):3785-90.
67. Paik J, Duncan T, Lindahl T, Sedgwick B. Sensitization of human carcinoma cells to alkylating agents by small interfering RNA suppression of 3-alkyladenine-DNA glycosylase. Cancer Res 2005;65(22):10472-7.
68. Sobol RW, Watson DE, Nakamura J*, et al.* Mutations associated with base excision repair deficiency and methylation-induced genotoxic stress. Proceedings of the National Academy of Science 2002;99(10):6860-5.
69. Liu L, Gerson SL. Therapeutic impact of methoxyamine: blocking repair of abasic sites in the base excision repair pathway. Current Opinion in Investigative Drugs 2004;5(6):623-7.
70. Palma JP, Rodriguez LE, Bontcheva-Diaz VD*, et al.* The PARP inhibitor, ABT-888 potentiates temozolomide: correlation with drug levels and reduction in PARP activity in vivo. Anticancer Res 2008;28(5A):2625-35.

71. Liu X, Shi Y, Guan R, *et al.* Potentiation of temozolomide cytotoxicity by poly(ADP)ribose polymerase inhibitor ABT-888 requires a conversion of single-stranded DNA damages to double-stranded DNA breaks. Mol Cancer Res 2008;6(10):1621-9.
72. Peralta-Leal A, Rodriguez MI, Oliver FJ. Poly(ADP-ribose)polymerase-1 (PARP-1) in carcinogenesis: potential role of PARP inhibitors in cancer treatment. Clin Transl Oncol 2008;10(6):318-23.
73. Stegh AH, Chin L, Louis DN, DePinho RA. What drives intense apoptosis resistance and propensity for necrosis in glioblastoma? A role for Bcl2L12 as a multifunctional cell death regulator. Cell Cycle 2008;7(18):2833-9.
74. Zong WX, Ditsworth D, Bauer DE, Wang ZQ, Thompson CB. Alkylating DNA damage stimulates a regulated form of necrotic cell death. Genes & Development 2004;18(11):1272-82.
75. Cohausz O, Blenn C, Malanga M, Althaus FR. The roles of poly(ADP-ribose)-metabolizing enzymes in alkylation-induced cell death. Cell Mol Life Sci 2008;65(4):644-55.
76. Kolthur-Seetharam U, Dantzer F, McBurney MW, de Murcia G, Sassone-Corsi P. Control of AIF-mediated cell death by the functional interplay of SIRT1 and PARP-1 in response to DNA damage. Cell Cycle 2006;5(8):873-7.
77. Yu SW, Andrabi SA, Wang H, *et al.* Apoptosis-inducing factor mediates poly(ADP-ribose) (PAR) polymer-induced cell death. Proceedings of the National Academy of Sciences of the United States of America 2006;103(48):18314-9.
78. Buelow B, Song Y, Scharenberg AM. The Poly(ADP-ribose) polymerase PARP-1 is required for oxidative stress-induced TRPM2 activation in lymphocytes. J Biol Chem 2008;283(36):24571-83.
79. Fonfria E, Marshall IC, Benham CD, *et al.* TRPM2 channel opening in response to oxidative stress is dependent on activation of poly(ADP-ribose) polymerase. British journal of pharmacology 2004;143(1):186-92.
80. Formentini L, Macchiarulo A, Cipriani G, *et al.* Poly(ADP-ribose) catabolism triggers AMP-dependent mitochondrial energy failure. J Biol Chem 2009;284(26):17668-76.
81. Ochs K, Lips J, Profittlich S, Kaina B. Deficiency in DNA polymerase ß provokes replication-dependent apoptosis via DNA breakage, Bcl-2 decline and caspase-3/9 activation. Cancer Res 2002;62(5):1524-30.
82. Horton JK, Stefanick DF, Wilson SH. Involvement of poly(ADP-ribose) polymerase activity in regulating Chk1-dependent apoptotic cell death. DNA Repair (Amst) 2005;4(10):1111-20.
83. Trivedi RN, Wang XH, Jelezcova E, Goellner EM, Tang J, Sobol RW. Human methyl purine DNA glycosylase and DNA polymerase ß expression collectively predict sensitivity to temozolomide. Molecular Pharmacology 2008;74(2):505-16.
84. Bonicalzi ME, Haince JF, Droit A, Poirier GG. Regulation of poly(ADP-ribose) metabolism by poly(ADP-ribose) glycohydrolase: where and when? Cell Mol Life Sci 2005;62(7-8):739-50.
85. Wyatt MD, Pittman DL. Methylating agents and DNA repair responses: Methylated bases and sources of strand breaks. Chem Res Toxicol 2006;19(12):1580-94.
86. Dantzer F, Ame JC, Schreiber V, Nakamura J, Menissier-de Murcia J, de Murcia G. Poly(ADP-ribose) polymerase-1 activation during DNA damage and repair. Methods Enzymol 2006;409:493-510.

87. Tang JB, Svilar D, Trivedi RN*, et al.* N-methylpurine DNA glycosylase and DNA polymerase beta modulate BER inhibitor potentiation of glioma cells to temozolomide. Neuro-oncology 2011;13(5):471-86.
88. Kanzawa T, Germano IM, Komata T, Ito H, Kondo Y, Kondo S. Role of autophagy in temozolomide-induced cytotoxicity for malignant glioma cells. Cell Death Differ 2004;11(4):448-57.
89. Yu SW, Andrabi SA, Wang H*, et al.* Apoptosis-inducing factor mediates poly(ADP-ribose) (PAR) polymer-induced cell death. Proc Natl Acad Sci U S A 2006;103(48):18314-9.
90. Xu Y, Huang S, Liu ZG, Han J. Poly(ADP-ribose) polymerase-1 signaling to mitochondria in necrotic cell death requires RIP1/TRAF2-mediated JNK1 activation. J Biol Chem 2006;281(13):8788-95.
91. Xu X, Chua CC, Kong J*, et al.* Necrostatin-1 protects against glutamate-induced glutathione depletion and caspase-independent cell death in HT-22 cells. J Neurochem 2007;103(5):2004-14.
92. Degterev A, Hitomi J, Germscheid M*, et al.* Identification of RIP1 kinase as a specific cellular target of necrostatins. Nat Chem Biol 2008;4(5):313-21.
93. Dumitriu IE, Voll RE, Kolowos W*, et al.* UV irradiation inhibits ABC transporters via generation of ADP-ribose by concerted action of poly(ADP-ribose) polymerase-1 and glycohydrolase. Cell Death Differ 2004;11(3):314-20.
94. Bentle MS, Reinicke KE, Bey EA, Spitz DR, Boothman DA. Calcium-dependent modulation of poly(ADP-ribose) polymerase-1 alters cellular metabolism and DNA repair. J Biol Chem 2006;281(44):33684-96.
95. Bey EA, Bentle MS, Reinicke KE*, et al.* An NQO1- and PARP-1-mediated cell death pathway induced in non-small-cell lung cancer cells by beta-lapachone. Proc Natl Acad Sci U S A 2007;104(28):11832-7.
96. Heeres JT, Hergenrother PJ. Poly(ADP-ribose) makes a date with death. Curr Opin Chem Biol 2007;11(6):644-53.
97. Lotze MT, Tracey KJ. High-mobility group box 1 protein (HMGB1): nuclear weapon in the immune arsenal. Nature reviews 2005;5(4):331-42.
98. Ditsworth D, Zong WX, Thompson CB. Activation of poly(ADP)-ribose polymerase (PARP-1) induces release of the pro-inflammatory mediator HMGB1 from the nucleus. J Biol Chem 2007;282(24):17845-54.
99. Prasad R, Liu Y, Deterding LJ*, et al.* HMGB1 is a cofactor in mammalian base excision repair. Mol Cell 2007;27(5):829-41.
100. Berger NA. Poly(ADP-ribose) in the cellular response to DNA damage. Radiat Res 1985;101(1):4-15.
101. Berger NA, Sims JL, Catino DM, Berger SJ. Poly(ADP-ribose) polymerase mediates the suicide response to massive DNA damage: studies in normal and DNA-repair defective cells. Princess Takamatsu Symp 1983;13:219-26.
102. Jacobson MK, Levi V, Juarez-Salinas H, Barton RA, Jacobson EL. Effect of carcinogenic N-alkyl-N-nitroso compounds on nicotinamide adenine dinucleotide metabolism. Cancer Res 1980;40(6):1797-802.
103. Formentini L, Moroni F, Chiarugi A. Detection and pharmacological modulation of nicotinamide mononucleotide (NMN) in vitro and in vivo. Biochemical pharmacology 2009;77(10):1612-20.

104. Hasmann M, Schemainda I. FK866, a highly specific noncompetitive inhibitor of nicotinamide phosphoribosyltransferase, represents a novel mechanism for induction of tumor cell apoptosis. Cancer Res 2003;63(21):7436-42.
105. Kauppinen TM, Chan WY, Suh SW, Wiggins AK, Huang EJ, Swanson RA. Direct phosphorylation and regulation of poly(ADP-ribose) polymerase-1 by extracellular signal-regulated kinases 1/2. Proc Natl Acad Sci U S A 2006;103(18):7136-41.
106. Rajamohan SB, Pillai VB, Gupta M*, et al.* SIRT1 promotes cell survival under stress by deacetylation-dependent deactivation of poly(ADP-ribose) polymerase 1. Mol Cell Biol 2009;29(15):4116-29.
107. Moubarak RS, Yuste VJ, Artus C*, et al.* Sequential activation of poly(ADP-ribose) polymerase 1, calpains, and Bax is essential in apoptosis-inducing factor-mediated programmed necrosis. Mol Cell Biol 2007;27(13):4844-62.
108. Hofseth LJ, Khan MA, Ambrose M*, et al.* The adaptive imbalance in base excision-repair enzymes generates microsatellite instability in chronic inflammation. Journal of Clinical Investigation 2003;112(12):1887-94.
109. Schreiber V, Dantzer F, Ame JC, de Murcia G. Poly(ADP-ribose): novel functions for an old molecule. Nat Rev Mol Cell Biol 2006;7(7):517-28.
110. Ethier C, Labelle Y, Poirier GG. PARP-1-induced cell death through inhibition of the MEK/ERK pathway in MNNG-treated HeLa cells. Apoptosis 2007;12(11):2037-49.
111. Wang Y, Kim NS, Li X*, et al.* Calpain activation is not required for AIF translocation in PARP-1-dependent cell death (parthanatos). J Neurochem 2009;110(2):687-96.
112. LeDoux SP, Wilson GL, Beecham EJ, Stevnsner T, Wassermann K, Bohr VA. Repair of mitochondrial DNA after various types of DNA damage in Chinese hamster ovary cells. Carcinogenesis 1992;13(11):1967-73.
113. Huang Q, Wu YT, Tan HL, Ong CN, Shen HM. A novel function of poly(ADP-ribose) polymerase-1 in modulation of autophagy and necrosis under oxidative stress. Cell Death Differ 2009;16(2):264-77.
114. Dali-Youcef N, Lagouge M, Froelich S, Koehl C, Schoonjans K, Auwerx J. Sirtuins: the 'magnificent seven', function, metabolism and longevity. Annals of medicine 2007;39(5):335-45.
115. Berger F, Lau C, Dahlmann M, Ziegler M. Subcellular compartmentation and differential catalytic properties of the three human nicotinamide mononucleotide adenylyltransferase isoforms. J Biol Chem 2005;280(43):36334-41.
116. Pieper AA, Walles T, Wei G*, et al.* Myocardial postischemic injury is reduced by polyADPripose polymerase-1 gene disruption. Mol Med 2000;6(4):271-82.
117. Endres M, Wang ZQ, Namura S, Waeber C, Moskowitz MA. Ischemic brain injury is mediated by the activation of poly(ADP-ribose)polymerase. J Cereb Blood Flow Metab 1997;17(11):1143-51.
118. Eliasson MJ, Sampei K, Mandir AS*, et al.* Poly(ADP-ribose) polymerase gene disruption renders mice resistant to cerebral ischemia. Nat Med 1997;3(10):1089-95.
119. Ha HC, Snyder SH. Poly(ADP-ribose) polymerase is a mediator of necrotic cell death by ATP depletion. Proc Natl Acad Sci U S A 1999;96(24):13978-82.
120. Wang S, Xing Z, Vosler PS*, et al.* Cellular NAD replenishment confers marked neuroprotection against ischemic cell death: role of enhanced DNA repair. Stroke 2008;39(9):2587-95.
121. Liu D, Gharavi R, Pitta M, Gleichmann M, Mattson MP. Nicotinamide prevents NAD+ depletion and protects neurons against excitotoxicity and cerebral ischemia: NAD+ consumption

by SIRT1 may endanger energetically compromised neurons. Neuromolecular Med 2009;11(1):28-42.
122. Masutani M, Suzuki H, Kamada N*, et al.* Poly(ADP-ribose) polymerase gene disruption conferred mice resistant to streptozotocin-induced diabetes. Proc Natl Acad Sci U S A 1999;96(5):2301-4.
123. Cardinal JW, Margison GP, Mynett KJ, Yates AP, Cameron DP, Elder RH. Increased susceptibility to streptozotocin-induced beta-cell apoptosis and delayed autoimmune diabetes in alkylpurine-DNA-N-glycosylase-deficient mice. Mol Cell Biol 2001;21(16):5605-13.
124. Burns N, Gold B. The effect of 3-methyladenine DNA glycosylase-mediated DNA repair on the induction of toxicity and diabetes by the beta-cell toxicant streptozotocin. Toxicol Sci 2007;95(2):391-400.
125. Pieper AA, Brat DJ, Krug DK*, et al.* Poly(ADP-ribose) polymerase-deficient mice are protected from streptozotocin-induced diabetes. Proc Natl Acad Sci U S A 1999;96(6):3059-64.
126. Garten A, Petzold S, Korner A, Imai S, Kiess W. Nampt: linking NAD biology, metabolism and cancer. Trends Endocrinol Metab 2009;20(3):130-8.
127. Zhu G, Chang P, Lippard SJ. Recognition of platinum-DNA damage by poly(ADP-ribose) polymerase-1. Biochemistry 2010;49(29):6177-83.
128. Pittelli M, Formentini L, Faraco G*, et al.* Inhibition of nicotinamide phosphoribosyltransferase: cellular bioenergetics reveals a mitochondrial insensitive NAD pool. J Biol Chem 2010;285(44):34106-14.
129. Alano CC, Tran A, Tao R, Ying W, Karliner JS, Swanson RA. Differences among cell types in NAD(+) compartmentalization: a comparison of neurons, astrocytes, and cardiac myocytes. Journal of neuroscience research 2007;85(15):3378-85.
130. Yang H, Yang T, Baur JA*, et al.* Nutrient-sensitive mitochondrial NAD+ levels dictate cell survival. Cell 2007;130(6):1095-107.
131. Ying W, Garnier P, Swanson RA. NAD+ repletion prevents PARP-1-induced glycolytic blockade and cell death in cultured mouse astrocytes. Biochem Biophys Res Commun 2003;308(4):809-13.
132. Ying W, Chen Y, Alano CC, Swanson RA. Tricarboxylic acid cycle substrates prevent PARP-mediated death of neurons and astrocytes. J Cereb Blood Flow Metab 2002;22(7):774-9.
133. Cipriani G, Rapizzi E, Vannacci A, Rizzuto R, Moroni F, Chiarugi A. Nuclear poly(ADP-ribose) polymerase-1 rapidly triggers mitochondrial dysfunction. J Biol Chem 2005;280(17):17227-34.
134. Zhou HZ, Swanson RA, Simonis U, Ma X, Cecchini G, Gray MO. Poly(ADP-ribose) polymerase-1 hyperactivation and impairment of mitochondrial respiratory chain complex I function in reperfused mouse hearts. American journal of physiology 2006;291(2):H714-23.
135. Lai Y, Chen Y, Watkins SC*, et al.* Identification of poly-ADP-ribosylated mitochondrial proteins after traumatic brain injury. J Neurochem 2008;104(6):1700-11.
136. Niere M, Kernstock S, Koch-Nolte F, Ziegler M. Functional localization of two poly(ADP-ribose)-degrading enzymes to the mitochondrial matrix. Mol Cell Biol 2008;28(2):814-24.
137. Sathornsumetee S, Rich JN. New treatment strategies for malignant gliomas. Expert Rev Anticancer Ther 2006;6(7):1087-104.
138. Pegg AE, Dolan ME, Moschel RC. Structure, function, and inhibition of O6-alkylguanine-DNA alkyltransferase. Prog Nucleic Acid Res Mol Biol 1995;51:167-223.

139. Friedman HS, Johnson SP, Dong Q*, et al.* Methylator resistance mediated by mismatch repair deficiency in a glioblastoma multiforme xenograft. Cancer Res 1997;57(14):2933-6.
140. Roos WP, Batista LF, Naumann SC*, et al.* Apoptosis in malignant glioma cells triggered by the temozolomide-induced DNA lesion O6-methylguanine. Oncogene 2007;26(2):186-97.
141. Caporali S, Falcinelli S, Starace G*, et al.* DNA damage induced by temozolomide signals to both ATM and ATR: role of the mismatch repair system. Molecular Pharmacology 2004;66(3):478-91.
142. Liu L, Gerson SL. Targeted modulation of MGMT: clinical implications. Clin Cancer Res 2006;12(2):328-31.
143. Hottiger MO, Hassa PO, Luscher B, Schuler H, Koch-Nolte F. Toward a unified nomenclature for mammalian ADP-ribosyltransferases. Trends in biochemical sciences;35(4):208-19.
144. Magni G, Orsomando G, Raffelli N, Ruggieri S. Enzymology of mammalian NAD metabolism in health and disease. Front Biosci 2008;13:6135-54.
145. Revollo JR, Grimm AA, Imai S. The NAD biosynthesis pathway mediated by nicotinamide phosphoribosyltransferase regulates Sir2 activity in mammalian cells. J Biol Chem 2004;279(49):50754-63.
146. Cea M, Zoppoli G, Bruzzone S*, et al.* APO866 activity in hematologic malignancies: a preclinical in vitro study. Blood 2009;113(23):6035-7; author reply 7-8.
147. Pogrebniak A, Schemainda I, Azzam K, Pelka-Fleischer R, Nussler V, Hasmann M. Chemopotentiating effects of a novel NAD biosynthesis inhibitor, FK866, in combination with antineoplastic agents. European journal of medical research 2006;11(8):313-21.
148. Watson M, Roulston A, Belec L*, et al.* The Small Molecule GMX1778 is a Potent Inhibitor of NAD+ Biosynthesis: Strategy for Enhanced Therapy in NAPRT1-Deficient Tumors. Mol Cell Biol 2009.
149. Alano CC, Garnier P, Ying W, Higashi Y, Kauppinen TM, Swanson RA. NAD+ depletion is necessary and sufficient for poly(ADP-ribose) polymerase-1-mediated neuronal death. J Neurosci 2010;30(8):2967-78.
150. Michelakis ED, Sutendra G, Dromparis P*, et al.* Metabolic modulation of glioblastoma with dichloroacetate. Science translational medicine 2010;2(31):31ra4.
151. Olesen UH, Christensen MK, Bjorkling F*, et al.* Anticancer agent CHS-828 inhibits cellular synthesis of NAD. Biochem Biophys Res Commun 2008;367(4):799-804.
152. Daponte A, Ascierto PA, Gravina A*, et al.* Temozolomide and cisplatin in avdanced malignant melanoma. Anticancer Res 2005;25(2B):1441-7.
153. Chen Z, Lu W, Garcia-Prieto C, Huang P. The Warburg effect and its cancer therapeutic implications. J Bioenerg Biomembr 2007;39(3):267-74.
154. Santra A, Kumar R, Sharma P, Bal C, Julka PK, Malhotra A. F-18 FDG PET-CT for predicting survival in patients with recurrent glioma: a prospective study. Neuroradiology 2011.
155. Fulco M, Sartorelli V. Comparing and contrasting the roles of AMPK and SIRT1 in metabolic tissues. Cell Cycle 2008;7(23):3669-79.
156. Shaw RJ, Kosmatka M, Bardeesy N*, et al.* The tumor suppressor LKB1 kinase directly activates AMP-activated kinase and regulates apoptosis in response to energy stress. Proc Natl Acad Sci U S A 2004;101(10):3329-35.
157. Shen Z, Wu Q, Yue L, Li HC, Shen ZZ, Shao ZM. [Function and prognostic value of tumor suppressor gene LKB1 in human breast carcinoma]. Zhonghua yi xue za zhi 2005;85(1):15-8.

158. Dowling RJ, Zakikhani M, Fantus IG, Pollak M, Sonenberg N. Metformin inhibits mammalian target of rapamycin-dependent translation initiation in breast cancer cells. Cancer Res 2007;67(22):10804-12.
159. Huang Q, Shen HM. To die or to live: the dual role of poly(ADP-ribose) polymerase-1 in autophagy and necrosis under oxidative stress and DNA damage. Autophagy 2009;5(2):273-6.
160. Cuervo AM. Autophagy and aging: keeping that old broom working. Trends Genet 2008;24(12):604-12.
161. Rabinowitz JD, White E. Autophagy and metabolism. Science 2010;330(6009):1344-8.
162. Munoz-Gamez JA, Rodriguez-Vargas JM, Quiles-Perez R, *et al.* PARP-1 is involved in autophagy induced by DNA damage. Autophagy 2009;5(1):61-74.
163. Egan DF, Shackelford DB, Mihaylova MM, *et al.* Phosphorylation of ULK1 (hATG1) by AMP-activated protein kinase connects energy sensing to mitophagy. Science 2011;331(6016):456-61.
164. Kim J, Kundu M, Viollet B, Guan KL. AMPK and mTOR regulate autophagy through direct phosphorylation of Ulk1. Nat Cell Biol 2011;13(2):132-41.
165. McLennan AG. The Nudix hydrolase superfamily. Cell Mol Life Sci 2006;63(2):123-43.
166. Fulco M, Cen Y, Zhao P, *et al.* Glucose restriction inhibits skeletal myoblast differentiation by activating SIRT1 through AMPK-mediated regulation of Nampt. Dev Cell 2008;14(5):661-73.
167. Pillai VB, Sundaresan NR, Kim G, *et al.* Exogenous NAD blocks cardiac hypertrophic response via activation of the SIRT3-LKB1-AMP-activated kinase pathway. J Biol Chem 2010;285(5):3133-44.
168. Bai P, Canto C, Brunyanszki A, *et al.* PARP-2 regulates SIRT1 expression and whole-body energy expenditure. Cell Metab 2011;13(4):450-60.
169. Bai P, Canto C, Oudart H, *et al.* PARP-1 inhibition increases mitochondrial metabolism through SIRT1 activation. Cell Metab 2011;13(4):461-8.
170. Lin SJ, Ford E, Haigis M, Liszt G, Guarente L. Calorie restriction extends yeast life span by lowering the level of NADH. Genes Dev 2004;18(1):12-6.
171. Ahn BH, Kim HS, Song S, *et al.* A role for the mitochondrial deacetylase Sirt3 in regulating energy homeostasis. Proc Natl Acad Sci U S A 2008;105(38):14447-52.
172. Seyfried TN, Kiebish MA, Marsh J, Shelton LM, Huysentruyt LC, Mukherjee P. Metabolic management of brain cancer. Biochim Biophys Acta 2010;1807(6):577-94.
173. Liu H, Knabb JR, Spike BT, Macleod KF. Elevated poly-(ADP-ribose)-polymerase activity sensitizes retinoblastoma-deficient cells to DNA damage-induced necrosis. Mol Cancer Res 2009;7(7):1099-109.
174. Magni G, Amici A, Emanuelli M, Orsomando G, Raffaelli N, Ruggieri S. Enzymology of NAD+ homeostasis in man. Cell Mol Life Sci 2004;61(1):19-34.
175. Olesen UH, Thougaard AV, Jensen PB, Sehested M. A preclinical study on the rescue of normal tissue by nicotinic acid in high-dose treatment with APO866, a specific nicotinamide phosphoribosyltransferase inhibitor. Mol Cancer Ther 2010;9(6):1609-17.
176. http://www.cancer.gov/cancertopics/druginfo/cisplatin.

APPENDIX A

Published OnlineFirst January 12, 2010; DOI:10.1158/1541-7786.MCR-09-0411

Molecular Cancer Research

Bioenergetic Metabolites Regulate Base Excision Repair–Dependent Cell Death in Response to DNA Damage

Jiang-bo Tang, Eva M. Goellner, Xiao-hong Wang, et al.

Mol Cancer Res 2010;8:67-79. Published OnlineFirst January 12, 2010.

Published OnlineFirst January 12, 2010; DOI:10.1158/1541-7786.MCR-09-0411

Molecular Cancer Research

DNA Damage and Cellular Stress Responses

Bioenergetic Metabolites Regulate Base Excision Repair–Dependent Cell Death in Response to DNA Damage

Jiang-bo Tang[1,2], Eva M. Goellner[1], Xiao-hong Wang[1], Ram N. Trivedi[1], Claudette M. St Croix[3], Elena Jelezcova[1], David Svilar[1], Ashley R. Brown[1], and Robert W. Sobol[1,2]

Abstract

Base excision repair (BER) protein expression is important for resistance to DNA damage–induced cytotoxicity. Conversely, BER imbalance [DNA polymerase β (Polβ) deficiency or repair inhibition] enhances cytotoxicity of radiation and chemotherapeutic DNA-damaging agents. Whereas inhibition of critical steps in the BER pathway result in the accumulation of cytotoxic DNA double-strand breaks, we report that DNA damage–induced cytotoxicity due to deficiency in the BER protein Polβ triggers cell death dependent on poly(ADP-ribose) (PAR) polymerase activation yet independent of PAR-mediated apoptosis-inducing factor nuclear translocation or PAR glycohydrolase, suggesting that cytotoxicity is not from PAR or PAR catabolite signaling. Cell death is rescued by the NAD^+ metabolite β-nicotinamide mononucleotide and is synergistic with inhibition of NAD^+ biosynthesis, showing that DNA damage–induced cytotoxicity mediated via BER inhibition is primarily dependent on cellular metabolite bioavailability. We offer a mechanistic justification for the elevated alkylation-induced cytotoxicity of Polβ-deficient cells, suggesting a linkage between DNA repair, cell survival, and cellular bioenergetics. *Mol Cancer Res; 8(1); 67–79. ©2010 AACR.*

Introduction

Efficacy of chemotherapy or radiation treatment is intimately dependent on DNA repair capacity (1). Robust repair of therapeutically induced DNA damage can provide significant resistance, whereas tumor-specific defects in DNA repair or inhibition of specific DNA repair proteins can provide therapeutic advantage (2). In particular, inhibiting base excision repair (BER) can be an effective means to improve response to temozolomide, radiation, bleomycin, and cisplatin, among other treatments (3-10). As with most DNA repair pathways, BER is a multistep mechanism composed of >20 proteins depending on the initial base lesion (3). However, inhibiting each step in the BER pathway will have different outcomes. DNA glycosylase inhibition or loss blocks BER initiation, leading to the accumulation of both cytotoxic (4) and mutagenic base lesions (5), the latter contributing to cellular dysfunction. In this regard, the preferred option is the inhibition of BER after repair initiation, promoting the accumulation of cytotoxic BER intermediates such as abasic sites and DNA single-strand breaks by inhibiting abasic site repair with methoxyamine and inhibiting the BER enzyme poly (ADP-ribose) polymerase 1 (PARP1) or by loss or inhibition of DNA polymerase β (Polβ; refs. 2, 6, 7). We refer to inhibition of the intermediate steps in BER as the induction of "BER failure" because repair is initiated yet is unable to be completed.

Importantly, understanding the mechanisms that are responsible for the increase in cell death due to BER inhibition or BER failure is critical in tailoring treatment as well as designing rational adjuvant or combination treatments that may further increase overall response. For example, inhibiting PARP1 has proven effective in improving temozolomide-induced cell death (8). Inhibition of PARP1 results in the accumulation of replication-mediated DNA double-strand breaks (DSB) and the onset of apoptosis (9, 10). This detailed understanding of the mechanism of cell death induced by combining a DNA-damaging agent (temozolomide) and a PARP1 inhibitor suggests that PARP1 inhibition would be effective against many tumors but may be ineffective against tumors that are resistant to apoptosis (11). Further, cell death induced by PARP1 inhibition suggested a requirement for homologous recombination in the cellular response to the accumulated DSBs,

Authors' Affiliations: [1]Department of Pharmacology and Chemical Biology, University of Pittsburgh School of Medicine and University of Pittsburgh Cancer Institute, Hillman Cancer Center; [2]Department of Human Genetics, University of Pittsburgh Graduate School of Public Health; [3]Center for Biological Imaging, Department of Cell Biology and Physiology, University of Pittsburgh, Pittsburgh, Pennsylvania

Note: Supplementary data for this article are available at Molecular Cancer Research Online (http://mcr.aacrjournals.org/).

J. Tang and E.M. Goellner contributed equally to this work.

Corresponding Author: Robert W. Sobol, Hillman Cancer Center, University of Pittsburgh Cancer Institute, Research Pavilion, Suite 2.6a, 5117 Centre Avenue, Pittsburgh, PA 15213-1863. Phone: 412-623-7764; Fax: 412-623-7761. E-mail: rws9@pitt.edu

doi: 10.1158/1541-7786.MCR-09-0411

Published OnlineFirst January 12, 2010; DOI:10.1158/1541-7786.MCR-09-0411

prompting preclinical and clinical trials of PARP1 inhibitors in the treatment of homologous recombination–defective tumors (2).

There are several BER proteins essential for the repair of temozolomide-induced DNA lesions. Using a mouse embryonic fibroblast cell model, we have shown that loss of Polβ can significantly improve the cytotoxic effect of temozolomide (12), suggesting that inhibition of Polβ may improve response to temozolomide in human tumor cells. Temozolomide is currently used in the treatment of glioblastoma (13), and it is therefore critical to evaluate the role of Polβ in glioma cell response to temozolomide treatment. No previous studies have investigated the role of Polβ in the response of human glioma tumor cells to temozolomide. Further, there is no mechanistic explanation for the increase in alkylation-induced cell death observed in cells that are deficient in Polβ beyond the evidence that cell death in mouse cells is the result of accumulation of unrepaired BER intermediates (7, 12).

Acute alkylation damage has been suggested to induce cell death by multiple mechanisms, including necrosis (14), caspase-3 and caspase-9 activation and the onset of apoptosis (15), apoptosis-inducing factor (AIF) translocation from the mitochondria to the nucleus (16-18), ADP-ribose–induced activation of the Ca^{2+} channel TRPM2, or AMP-mediated inhibition of ATP transport (19-21). In most, if not all, cases, cell death has been attributed to the direct action of either PAR formed by PARP1 activation or PAR catabolites that accumulate after PAR degradation by the catabolic enzyme PAR glycohydrolase (PARG). Polβ-deficient mouse cells are hypersensitive to the cell killing effects of alkylating agents due to failure to repair the 5′-deoxyribose phosphate (5′-dRP) BER intermediate (22). However, the exact downstream signaling events and mechanism of cytotoxicity specifically induced by the unrepaired 5′-dRP lesion remain unclear. Previous studies in mouse cells have not been conclusive. One report suggested that the absence of Polβ led to damage-induced cell death via apoptosis (23), whereas a later study proposed a necrotic form of cell death for both wild-type (WT) and Polβ-deficient cells (24), similar to what has been proposed as a general mechanism of alkylation-induced cell death in mouse fibroblasts (14). However, this latter study required the use of apoptosis-deficient cells to observe necrotic cell death (14). None of these previous studies have identified a mechanism of cell death specific to Polβ deficiency and BER failure or a failure to repair the cytotoxic BER intermediate 5′-dRP.

The studies described herein were designed to specifically define the mechanism of cell death in human tumor cells resulting from failure to repair the BER intermediate 5′-dRP due to "inhibition of" or a "deficiency in" Polβ (BER failure). We have hypothesized that PARP1 functions in BER as both a complex coordinator and a molecular repair sensor. As a BER molecular sensor, we suggest that PARP1 facilitates cell death in response to incomplete BER or BER failure. In support of this hypothesis, we show that a specific BER intermediate, a single-strand DNA strand break containing a 3′-OH and 5′-dRP, is an *in vivo* substrate in human cells that activates PARP1 in the context of BER and that elevated cytotoxicity observed in Polβ-deficient human cells is controlled by the activation of PARP1. Further, we provide clear evidence that following BER failure human cells die independent of RIP1 activation or AIF translocation, thus ruling out PAR as the cell death signal that is initiated on BER failure. Further, we show that the observed cell death in Polβ-deficient cells is unrelated to the accumulation of PAR catabolites, such as ADP-ribose or AMP, yet is dependent on NAD^+ metabolite bioavailability or the bioenergetic capacity of the cell.

This study provides mechanistic insight into why Polβ deficiency leads to cell death, defines the mode of death, and offers a mechanistic link between BER failure and energy metabolism—the novel finding that DNA damage–induced cytotoxicity mediated via BER inhibition is primarily dependent on cellular metabolite bioavailability. Finally, we offer a mechanistic justification for the elevated alkylation-induced cytotoxicity of Polβ-deficient cells, suggesting a linkage between DNA repair, cell survival, and cellular bioenergetics.

Materials and Methods

Cell Culture and Cell Line Development

The cell line LN428 is an established glioblastoma-derived cell line with mutations in p53 and deletions in $p14^{ARF}$ and p16 and is WT for PTEN (25, 26). LN428 cells were kindly provided by Ian Pollack (University of Pittsburgh, Pittsburgh, PA) and cultured in α-Eagle's MEM supplemented with 10% heat-inactivated fetal bovine serum, glutamine, antibiotic/antimycotic, and gentamicin. MDA-MB-231 cells and derivatives were described previously (27). Cell lines expressing human MPG (WT), human MPG (N169D), FLAG-Polβ(WT), and FLAG-Polβ(K72A) were developed by transfection using FuGene 6 transfection reagent (Roche Diagnostic Corp.) according to the manufacturer's protocol. Transfected cell lines were cultured in G418 and/or puromycin for 2 wk, and individual clones stably expressing human MPG or Polβ were selected. It was recently suggested that $p14^{ARF}$ deficiency results in proteosome-mediated degradation of Polβ (28). Although LN428 cells are deficient in $p14^{ARF}$ (26), we note that the expression levels of Polβ are stable. Lentiviral particles were generated by cotransfection of plasmid pCDF1-MCS1-EF1-copGFP (control) or pSIF-H1-hPOLB1-copGFP (Polβ shRNA) together with pFIV-34N and pVSV-G into 293-FT cells (29) using FuGene 6 transfection reagent. Forty-eight hours after transfection, lentivirus-containing supernatant was collected and passed through 0.45-μm filters to isolate the viral particles. Lentiviral transduction was done as described earlier (27). Briefly, 6.0×10^4 cells were seeded into six-well plates 24 h before transduction. Cells were transduced for 18 h at 32°C and cultured for 72 h at 37°C. Cells expressing copGFP only or both copGFP and Polβ-specific shRNA

Published OnlineFirst January 12, 2010; DOI:10.1158/1541-7786.MCR-09-0411

were isolated by fluorescence-activated cell sorting, and Polβ-KD was confirmed by immunoblot analysis. All the cell lines developed and used in this study are described in Supplementary Table S1.

Chemicals and Reagents

α-Eagle's MEM was from Mediatech. RPMI 1640 and DMEM were from Cambrex Bioscience Group and Biowhittaker, respectively. Fetal bovine serum, heat-inactivated fetal bovine serum, penicillin/streptomycin/amphotericin, glutamine, and antibiotic/antimycotic were from Invitrogen. Temozolomide (NSC 362856; IUPAC name: 3-methyl-2-oxo-1,3,4,5,8-pentazabicyclo[4.3.0]nona-4,6,8-triene-7-carbooxamide; CAS number: 856622-93-1; ref. 30) was obtained from the National Cancer Institute Developmental Therapeutics Program. A temozolomide stock solution was prepared in DMSO at 100 mmol/L. MMS was from Sigma-Aldrich. Puromycin, gentamicin, and neomycin were purchased from Clontech Laboratories, Irvine Scientific, and Invitrogen, respectively. PJ34 was purchased from Calbiochem. FK-866 {(*E*)-[4-(1-benzoylpiperidin-4-yl)butyl]-3-pyridin-3-yl)acrylamide} was obtained from the National Institute of Mental Health Chemical Synthesis and Drug Supply Program (NIMH F-901; ref. 31). NMN was obtained from Sigma, and NA was obtained from Fisher.

Plasmid Expression and RNA Interference Vectors

Human MPG (WT) was expressed using the plasmid pRS1422, as described previously (27). The MPG expression plasmid (pRS1422) was then mutated at residue N169 using the QuikChange XL Site-Directed Mutagenesis kit (Stratagene) to yield pIRES-Neo-MPG-N169D. The expression plasmid for FLAG-tagged WT human Polβ was generated by PCR amplification of the human Polβ cDNA using a FLAG-containing forward oligonucleotide and cloned into pENTR/D-TOPO as we described previously (27). pENTER/FLAG-Polβ(WT) was then mutated at residue K72 as described above to yield pENTER/FLAG-Polβ(K72A). FLAG-Polβ(WT) and FLAG-Polβ(-K72A) were subsequently cloned into a Gateway-modified pIRES-Puro vector by TOPO cloning, as we have described previously (27). The FIV-based lentiviral shRNA expression vector system specific for human Polβ was as described previously (27) but was modified for copGFP expression (pSIF-H1-hPOLB1-copGFP). Lentiviral particles for coexpression of PARG shRNA and TurboGFP were prepared by transfection of four plasmids [the control plasmid pLK0.1-Puro-tGFP or the human PARG-specific shRNA plasmid pLK0.1-Puro-PARGshRNA4 plus pMD2.g(VSVG), pRSV-REV, and pMDLg/pRRE] into 293-FT cells (29, 32) using FuGene 6 transfection reagent. Culture medium from transfected cells was collected 48 h after transfection to isolate the viral particles, passed through 0.45-μm filters, used immediately, or stored at −80°C in single-use aliquots. Transduction of LN428 cells with control lentivirus (GFP expression only) and human PARG-specific shRNA lentivirus was completed as follows: Briefly, 6.0×10^4 cells were seeded into six-well plates and incubated for 24 to 30 h at 10% CO_2 at 37°C. Cells were transduced for 18 h with virus at 32°C and cultured for 72 h at 37°C before isolation of the GFP-expressing population by fluorescence-activated cell sorting using the University of Pittsburgh Cancer Institute Flow Cytometry Facility. Cells were then cultured to expand the population and analyzed for expression of PARG by quantitative reverse transcription-PCR.

Quantitative Reverse Transcription-PCR Analysis

Expression of PARG and Polβ mRNA was measured by quantitative reverse transcription-PCR using an Applied Biosystems StepOnePlus system. Briefly, 80,000 cells were lysed and reverse transcribed using the Applied Biosystems Taqman Gene Expression Cells-to-CT kit. Each sample was analyzed in triplicate and the results are an average of all three analyses. Analysis of mRNA expression was conducted as per the manufacturer ($\Delta\Delta C_T$ method) using Applied Biosystems Taqman Gene Expression Assays (human Polβ: Hs00160263_m1; human PARG: Hs00608254_m1) and normalized to the expression of human β-actin (part 4333762T).

Cell Extract Preparation and Western Blot

Nuclear extracts were prepared and protein concentration was determined as we described previously (12). Twenty micrograms of protein were loaded on a precast 4% to 20% NuPAGE Tris-glycine gel (Invitrogen). For whole-cell extracts used in PAR formation assays, 3×10^6 cells were seeded into a 100-mm cell culture dish 24 h before drug treatment. Cells were either treated with temozolomide only or preexposed to a PARP inhibitor (PJ34 or DR2313) followed by PARP inhibitor plus temozolomide treatment. After treatment, cells were washed twice with cold PBS, collected, and lysed with 400 μL of 2× Laemmli buffer [2% SDS, 20% glycerol, 62.5 mmol/L Tris-HCl (pH 6.8), 0.01% bromphenol blue]. Samples were boiled for 8 min and extract from ~1.5×10^5 cells was loaded onto each lane on a 4% to 12% precast NuPAGE Tris-glycine gel for immunoblot assay.

The following primary antibodies were used in immunoblot assays: anti-human MPG monoclonal antibody (clone 506-3D; ref. 27), anti-Polβ monoclonal antibody (clone 61; Thermo Fisher Scientific), anti-APE1 (EMD Biosciences), anti–proliferating cell nuclear antigen (PCNA; Santa Cruz Biotechnology), anti-FLAG (M2 monoclonal antibody; Sigma-Aldrich), anti-PAR (clone 10H, kindly provided by M. Ziegler, University of Bergen, Bergen, Norway), anti-PARP1 (BD Pharmingen), and anti-human HMGB1 (R&D Systems).

Cell Cytotoxicity Assay

Temozolomide-induced cytotoxicity was determined by an MTS assay, a modified MTT assay as described previously (12). Results were calculated from the average of three or four separate experiments and are reported as the percentage of treated cells relative to the cells without treatment (% control). For PJ34, cells were preexposed to the inhibitor

Published OnlineFirst January 12, 2010; DOI:10.1158/1541-7786.MCR-09-0411

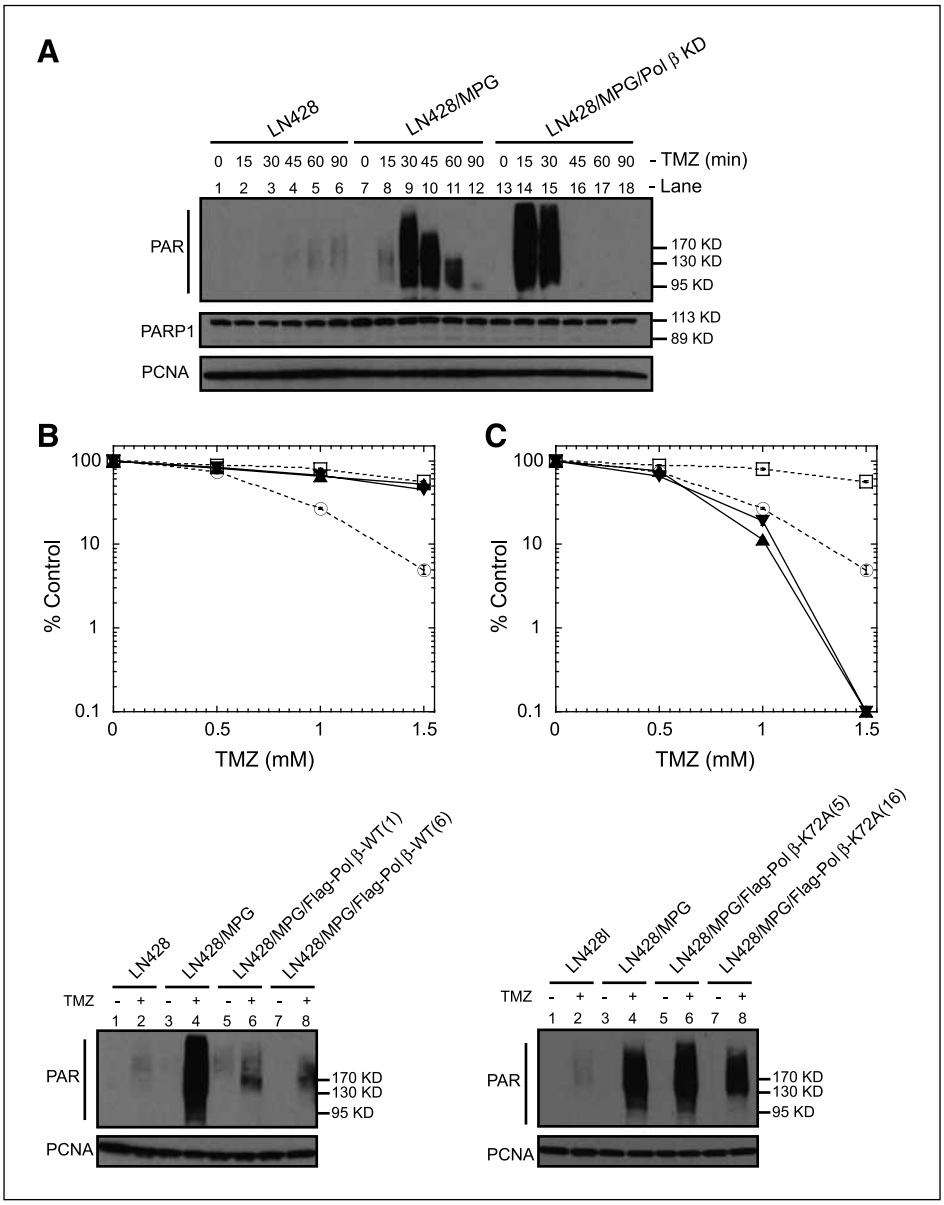

FIGURE 1. PARP activation due to BER failure. **A.** Immunoblot of PAR to determine activation of PARP in the cell lines indicated before and after exposure to temozolomide (*TMZ*; 1.5 mmol/L) for the time indicated. PARP1 and PCNA protein expression levels are also shown. **B.** Top, temozolomide-induced cytotoxicity in LN428, LN428/MPG, and two clones of LN428/MPG cells complemented with FLAG-Polβ(WT). After treatment (48 h), viable cells were determined using a modified MTT assay. Plots show the % viable cells as compared with untreated (control) cells. Means are calculated from quadruplicate values in each experiment. Points, mean of three independent experiments; bars, SE. □, LN428; ○, LN428/MPG; ▲, LN428/MPG/FLAG-Polβ(WT), clones 1 and 6. Bottom, immunoblot of PAR to determine activation of PARP1 after exposure to temozolomide (1.5 mmol/L) for the time indicated. PCNA is shown as a loading control. **C.** Top, temozolomide-induced cytotoxicity in LN428, LN428/MPG, and two clones of LN428/MPG cells complemented with FLAG-Polβ(K72A), measured as in **B**. □, LN428; ○, LN428/MPG; ▲, LN428/MPG/FLAG-Polβ(K72A), clones 5 and 16. Bottom, immunoblot of PAR to determine activation of PARP1 after exposure to temozolomide (1.5 mmol/L) for the time indicated. PCNA is shown as a loading control.

for 30 min and then treated with temozolomide in the presence of the inhibitor for 48 h. For NA and NMN, cells were preexposed to each for 24 h (concentrations as indicated in the legend) and then treated with temozolomide (1.0 mmol/L) in the presence of NA or NMN for 48 h. The effect on cell growth and survival was determined by an MTS assay, as described previously (12).

HMGB1 Release Assay

Cells were pretreated with medium alone or with PARP inhibitor (PJ34) for 30 min before cotreatment with PJ34 (2 μmol/L) and temozolomide (1.5 mmol/L) for 12 h. Cell culture medium was then collected and passed through 0.45-μm filters. Immobilized heparin (Thermo Fisher Scientific) slurry (100 μL) and 1 mL of medium were mixed and rotated at 4°C for 2 h before centrifugation at 8,000 × *g* to pull down HMGB1 bound to immobilized heparin (33). Pellets were boiled with 100 μL of 2× Laemmli buffer, and supernatants were used for immunoblot assay after brief centrifugation.

PAR Assay

Cells (1.5×10^6) were seeded in 100-mm dishes 24 h before treatment. For the FK-866 experiments, cells were then incubated in the presence of FK-866 (10 nmol/L) or DMSO for an additional 24 h. Medium was then removed and replaced with fresh medium or medium supplemented with PJ34 (2 μmol/L). After 30 min, cells

Published OnlineFirst January 12, 2010; DOI:10.1158/1541-7786.MCR-09-0411

were lysed immediately (0 time point) or medium was replaced with temozolomide for the times indicated in the figure legends. Extracts were prepared by washing the cells with PBS and preparing cell extract with 400 μL of 2× Laemmli buffer. Cell extract (20 μL) was analyzed by immunoblot with a 4,000-fold dilution of an anti-PAR primary antibody (clone 10H) followed by a 5,000-fold dilution of the horseradish peroxidase–conjugated secondary goat anti-mouse antibody.

Immunofluorescence and Confocal Microscopy

Cells were cultured on glass coverslips for 24 h before treatment with MMS or medium control. One hour after treatment, cells were washed and allowed to recover in medium for 5 h. Cells were then fixed with 4% paraformaldehyde for 20 min, permeabilized with 0.5% Triton X-100 for 15 min, and blocked with 2% bovine serum albumin for 1 h, all at room temperature. AIF was detected by incubating 1 h at room temperature with an anti-AIF antibody (Santa Cruz Biotechnology) at 1:100 dilution followed by goat anti-mouse Alexa Fluor 488 (Molecular Probes) at 1:500, Alexa Fluor 647 phalloidin actin stain at 1:250 (Molecular Probes), and 5 μmol/L DRAQ5 nuclear stain for 1 h at room temperature. Slides were mounted and imaged on the Olympus FluoView 500 confocal microscope.

NAD^+ and ATP Measurements

Cells were seeded 24 h before treatment with MMS or medium control. NAD^+: 1 h after treatment, cells were trypsinized and counted and 1×10^5 cells were pelleted. NAD^+ lysates were prepared and NAD^+ measurements were obtained using the EnzyChrom NAD^+/NADH Assay kit (BioAssay Systems). ATP: 1 h after treatment, cells were washed and allowed to recover in normal medium for 1 h. Cells were then lysed and ATP content was measured by luminescent output using the ATPlite assay kit (Perkin-Elmer).

FK-866 Cytotoxicity Assay

Cells were seeded in 96-well plates 24 h before treatment. Cells were pretreated with 10 nmol/L FK-866 or DMSO control for 24 h and then exposed to MMS for 1 h. The cells were then washed with medium and allowed to recover for 48 h before assaying for cytotoxicity by an MTS assay previously described (12, 27). Results shown are the average of three independent experiments and reported as percent survival of MMS-treated cells compared with control wells.

Results

Hyperactivation of PARP due to Polβ Deficiency and Failure to Repair the BER Intermediate 5′-dRP

BER is a finely tuned process that requires balanced expression of several proteins to avoid accumulation of mutagenic or cytotoxic repair intermediates (3). To understand how alterations in BER enzyme activity in human tumor cells lead to DNA damage–induced cell sensitivity, we developed human glioma (LN428) cell lines with a functional deficiency in Polβ by increasing expression of N-methylpurine DNA glycosylase (MPG) and depleting the cell of Polβ by stable lentiviral-mediated expression of short hairpin RNA (shRNA). As we have reported, human cells with elevated expression of MPG are sensitive to alkylation damage due to a deficiency in Polβ (27), a phenotype that is enhanced by Polβ knockdown (Polβ-KD). Conversely, reexpression of Polβ eliminated the alkylation hypersensitive phenotype (Supplementary Figs. S1 and S2). These cells (LN428/MPG and LN428/MPG/Polβ-KD cells) are therefore functionally deficient in Polβ and were used to determine the mechanism that mediates the enhanced DNA damage–induced cell death resulting from Polβ deficiency.

The DNA binding and signaling molecules PARP1 and PARP2 have each been implicated in BER (3). PARP1 facilitates BER complex formation, and it has been postulated that local strand break–induced activation of PARP1 and the resultant synthesis of PAR mediate recruitment of the BER proteins XRCC1 and Polβ to stimulate DNA repair (34). We therefore have hypothesized that in cells that fail to complete BER (e.g., when 5′-dRP lesions are not repaired; herein referred to as BER failure), PARP1 is hyperactivated and functions as a DNA damage signaling protein that triggers cell death. To determine whether PARP is activated by the BER intermediate (5′-dRP) *in vivo*, we exposed the control (LN428) and corresponding BER-defective cells (Polβ-deficient LN428/MPG and LN428/MPG/Polβ-KD cells) to temozolomide for up to 90 minutes. Whole-cell extracts were probed by immunoblot for PAR accumulation following temozolomide exposure (Fig. 1A). The level of PAR accumulation was shown to correlate with the extent of the BER defect. PARP activation was elevated in the LN428/MPG cells (an intermediate level of sensitivity), with the highest level of PAR observed 30 minutes following exposure to temozolomide, whereas essentially no PARP activation was observed in the LN428 cells (Fig. 1A). In the more sensitive cell line (LN428/MPG/Polβ-KD), PARP activation was more robust and rapid as compared with that of the LN428/MPG cell line (Fig. 1A), as PAR reached its highest level at 15 minutes after exposure to temozolomide. Comparable results were also observed in a Polβ-defective breast cancer cell line, where elevated temozolomide-induced PARP activation is restricted to the cells with Polβ deficiency (Supplementary Fig. S2B and C). Conversely, exposure to etoposide resulted in a low level of PARP activation at all time points for all three cell lines LN428, LN428/MPG, and LN428/MPG/Polβ-KD (Supplementary Fig. S2D). Thus, PARP activation is elevated in BER-defective (Polβ-deficient) cells following alkylation damage.

Because the combination of alkylating agent treatment and Polβ deficiency triggers PARP activation, we next validated the significance and specificity of this finding by reexpression of Polβ in the LN428/MPG and LN428/MPG/Polβ-KD cells. We find that the BER-deficient phenotype (increased cellular sensitivity to alkylating agents) observed

Published OnlineFirst January 12, 2010; DOI:10.1158/1541-7786.MCR-09-0411

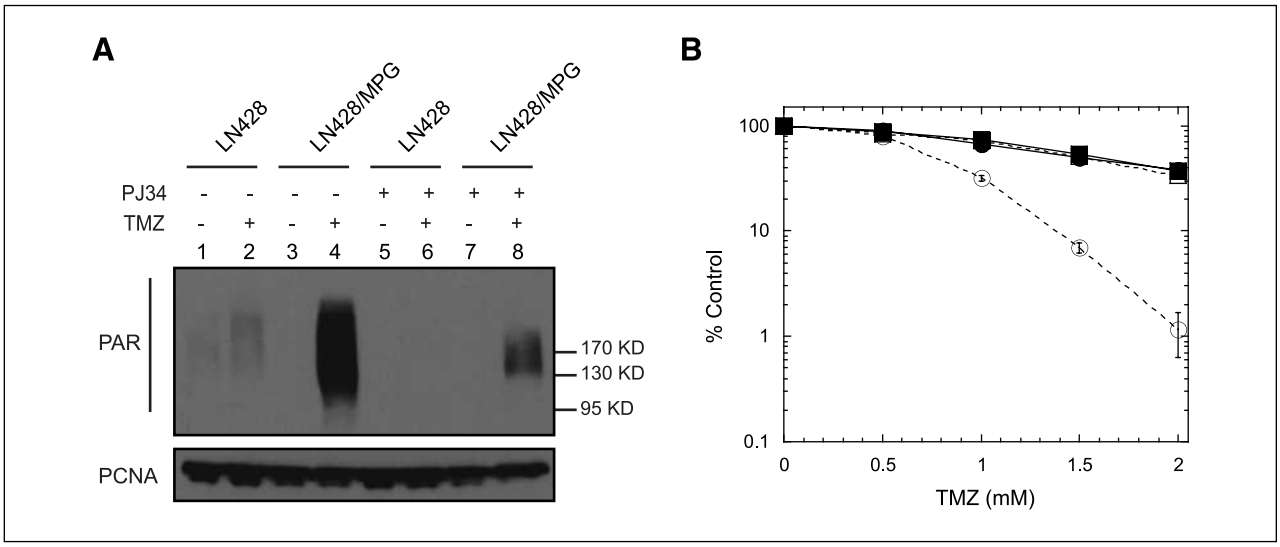

FIGURE 2. PARP activation mediates cellular hypersensitivity in BER-defective cells. **A.** Temozolomide-induced PARP activation in LN428 and LN428/MPG cells in the presence or absence of the PARP1/PARP2 inhibitor PJ34. Cells were pretreated with PJ34 (4 μmol/L) or vehicle control for 30 min before exposure to temozolomide (1.5 mmol/L) plus PJ34 (2 μmol/L) for another 30 min. PCNA was used as a loading control. **B.** Temozolomide-induced cytotoxicity (LN428 and LN428/MPG cell lines) in the presence (*solid lines*) or absence (*dashed lines*) of the PARP1/PARP2 inhibitor PJ34. Viable cells were measured 48 h after exposure as in Fig. 1B. □ and ■, LN428; ○ and ●, LN428/MPG.

in both the LN428/MPG and the LN428/MPG/Polβ-KD cells was reversed by complementation (expression) of FLAG-Polβ(WT) (Fig. 1B, *top*; Supplementary Fig. S1E) but not the 5′-dRP lyase–deficient (K72A) mutant of Polβ (Fig. 1C, *top*). Similarly, we find that complementation with FLAG-Polβ(WT) but not with the Polβ 5′-dRP lyase mutant eliminated the temozolomide-induced activation of PARP observed in BER-defective cells (Fig. 1B and C, *bottom*). These data therefore suggest that the Polβ-specific BER intermediate (5′-dRP lesion) triggers rapid and robust PARP1 activation *in vivo*, triggering the onset of cytotoxicity.

The correlation between PARP activation and alkylation sensitivity prompted us to determine if inhibition of PARP reverses the cellular hypersensitivity of Polβ-deficient human tumor cells. We inhibited activation of PARP by pretreatment and cotreatment with the PARP1/PARP2 inhibitors PJ34 or DR2313. Inhibition of PARP by PJ34 significantly reduced the level of temozolomide-induced PARP activation in the Polβ-deficient cells (LN428/MPG; Fig. 2A, *lanes 3* and *4* and *lanes 7* and *8*). We next assayed if PARP inhibition can rescue the alkylation-sensitive phenotype of LN428/MPG cells, as determined by an MTS assay 48 hours after temozolomide exposure. Most importantly, we find that PARP inhibition by either PJ34 or DR2313 treatment converted the LN428/MPG cells from a sensitive phenotype to a resistant phenotype (Fig. 2B; Supplementary Fig. S3A). Rescue by PARP inhibition was also observed in Polβ-deficient MDA-MB-231 cells (Supplementary Fig. S3B). It remains to be determined if this resistant phenotype is long lived. In photoreceptor, PC12, SH-SY5Y, and HeLa cells, PARP inhibition is cytoprotective, as we observe herein (35-37). Further studies will determine if this resistant phenotype reported here persists or if the BER failure–induced single-strand breaks lead to the formation of DSBs and the onset of apoptosis after several rounds of replication (9). Regardless, these studies support our hypothesis that PARP hyperactivation mediates the alkylation-sensitive phenotype of Polβ-deficient cells.

Unrepaired BER Intermediates (5′-dRP Lesions) Trigger Cell Death via Energy Depletion in the Absence of PAR or PAR Catabolite–Mediated Signaling

Several different mechanisms have been attributed to PARP1 activation–induced cell death. We first evaluated the involvement of caspase-dependent cell death in control cells as compared with the corresponding Polβ-deficient cells following temozolomide treatment. These experiments (Supplementary Fig. S4A and B) rule out a caspase-dependent response due to BER failure, in line with our previous report (27). Although it has been shown that an autophagic response contributes to temozolomide-induced cell death in some cells (38), temozolomide hypersensitivity of Polβ-deficient cells is not affected by the autophagy inhibitor 3-methyladenine (Supplementary Fig. S4C). In support of this observation, we did not observe increased LC3 puncta in BER-defective cells following temozolomide exposure (27).

A major mechanism that has been attributed to PARP activation–induced cell death is direct PAR signaling to the mitochondria, where PAR mediates translocation of AIF from the mitochondria to the nucleus to induce caspase-independent cell death (16-18) via a mechanism that requires receptor (tumor necrosis factor receptor superfamily)–interacting serine-threonine kinase 1 (RIP1) activation (see model; Fig. 3A; ref. 39). RIP1 can be inhibited

Published OnlineFirst January 12, 2010; DOI:10.1158/1541-7786.MCR-09-0411

by necrostatins, small-molecule inhibitors shown to inhibit cell death (40, 41). Therefore, we investigated the role of RIP1 in the PARP-mediated cell death we observed by inhibiting RIP1 with necrostatin-1 (41) and evaluating the effect of RIP1 inhibition on DNA damage–induced cell survival in both control and Polβ-deficient cells. However, inhibition of RIP1 did not prevent cell death in either the parental or the Polβ-deficient cells (Supplementary Fig. S5), suggesting but not proving that AIF translocation may not be related to the observed cell death.

We therefore next evaluated the subcellular localization of AIF in control and Polβ-deficient cells following exposure to the alkylating agents methyl methanesulfonate (MMS) or temozolomide as compared with vehicle (medium) by immunofluorescent staining and confocal microscopy (Fig. 3B) or by subcellular fractionation and immunoblot analysis (Supplementary Fig. S6). In line with the RIP1 inhibition data above, alkylating agent treatment of Polβ-deficient cells did not alter the subcellular localization of AIF (Fig. 3B; Supplementary Fig. S6). All the detectable AIF was localized to the mitochondria in both cell lines regardless of agent or time of exposure (up to 12 hours), thus ruling out PAR as a cell death signal on BER failure.

In the absence of a PAR-mediated cell death process (AIF translocation), it is possible that cell death is initiated via the rapid breakdown of PAR (see Fig. 1A) by the degradative enzyme PARG and the accumulation of the PAR catabolites ADP-ribose, ribose-5-phosphate, and/or AMP (see model; Fig. 3A; ref. 42). ADP-ribose acts as a second

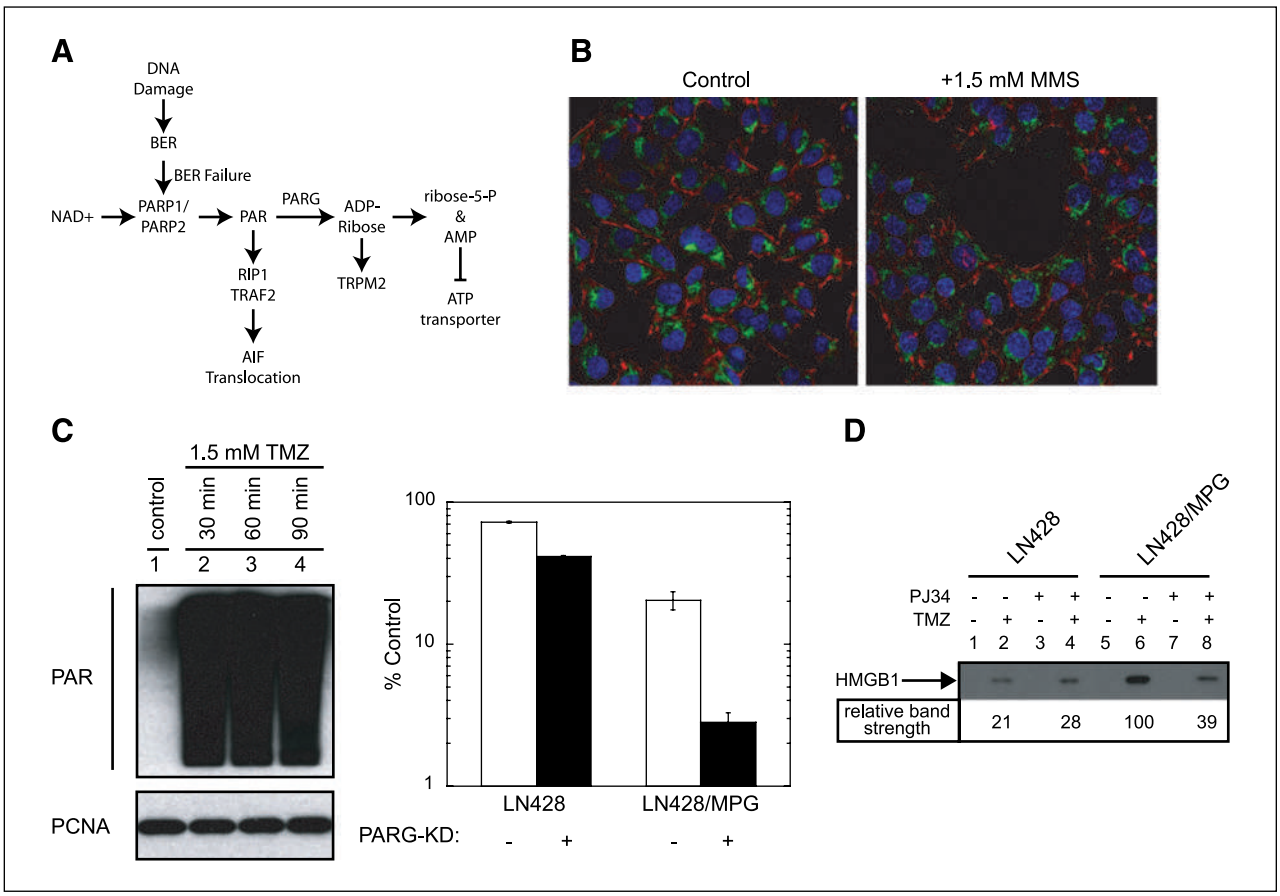

FIGURE 3. Absence of PAR or PAR catabolite–mediated cell death following BER failure. **A.** Model depicting the nexus of BER, the synthesis of PAR, and the generation of PAR catabolites in response to BER failure–induced PARP1/PARP2 hyperactivation. **B.** Absence of mitochondria to nucleus translocation of AIF due to BER failure as determined by confocal microscopy. BER-deficient cells (LN428/MPG) were treated with medium (*left*) or 1.5 mmol/L MMS (*right*) for 1 h and then washed and allowed to recover in medium for 5 h before fixation and staining for AIF (*green*), actin (*red*), and nucleus (*blue*). **C.** PARG-KD prevented degradation of DNA damage–induced PAR. Left, immunoblot of PAR to determine the degradation of PAR in LN428/MPG/PARG-KD cells following treatment with 1.5 mmol/L temozolomide. PCNA protein expression level was shown as a loading control. Right, preventing generation of PAR catabolites from degradation of PAR via PARG-KD enhances temozolomide-induced cytotoxicity. LN428 and LN428/MPG cells with (*black columns*) or without (*white columns*) PARG-KD were exposed to temozolomide (1 mmol/L) or vehicle control (DMSO) for 48 h. Viable cells were determined as in Fig. 1B and reported as percentage relative to vehicle control–treated cells (% control). Columns, mean of three independent experiments; bars, SE. **D.** HMGB1 released into the cell culture medium, as shown by immunoblot. LN428 and LN428/MPG cells were pretreated with PJ34 (4 μmol/L) or vehicle control for 30 min and then exposed to temozolomide (1.5 mmol/L) with or without PJ34 (2 μmol/L) for 12 h. HMGB1 was then captured using immobilized heparin and analyzed by immunoblot, as described in Materials and Methods.

Published OnlineFirst January 12, 2010; DOI:10.1158/1541-7786.MCR-09-0411

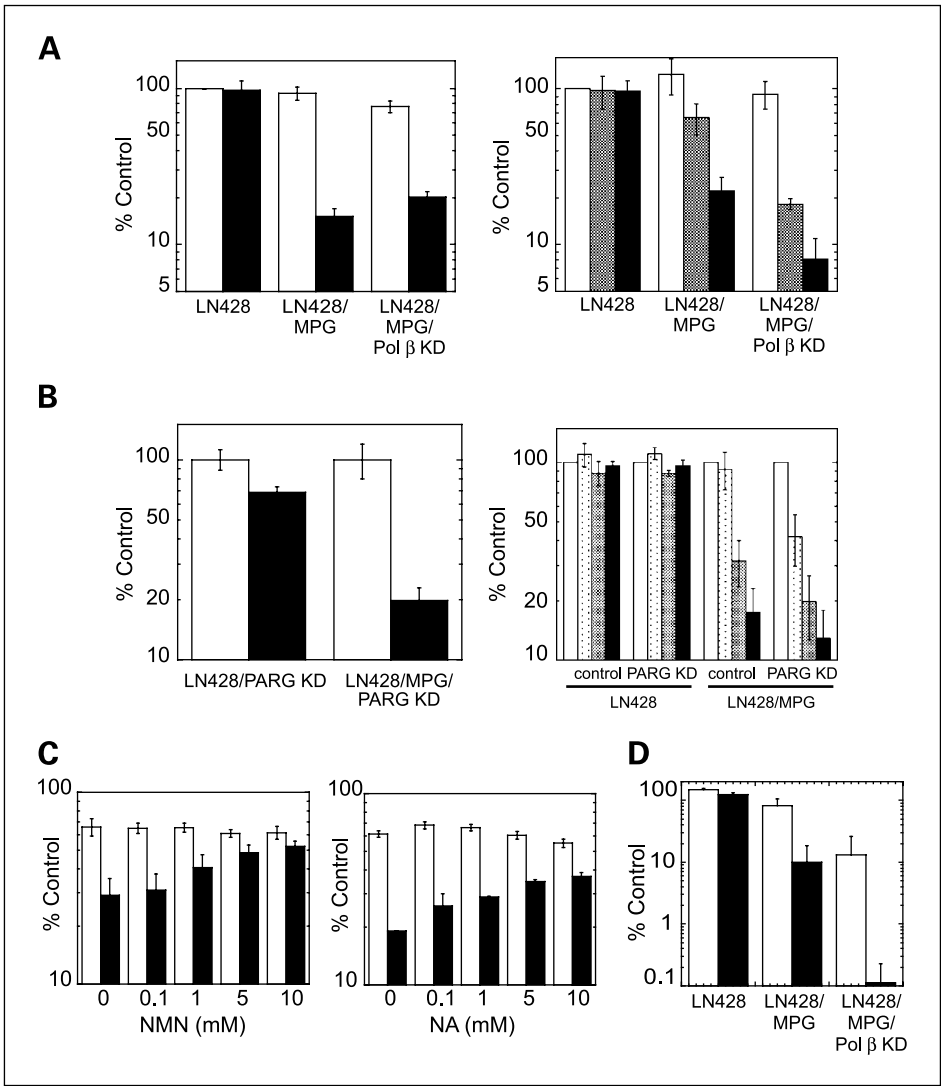

FIGURE 4. BER failure–induced cell death depends on NAD^+ availability. **A.** Alkylation damage promotes NAD^+ and ATP depletion in BER-defective cells. Left, NAD^+ content. Cells were treated with medium (*white columns*) or 0.5 mmol/L MMS (*black columns*) for 1 h before collection for NAD^+ content analysis via enzymatic assay as described in Materials and Methods. Right, ATP content. Cells were treated with medium (*white columns*), 0.5 mmol/L MMS (*gray columns*), or 1.5 mmol/L MMS (*black columns*) for 1 h. ATP content was measured after 1-h recovery in normal medium via the luminescence ATP assay described in Materials and Methods. NAD^+ levels or ATP levels shown are the average of three independent experiments and are reported as percent control of the untreated control cell line. **B.** PARG-KD does not rescue alkylation damage–induced NAD^+ and ATP depletion in BER-defective cells. Left, NAD^+ content. PARG-KD cell lines were treated with medium (*white columns*) or 0.5 mmol/L temozolomide (*black columns*) for 1 h before collection for NAD^+ content analysis as described in Materials and Methods. Right, ATP content. PARG-KD cells were treated with medium (*white columns*), 0.5 mmol/L temozolomide (*dotted columns*), 1.0 mmol/L temozolomide (*gray columns*), or 1.5 mmol/L temozolomide (*black columns*) for 1 h. ATP content was measured after 1-h recovery in normal medium via the luminescence ATP assay described in Materials and Methods. NAD^+ levels or ATP levels shown are the average of three independent experiments and are reported as percent control of the untreated control cell line. **C.** Bioenergetic metabolites rescue Polβ-deficient cells from DNA damage–induced cell death. LN428 and LN428/MPG cells were pretreated with NMN, NA, or vehicle control (medium) for 24 h and then exposed to temozolomide (1 mmol/L) in the presence or absence of NMN or NA for 48 h. Viable cells were measured as in Fig. 1B and reported as percentage relative to vehicle control–treated cells (% control). Columns, mean of three independent experiments; bars, SE. **D.** NAD^+ biosynthesis inhibition augments BER failure–induced cell death. Cells were pretreated for 24 h with a nontoxic 10 nmol/L dose of FK-866 (*black columns*) or DMSO (*white columns*). Cells were then exposed to medium control or MMS (0.5 mmol/L) for 1 h. Viable cells were determined as in Fig. 1B. Columns, mean of three independent experiments; bars, SE.

messenger to activate the cation channel TRPM2 to trigger Ca^{2+} influx, resulting in cell death (19, 20), or inhibits ATP-binding cassette transporters (43), whereas elevated AMP can block ATP transport, leading to ATP depletion and cell death (21). To investigate the possibility that PAR catabolites contribute to PARP-mediated cell death in Polβ-deficient cells, we first blocked Ca^{2+} influx with BAPTA-AM, shown recently by Bentle et al. (44) and Bey et al. (45) to

Published OnlineFirst January 12, 2010; DOI:10.1158/1541-7786.MCR-09-0411

abrogate PARP1 activation–induced cell death. Unlike that observed following DNA damage from reactive oxygen species or oxidative stress, BAPTA-AM did not prevent the elevated damage-induced cell death in Polβ-deficient cells (Supplementary Fig. S7). However, as there may be multiple mechanisms of PAR catabolite–induced cell death, we next knocked down expression of PARG by stable transduction of both cell lines with a lentivirus-expressing shRNA specific to PARG. Expression of PARG mRNA is reduced to 35% as compared with the green fluorescent protein (GFP) control cells when determined by quantitative reverse transcription-PCR (data not shown). Importantly, we found no evidence for PAR-degrading activity in the cells with stable depletion of PARG (Fig. 3C, *left*). When exposed to an alkylating agent, BER-deficient PARG-KD cells accumulate significant levels of PAR with no evidence for PAR degradation (Fig. 3C, *left, lanes 2-4*). This is in contrast to the presence of PARG when the PAR molecule is degraded within 60 to 90 minutes (Fig. 1, *lanes 7-12*). These data show that these PARG-KD cells do not degrade PAR and, hence, do not accumulate PAR catabolites, providing an opportunity to determine if PAR catabolites contribute to cell death in these cells. As shown in Fig. 3C (*right*), PARG-KD did not rescue or reverse the enhanced damage-induced cell death phenotype of Polβ-deficient (LN428/MPG) cells. In fact, PARG-KD cells (*black columns*) were more sensitive to the cell killing effect of the alkylating agent temozolomide as compared with the PARG-expressing cells (*white columns*; Fig. 3C, *right*). The inability of necrostatins to abrogate the response and the lack of PAR-mediated AIF translocation strongly suggest that PAR is not acting as a signaling molecule to induce cell death, as has been suggested (46, 47). Further, the inability of BAPTA-AM and, most importantly, PARG-KD to reverse the alkylation-sensitive phenotype of Polβ-deficient cells also suggests that the observed cell death is unrelated to the accumulation of PAR catabolites such as ADP-ribose or AMP. Finally, one of the hallmarks of caspase-independent cell death is secretion of HMGB1 into the extracellular space (48, 49). A significant level of HMGB1 was secreted into the culture medium following exposure of the BER-defective cells (LN428/MPG) to temozolomide as compared with that of the control LN428 cells (Fig. 3D). HMGB1 release was mediated through PARP activation, likely due to PARP1 modification (49), as PARP inhibition greatly reduced the release of HMGB1 (Fig. 3D). It is unclear how or if HMGB1 release due to failed BER is related to the recently reported role of HMGB1 in BER (50).

An alternate process of cell death due to PARP1 activation was originally proposed by Berger (51, 52) to involve energy (NAD^+ and ATP) depletion, in support of an earlier observation by Jacobson and colleagues (53) showing a decrease in NAD^+ concurrent with an increase in PAR synthesis. We therefore measured NAD^+ and ATP levels in the control (LN428) and Polβ-deficient (LN428/MPG and LN428/MPG/Polβ-KD) cells before and after exposure to MMS or temozolomide. In line with the cytotoxicity and PARP1 activation results described above, exposure of Polβ-deficient cells to MMS or temozolomide led to a rapid and drastic depletion of both NAD^+ and ATP, whereas the NAD^+ and ATP levels in the control cells were not affected (Fig. 4A). We next measured the effect of alkylation damage on the corresponding cells depleted of PARG (PARG-KD). If PAR catabolites trigger cell death, we would expect that NAD^+ and ATP loss would be attenuated in PARG-KD cells. However, exposure of Polβ-deficient PARG-KD cells to temozolomide led to enhanced depletion of both NAD^+ and ATP (Fig. 4B). The absence of PAR or PAR catabolite–mediated cell death, together with the specific loss of NAD^+ and ATP (Fig. 4A) even when the formation of PAR catabolites is prevented (Fig. 4B), suggests that the BER failure response is linked to the cellular bioenergetic capacity of the cell.

For this paradigm to hold, we hypothesized that the availability of bioenergetic metabolites would affect the survival of Polβ-deficient cells exposed to an alkylating agent. In line with this hypothesis, we find that supplementation of the cells with either β-nicotinamide mononucleotide (NMN; ref. 54) or nicotinic acid (NA) reversed the DNA damage–induced phenotype, rendering the Polβ-deficient cells (*black columns*) completely (NMN) or 80% (NA) resistant to the cell killing effects of the alkylating agent as compared with the BER-proficient cells (*white columns*; Fig. 4C). Conversely, we anticipated that the hypersensitive phenotype of Polβ-deficient cells would be exacerbated by a reduction in the cellular level of NAD^+ and related bioenergetic metabolites. We therefore evaluated the effect of transient NAD^+ depletion on the observed BER failure response by pretreating cells with FK-866, a highly specific noncompetitive small-molecule inhibitor of nicotinamide phosphoribosyltransferase, a critical enzyme in the NAD^+ biosynthetic salvage pathway that catalyzes the synthesis of NMN (31). Most importantly, the sensitivity of control cells to alkylation damage was not altered by FK-866 treatment. However, the BER-deficient cells are 9-fold more sensitive to MMS following a nontoxic (10 nmol/L) treatment with FK-866 as compared with the untreated cells (Fig. 4D), although PAR synthesis after the combined FK-866 + MMS treatment is attenuated (Supplementary Fig. S8). These results support our overall hypothesis that the BER failure phenotype of Polβ-deficient cells is mediated by BER intermediate (5′-dRP)–induced PARP1 activation and induction of caspase-independent cell death that is uniquely dependent on the availability of bioenergetic metabolites such as NMN and NAD^+.

Discussion

The requirement for BER in general and Polβ more specifically in the repair of genomic DNA base damage, particularly DNA damage induced by alkylating agents such as the chemotherapeutic temozolomide and the SN1 and SN2 alkylating agents *N*-methyl-*N*′-nitro-*N*-nitrosoguanidine (MNNG) and MMS, respectively (7, 12), elevates the significance of characterizing the mechanism responsible for Polβ deficiency–induced cell death (e.g., a failure to

Published OnlineFirst January 12, 2010; DOI:10.1158/1541-7786.MCR-09-0411

complete repair of the BER intermediate 5′-dRP in the absence of Polβ). As evidenced recently by the development of clinically significant PARP1 inhibitors, identifying BER proteins critical for response to DNA-damaging agents (e.g., chemotherapy) can have broad human health implications. Equally important is a clear understanding of the mechanism(s) that contributes to the enhanced cell death observed on DNA repair inhibition. For example, PARP1 inhibition triggers apoptosis via the accumulation of DSBs (9, 10) and a requirement for homologous recombination proteins such as BRCA1 and BRCA2 (2). To this end, we have developed a unique series of genetically modified human tumor cell lines as models of Polβ deficiency that accumulate the cytotoxic BER intermediate 5′-dRP following exposure to alkylating agents (temozolomide, MMS, and MNNG). By directly comparing BER-defective (Polβ-deficient) and BER-competent isogenic human cell lines, the cellular, biochemical, and signaling responses to DNA base damage can be defined as either global (nonspecific) or BER (Polβ)–specific effects, the latter resulting from a cellular response to the inability to complete BER, referred to herein as BER failure. We have then used this system to define the mechanism of cell death resulting from Polβ loss/inhibition or BER failure and propose and test paradigms to enhance the cell death response.

From these studies, we find that the unrepaired BER intermediates that accumulate on DNA-damaging agent exposure when Polβ is deficient will activate PARP1, leading to a rapid onset of PARP1-dependent, caspase-independent cell death with little or no role for a caspase-dependent or autophagy-dependent process in the response. It remains to be determined if the BER failure–induced cell death observed herein is dependent on extracellular signal-regulated kinase 1/2–mediated PARP1 phosphorylation (55) and SIRT1-regulated deacetylation of PARP1 (56) or if the observed PARP1-induced cell death requires BAX, calpain, and c-Jun NH_2-terminal kinase activation (57). Coincident with damage-induced necrosis in Polβ-deficient cells is PARP1-dependent HMGB1 secretion (49), a hallmark of caspase-independent cell death and inflammation signaling. HMGB1 functions in the extracellular space as a robust RAGE ligand and inflammatory cytokine or damage-associated molecular pattern molecule (48), suggesting that BER failure and the resulting PARP1 activation may trigger an inflammatory response in tissues with a BER imbalance such as ulcerative colitis (58).

There are multiple PARP1 activation–induced cell death mechanisms, as outlined in the diagram shown in Fig. 3A. In one, it is suggested that PAR, the product of PARP1 activation, is a cell death molecule. In this process, PAR initiates the translocation of AIF from the mitochondria to the nucleus by a RIP1-dependent mechanism (Fig. 3A; refs. 16-18, 39). Uniquely, PAR generated due to BER failure does not seem to trigger cell death via RIP1 activation nor does PAR function as a signal to initiate AIF translocation. PARP1 is involved in many DNA repair processes, including homologous recombination and nonhomologous end joining, in response to DSBs and has a role in telomere maintenance (59, 60). The question remains if PAR generated via BER failure is of a unique chemical makeup as compared with PAR generated from DSB-induced PARP1 activation. One possible explanation for the absence of a role for AIF in this study is the concentration of DNA-damaging agents used. In this report, we have used temozolomide or MMS at a maximum concentration of 1.5 mmol/L or MNNG at a concentration of 5 μmol/L, resulting in 90% to 95% cell death in the BER-deficient cells with little or no cell death in the control cells (Supplementary Fig. S2A). Many reports of PAR-induced AIF translocation include MNNG concentrations of 100 and 500 μmol/L (35, 57, 61). Such high concentrations of DNA-damaging gents (e.g., MNNG at 20× and 100× that used herein) have the potential to directly induce DNA DSBs and create overwhelming levels of both nuclear and mitochondrial genome damage (62) as well as the possibility of direct protein alkylation. Regardless, it is clear that the cell death initiated by BER failure is independent of RIP1 activation and AIF translocation, thus ruling out PAR as the cell death signal that is initiated on BER failure.

One explanation for the absence of PAR-mediated cell death is the rapid catabolism of PAR by PARG (42). In this study, we find that PAR synthesized due to PARP activation is degraded within 90 minutes (Fig. 1). As summarized in Fig. 3A, the breakdown products of PAR (PAR catabolites) are also likely mediators of cell death, including ADP-ribose (activator of the Ca^{2+} channel TRPM2) and AMP (inhibitor of ATP transport; refs. 19-21). However, PARG knockdown did not reverse the DNA damage–sensitive phenotype of Polβ-deficient cells (Fig. 3C), suggesting that damage-dependent cell death in Polβ-deficient cells is not initiated by PAR catabolites. Conversely, the PAR catabolite AMP may provide a protective phenotype by activation of AMP kinase, induction of autophagy, and enhanced ATP synthesis, as recently reported following reactive oxygen species–induced DNA damage and PARP1 activation (63). Although loss of AMP kinase activation and induction of autophagy on PARG-KD could explain, in part, the enhanced cell death observed in the PARG-KD cells (Fig. 3C), we suggest this is unlikely because in this study autophagy is not involved (Supplementary Fig. S4C) and the activation of AMP kinase, if any, does not seem to overcome the damage-induced cell death phenotype resulting from BER failure in the PARG-proficient cells. Regardless, it is interesting to speculate that PARG may regulate AMP kinase activation in response to reactive oxygen species–induced PARP1 activation (63). In all, these studies imply that the alkylation-sensitive phenotype of Polβ-deficient cells is unrelated to the accumulation of PAR catabolites, such as ADP-ribose or AMP, and is likely wholly dependent on the metabolite bioavailability or bioenergetic capacity of the cell.

The overriding response to the loss of Polβ and an inability to complete BER (BER failure) is energy failure or depletion of bioenergetic metabolites with no evidence for cell death triggered by PAR or the PAR catabolites ADP-ribose or AMP. The energy collapse or depletion of

Published OnlineFirst January 12, 2010; DOI:10.1158/1541-7786.MCR-09-0411

NAD^+ and ATP due to BER failure is offset by elevated levels of NMN (54) and is negatively affected by NAD^+ biosynthesis inhibition (FK-866), suggesting that (*a*) FK-866 (APO866) and related clinically useful NAD^+ biosynthesis inhibitors might be combined with temozolomide and BER inhibitors to improve temozolomide response and (*b*) any stress on or defects in the NAD^+ biosynthesis pathway such as overactivation of SIRT1 (64) or attenuating defects in nicotinamide phosphoribosyltransferase, NMNAT1, or related NAD biosynthetic enzymes (65) may have significant effects on cell survival following BER failure.

Similar phenotypes (stress-induced PARP1 activation and cell survival dependent on NAD^+ metabolites) have been observed in diverse human cell types and mammalian organ systems, stressing the significance of these findings. PARP1 activation and the resulting "NAD^+ depletion"–mediated or ATP depletion–mediated cell death play critical roles in tissue injury from cerebral and myocardial ischemia (66-69). Analogous to the studies described herein, cellular protection from cerebral ischemia is provided by NAD^+ metabolite supplementation (70, 71). Similarly, streptozotocin-induced diabetes results from PARP1 activation, energy imbalance, and cell death dependent on the BER enzyme MPG (72-75). Most importantly, cellular NAD^+ metabolism plays an essential role in pancreatic β-cell viability and insulin secretion (76). With the observation that BER failure triggers NAD^+ depletion, it is interesting to speculate if overall BER capacity controls susceptibility to ischemia or streptozotocin-induced and age-related diabetes onset via neuronal or β-cell death from loss of bioenergetic metabolites after BER failure. The onset of these physiologically significant outcomes (stroke, neurodegeneration, ischemia, and diabetes) involves PARP1 activation, NAD^+ depletion, and cell death, similar to that reported here. Although a portion of the environmental and endogenous stressors that induce these phenotypes via PARP1 activation will directly induce DNA single-strand breaks, it is reasonable to presume that a significant proportion of cell death related to stroke, retinal degeneration, ischemia, and diabetes may initiate from genomic DNA base damage, requiring repair by the BER machinery. As such, the failure to repair the DNA damage and the resulting accumulation of DNA repair intermediates (BER failure) may be the trigger of PARP1 activation and cell death.

In summary, these studies suggest that PARP1 functions as a BER molecular sensor protein to induce caspase-independent cell death following BER failure and provides mechanistic insight into why Polβ deficiency leads to cell death. Further, we show that the observed DNA damage–dependent cell death in Polβ-deficient cells is unrelated to the accumulation of PAR catabolites, such as ADP-ribose or AMP, yet is dependent on NAD^+ metabolite bioavailability or bioenergetic capacity of the cell, suggesting a linkage between DNA repair capacity, cell survival, and cellular bioenergetic metabolites. Finally, these studies have potentially important implications for therapeutic development as it relates to a chemotherapy-induced synthetic lethality approach to cancer therapy involving the combination of a chemotherapeutic DNA-damaging agent, a DNA repair inhibitor, and a regulator or inhibitor of NAD^+ biosynthesis.

Disclosure of Potential Conflicts of Interest

No potential conflicts of interest were disclosed.

Acknowledgments

We thank Ian Pollack for the LN428 cells; M. Ziegler for the PAR antibody (clone 10H); L. Zhang (University of Pittsburgh, Pittsburgh, PA) for help with the mitochondria isolation; and P. Opresko, L. Niedernhofer, K. Almeida, B. Van Houten, M.K. Jacobson, and M. Ziegler for advice.

Grant Support

American Cancer Society; Susan G. Komen Breast Cancer Foundation; NIH grants 1R01-AG24364, P20-CA103730, R01-NS37704, 1P20-CA132385, and 1P50-CA097190; National Brain Tumor Society; and University of Pittsburgh Cancer Institute (R.W. Sobol) and University of Pittsburgh Department of Pharmacology and Chemical Biology and John S. Lazo Cancer Pharmacology Fellowship (E.M. Goellner).

The costs of publication of this article were defrayed in part by the payment of page charges. This article must therefore be hereby marked *advertisement* in accordance with 18 U.S.C. Section 1734 solely to indicate this fact.

Received 9/11/09; revised 11/5/09; accepted 11/8/09; published OnlineFirst 1/12/10.

References

1. Sarkaria JN, Kitange GJ, James CD, et al. Mechanisms of chemoresistance to alkylating agents in malignant glioma. Clin Cancer Res 2008;14:2900–8.
2. Ashworth A. A synthetic lethal therapeutic approach: poly(ADP) ribose polymerase inhibitors for the treatment of cancers deficient in DNA double-strand break repair. J Clin Oncol 2008;26:3785–90.
3. Almeida KH, Sobol RW. A unified view of base excision repair: lesion-dependent protein complexes regulated by post-translational modification. DNA Repair 2007;6:695–711.
4. Paik J, Duncan T, Lindahl T, Sedgwick B. Sensitization of human carcinoma cells to alkylating agents by small interfering RNA suppression of 3-alkyladenine-DNA glycosylase. Cancer Res 2005;65:10472–7.
5. Sobol RW, Watson DE, Nakamura J, et al. Mutations associated with base excision repair deficiency and methylation-induced genotoxic stress. Proc Natl Acad Sci U S A 2002;99:6860–5.
6. Liu L, Gerson SL. Therapeutic impact of methoxyamine: blocking repair of abasic sites in the base excision repair pathway. Curr Opin Investig Drugs 2004;5:623–7.

Published OnlineFirst January 12, 2010; DOI:10.1158/1541-7786.MCR-09-0411

7. Sobol RW, Horton JK, Kuhn R, et al. Requirement of mammalian DNA polymerase-β in base-excision repair. Nature 1996;379:183–6.
8. Palma JP, Rodriguez LE, Bontcheva-Diaz VD, et al. The PARP inhibitor, ABT-888 potentiates temozolomide: correlation with drug levels and reduction in PARP activity *in vivo*. Anticancer Res 2008;28: 2625–35.
9. Liu X, Shi Y, Guan R, et al. Potentiation of temozolomide cytotoxicity by poly(ADP)ribose polymerase inhibitor ABT-888 requires a conversion of single-stranded DNA damages to double-stranded DNA breaks. Mol Cancer Res 2008;6:1621–9.
10. Peralta-Leal A, Rodriguez MI, Oliver FJ. Poly(ADP-ribose)polymerase-1 (PARP-1) in carcinogenesis: potential role of PARP inhibitors in cancer treatment. Clin Transl Oncol 2008;10:318–23.
11. Stegh AH, Chin L, Louis DN, DePinho RA. What drives intense apoptosis resistance and propensity for necrosis in glioblastoma? A role for Bcl2L12 as a multifunctional cell death regulator. Cell Cycle 2008; 7:2833–9.
12. Trivedi RN, Almeida KH, Fornsaglio JL, Schamus S, Sobol RW. The role of base excision repair in the sensitivity and resistance to temozolomide mediated cell death. Cancer Res 2005;65:6394–400.
13. Hegi ME, Liu L, Herman JG, et al. Correlation of O^6-methylguanine methyltransferase (MGMT) promoter methylation with clinical outcomes in glioblastoma and clinical strategies to modulate MGMT activity. J Clin Oncol 2008;26:4189–99.
14. Zong WX, Ditsworth D, Bauer DE, Wang ZQ, Thompson CB. Alkylating DNA damage stimulates a regulated form of necrotic cell death. Genes Dev 2004;18:1272–82.
15. Cohausz O, Blenn C, Malanga M, Althaus FR. The roles of poly(ADP-ribose)-metabolizing enzymes in alkylation-induced cell death. Cell Mol Life Sci 2008;65:644–55.
16. Kolthur-Seetharam U, Dantzer F, McBurney MW, de Murcia G, Sassone-Corsi P. Control of AIF-mediated cell death by the functional interplay of SIRT1 and PARP-1 in response to DNA damage. Cell Cycle 2006;5:873–7.
17. Yu SW, Andrabi SA, Wang H, et al. Apoptosis-inducing factor mediates poly(ADP-ribose) (PAR) polymer-induced cell death. Proc Natl Acad Sci U S A 2006;103:18314–9.
18. Yu SW, Wang H, Poitras MF, et al. Mediation of poly(ADP-ribose) polymerase-1-dependent cell death by apoptosis-inducing factor. Science 2002;297:259–63.
19. Buelow B, Song Y, Scharenberg AM. The poly(ADP-ribose) polymerase PARP-1 is required for oxidative stress-induced TRPM2 activation in lymphocytes. J Biol Chem 2008;283:24571–83.
20. Fonfria E, Marshall IC, Benham CD, et al. TRPM2 channel opening in response to oxidative stress is dependent on activation of poly(ADP-ribose) polymerase. Br J Pharmacol 2004;143:186–92.
21. Formentini L, Macchiarulo A, Cipriani G, et al. Poly(ADP-ribose) catabolism triggers AMP-dependent mitochondrial energy failure. J Biol Chem 2009;284:17668–76.
22. Sobol RW, Prasad R, Evenski A, et al. The lyase activity of the DNA repair protein β-polymerase protects from DNA-damage-induced cytotoxicity. Nature 2000;405:807–10.
23. Ochs K, Lips J, Profittlich S, Kaina B. Deficiency in DNA polymerase β provokes replication-dependent apoptosis via DNA breakage, Bcl-2 decline and caspase-3/9 activation. Cancer Res 2002;62:1524–30.
24. Horton JK, Stefanick DF, Wilson SH. Involvement of poly(ADP-ribose) polymerase activity in regulating Chk1-dependent apoptotic cell death. DNA Repair (Amst) 2005;4:1111–20.
25. Park MJ, Kim MS, Park IC, et al. PTEN suppresses hyaluronic acid-induced matrix metalloproteinase-9 expression in U87MG glioblastoma cells through focal adhesion kinase dephosphorylation. Cancer Res 2002;62:6318–22.
26. Ishii N, Maier D, Merlo A, et al. Frequent co-alterations of TP53, p16/CDKN2A, p14ARF, PTEN tumor suppressor genes in human glioma cell lines. Brain Pathol 1999;9:469–79.
27. Trivedi RN, Wang XH, Jelezcova E, Goellner EM, Tang J, Sobol RW. Human methyl purine DNA glycosylase and DNA polymerase β expression collectively predict sensitivity to temozolomide. Mol Pharmacol 2008;74:505–16.
28. Parsons JL, Tait PS, Finch D, et al. Ubiquitin ligase ARF-BP1/Mule modulates base excision repair. EMBO J 2009;28:3207–15.
29. Poeschla EM, Wong-Staal F, Looney DJ. Efficient transduction of nondividing human cells by feline immunodeficiency virus lentiviral vectors. Nat Med 1998;4:354–7.
30. Sobol RW. Temozolomide. In: Schwab M, editor. Encyclopedia of cancer. 2nd ed. Berlin, Heidelberg, New York: Springer; 2009.
31. Hasmann M, Schemainda I. FK866, a highly specific noncompetitive inhibitor of nicotinamide phosphoribosyltransferase, represents a novel mechanism for induction of tumor cell apoptosis. Cancer Res 2003;63:7436–42.
32. Rubinson DA, Dillon CP, Kwiatkowski AV, et al. A lentivirus-based system to functionally silence genes in primary mammalian cells, stem cells and transgenic mice by RNA interference. Nat Genet 2003;33:401–6.
33. Palumbo R, Sampaolesi M, De Marchis F, et al. Extracellular HMGB1, a signal of tissue damage, induces mesoangioblast migration and proliferation. J Cell Biol 2004;164:441–9.
34. Dantzer F, Ame JC, Schreiber V, Nakamura J, Menissier-de Murcia J, de Murcia G. Poly(ADP-ribose) polymerase-1 activation during DNA damage and repair. Methods Enzymol 2006;409:493–510.
35. Ethier C, Labelle Y, Poirier GG. PARP-1-induced cell death through inhibition of the MEK/ERK pathway in MNNG-treated HeLa cells. Apoptosis 2007;12:2037–49.
36. Paquet-Durand F, Silva J, Talukdar T, et al. Excessive activation of poly(ADP-ribose) polymerase contributes to inherited photoreceptor degeneration in the retinal degeneration 1 mouse. J Neurosci 2007; 27:10311–9.
37. Iwashita A, Yamazaki S, Mihara K, et al. Neuroprotective effects of a novel poly(ADP-ribose) polymerase-1 inhibitor, 2-{3-[4-(4-chlorophenyl)-1-piperazinyl] propyl}-4(3*H*)-quinazolinone (FR255595), in an *in vitro* model of cell death and in mouse 1-methyl-4-phenyl-1,2,3,6-tetrahydropyridine model of Parkinson's disease. J Pharmacol Exp Ther 2004;309:1067–78.
38. Kanzawa T, Germano IM, Komata T, Ito H, Kondo Y, Kondo S. Role of autophagy in temozolomide-induced cytotoxicity for malignant glioma cells. Cell Death Differ 2004;11:448–57.
39. Xu Y, Huang S, Liu ZG, Han J. Poly(ADP-ribose) polymerase-1 signaling to mitochondria in necrotic cell death requires RIP1/TRAF2-mediated JNK1 activation. J Biol Chem 2006;281:8788–95.
40. Xu X, Chua CC, Kong J, et al. Necrostatin-1 protects against glutamate-induced glutathione depletion and caspase-independent cell death in HT-22 cells. J Neurochem 2007;103:2004–14.
41. Degterev A, Hitomi J, Germscheid M, et al. Identification of RIP1 kinase as a specific cellular target of necrostatins. Nat Chem Biol 2008;4:313–21.
42. Bonicalzi ME, Haince JF, Droit A, Poirier GG. Regulation of poly (ADP-ribose) metabolism by poly(ADP-ribose) glycohydrolase: where and when? Cell Mol Life Sci 2005;62:739–50.
43. Dumitriu IE, Voll RE, Kolowos W, et al. UV irradiation inhibits ABC transporters via generation of ADP-ribose by concerted action of poly(ADP-ribose) polymerase-1 and glycohydrolase. Cell Death Differ 2004;11:314–20.
44. Bentle MS, Reinicke KE, Bey EA, Spitz DR, Boothman DA. Calcium-dependent modulation of poly(ADP-ribose) polymerase-1 alters cellular metabolism and DNA repair. J Biol Chem 2006;281: 33684–96.
45. Bey EA, Bentle MS, Reinicke KE, et al. An NQO1- and PARP-1-mediated cell death pathway induced in non-small-cell lung cancer cells by β-lapachone. Proc Natl Acad Sci U S A 2007;104:11832–7.
46. Heeres JT, Hergenrother PJ. Poly(ADP-ribose) makes a date with death. Curr Opin Chem Biol 2007;11:644–53.
47. Andrabi SA, Kim NS, Yu SW, et al. Poly(ADP-ribose) (PAR) polymer is a death signal. Proc Natl Acad Sci U S A 2006;103:18308–13.
48. Lotze MT, Tracey KJ. High-mobility group box 1 protein (HMGB1): nuclear weapon in the immune arsenal. Nat Rev 2005;5:331–42.
49. Ditsworth D, Zong WX, Thompson CB. Activation of poly(ADP)-ribose polymerase (PARP-1) induces release of the pro-inflammatory mediator HMGB1 from the nucleus. J Biol Chem 2007;282:17845–54.
50. Prasad R, Liu Y, Deterding LJ, et al. HMGB1 is a cofactor in mammalian base excision repair. Mol Cell 2007;27:829–41.
51. Berger NA. Poly(ADP-ribose) in the cellular response to DNA damage. Radiat Res 1985;101:4–15.

Published OnlineFirst January 12, 2010; DOI:10.1158/1541-7786.MCR-09-0411

52. Berger NA, Sims JL, Catino DM, Berger SJ. Poly(ADP-ribose) polymerase mediates the suicide response to massive DNA damage: studies in normal and DNA-repair defective cells. Princess Takamatsu Symp 1983;13:219–26.
53. Jacobson MK, Levi V, Juarez-Salinas H, Barton RA, Jacobson EL. Effect of carcinogenic *N*-alkyl-*N*-nitroso compounds on nicotinamide adenine dinucleotide metabolism. Cancer Res 1980;40:1797–802.
54. Formentini L, Moroni F, Chiarugi A. Detection and pharmacological modulation of nicotinamide mononucleotide (NMN) *in vitro* and *in vivo*. Biochem Pharmacol 2009;77:1612–20.
55. Kauppinen TM, Chan WY, Suh SW, Wiggins AK, Huang EJ, Swanson RA. Direct phosphorylation and regulation of poly(ADP-ribose) polymerase-1 by extracellular signal-regulated kinases 1/2. Proc Natl Acad Sci U S A 2006;103:7136–41.
56. Rajamohan SB, Pillai VB, Gupta M, et al. SIRT1 promotes cell survival under stress by deacetylation-dependent deactivation of poly (ADP-ribose) polymerase 1. Mol Cell Biol 2009;29:4116–29.
57. Moubarak RS, Yuste VJ, Artus C, et al. Sequential activation of poly (ADP-ribose) polymerase 1, calpains, and Bax is essential in apoptosis-inducing factor-mediated programmed necrosis. Mol Cell Biol 2007;27:4844–62.
58. Hofseth LJ, Khan MA, Ambrose M, et al. The adaptive imbalance in base excision-repair enzymes generates microsatellite instability in chronic inflammation. J Clin Invest 2003;112:1887–94.
59. Schreiber V, Dantzer F, Ame JC, de Murcia G. Poly(ADP-ribose): novel functions for an old molecule. Nat Rev Mol Cell Biol 2006;7:517–28.
60. Hassa PO, Haenni SS, Elser M, Hottiger MO. Nuclear ADP-ribosylation reactions in mammalian cells: where are we today and where are we going? Microbiol Mol Biol Rev 2006;70:789–829.
61. Wang Y, Kim NS, Li X, et al. Calpain activation is not required for AIF translocation in PARP-1-dependent cell death (parthanatos). J Neurochem 2009;110:687–96.
62. LeDoux SP, Wilson GL, Beecham EJ, Stevnsner T, Wassermann K, Bohr VA. Repair of mitochondrial DNA after various types of DNA damage in Chinese hamster ovary cells. Carcinogenesis 1992;13:1967–73.
63. Huang Q, Wu YT, Tan HL, Ong CN, Shen HM. A novel function of poly(ADP-ribose) polymerase-1 in modulation of autophagy and necrosis under oxidative stress. Cell Death Differ 2009;16:264–77.
64. Dali-Youcef N, Lagouge M, Froelich S, Koehl C, Schoonjans K, Auwerx J. Sirtuins: the 'magnificent seven', function, metabolism and longevity. Ann Med 2007;39:335–45.
65. Berger F, Lau C, Dahlmann M, Ziegler M. Subcellular compartmentation and differential catalytic properties of the three human nicotinamide mononucleotide adenylyltransferase isoforms. J Biol Chem 2005;280:36334–41.
66. Pieper AA, Walles T, Wei G, et al. Myocardial postischemic injury is reduced by polyADPripose polymerase-1 gene disruption. Mol Med 2000;6:271–82.
67. Endres M, Wang ZQ, Namura S, Waeber C, Moskowitz MA. Ischemic brain injury is mediated by the activation of poly(ADP-ribose)polymerase. J Cereb Blood Flow Metab 1997;17:1143–51.
68. Eliasson MJ, Sampei K, Mandir AS, et al. Poly(ADP-ribose) polymerase gene disruption renders mice resistant to cerebral ischemia. Nat Med 1997;3:1089–95.
69. Ha HC, Snyder SH. Poly(ADP-ribose) polymerase is a mediator of necrotic cell death by ATP depletion. Proc Natl Acad Sci U S A 1999;96:13978–82.
70. Wang S, Xing Z, Vosler PS, et al. Cellular NAD replenishment confers marked neuroprotection against ischemic cell death: role of enhanced DNA repair. Stroke 2008;39:2587–95.
71. Liu D, Gharavi R, Pitta M, Gleichmann M, Mattson MP. Nicotinamide prevents NAD^+ depletion and protects neurons against excitotoxicity and cerebral ischemia: NAD^+ consumption by SIRT1 may endanger energetically compromised neurons. Neuromolecular Med 2009;11:28–42.
72. Masutani M, Suzuki H, Kamada N, et al. Poly(ADP-ribose) polymerase gene disruption conferred mice resistant to streptozotocin-induced diabetes. Proc Natl Acad Sci U S A 1999;96:2301–4.
73. Cardinal JW, Margison GP, Mynett KJ, Yates AP, Cameron DP, Elder RH. Increased susceptibility to streptozotocin-induced β-cell apoptosis and delayed autoimmune diabetes in alkylpurine-DNA-*N*-glycosylase-deficient mice. Mol Cell Biol 2001;21:5605–13.
74. Burns N, Gold B. The effect of 3-methyladenine DNA glycosylase-mediated DNA repair on the induction of toxicity and diabetes by the β-cell toxicant streptozotocin. Toxicol Sci 2007;95:391–400.
75. Pieper AA, Brat DJ, Krug DK, et al. Poly(ADP-ribose) polymerase-deficient mice are protected from streptozotocin-induced diabetes. Proc Natl Acad Sci U S A 1999;96:3059–64.
76. Garten A, Petzold S, Korner A, Imai S, Kiess W. Nampt: linking NAD biology, metabolism and cancer. Trends Endocrinol Metab 2009;20:130–8.

Supplemental Material

Supplemental Data include Figure S1-S8, the figure legends, Materials & Methods and Table S1.

Materials and Methods

Chemicals and reagents

MMS, Etoposide and 3-Methyladenine were from Sigma-Aldrich. MNNG (CAS# 70-25-7; IUPAC 1-methyl-2-nitro-1-nitrosoguanidine) was obtained from TCI America (Cat# M0527), dissolved in DMSO to a stock concentration of 10mM, filtered through a 0.22uM filter and stored until needed at -20˚C. DR2313 and Z-VAD.fmk were purchased from Calbiochem. BAPTA-AM was obtained from InVitrogen (cat# B-1205). Necrostatin-1 was obtained from Sigma (cat# N9037).

Caspase-3 and caspase-9 activation assay

Caspase-3 and caspase-9 activation was measured using a caspase-3 and caspase-9 colorimetric activity assay kit as described earlier (1). Briefly, the assay is based on the spectrophotometric identification of p-nitroaniline (pNA) after cleavage of a labeled DEVD-Pna (caspase-3) or LEHD-Pna (caspase-9) substrate. For the caspase-3 and caspase-9 activation assay, 0.75 $x10^6$ cells were seeded in 100mm dishes. 24 hours after seeding, the cells (LN428 and LN428/MPG) were treated with 3.0 mM and 1.5 mM TMZ, respectively (corresponding to equitoxic dose of TMZ for each cell line) or media for 24 hours. Separately, cells were also treated with 60 μM ETO or media for 24 hours. After induction of apoptosis with TMZ or ETO, the cell pellet (containing approximately $2x10^6$ cells) was re-suspended in 1x cell lysis buffer and the supernatant (cytosolic extract) was used to measure caspase-3 or caspase-9 activation. Samples were mixed with assay mixture in a 96-well plate and incubated for 2 hours at 37˚C and absorbance was measured at 405nm. The fold increase in

caspase-3 or caspase-9 activation was calculated by comparing the OD from the TMZ or ETO samples with the OD from the untreated control samples.

Subcellular fractionation and analysis of AIF expression

Cells were seeded into 100 mm cell culture dishes at 3 X 10^6 cells / dish. 24 hours later, cells were treated with TMZ (1.5 mM) for different periods of time before washing with cold PBS and subjecting to subcellular fractionation, essentially as described (2). Briefly, following treatment and washing, cells were collected by scraping using a rubber scraper. Cells were pelleted (400g, 5 min at 4˚C). The cell pellet was resuspended in 1 ml of cold homogenization buffer (0.25 M Sucrose, 10 mM HEPES pH 7.4, 1 mM EGTA) and the cell suspension was homogenized in a 2 ml Wheaton Dounce Homogenizer on ice. The homogenate was centrifuged at 1,000 x g for 15 minutes at 4˚C to obtain the nuclear pellet, and the supernatant was then centrifuged at 10,000 x g for 15 minutes at 4˚C to pellet mitochondria.

Cell cytotoxicity assay

TMZ or etoposide (ETO) induced cytotoxicity was determined by an MTS assay, a modified MTT assay as described previously (3). Results were calculated from the average of three or four separate experiments and are reported as the percentage of treated cells relative to the cells without treatment (% Control). For PJ34, DR2313, Z-VAD.fmk, 3-Methyladenine (3-MA), Necrostatin-1 and BAPTA-AM, cells were pre-exposed to those inhibitors for 30 minutes (PJ34, DR2313, Necrostatin-1 and BAPTA-AM) or one hour (Z-VAD.fmk and 3-MA) and were then treated with TMZ in the presence of those inhibitors for 48 hours. The impact on cell growth and survival was determined by an MTS assay, as described previously (3).

Figure Legends

Figure S1. Alkylation sensitivity mediated by a deficiency in Pol ß-mediated DNA repair

(A) Characterization of glioma cell lines. Expression level of BER proteins including MPG, Pol ß and APE1 are shown for LN428 glioma cells (LN428), LN428 cells transduced by GFP expressing lentivirus (LN428/GFP), LN428 cells transfected with plasmid pIRES.neo.MPG to over-express MPG (LN428/MPG), MPG over-expressing glioma cells expressing GFP (LN428/MPG/GFP) or co-expressing GFP and Pol ß shRNA (LN428/MPG/Polß-KD). PCNA was used as a loading control.

(B) Cell sensitivity to TMZ. Cells were cultured in 96-well plates for 24 hours prior to exposure to TMZ, measured as in Figure 1B. [LN428, open square; LN428/MPG, open circle; LN428/MPG/Polß-KD, open diamond]

(C) Cell sensitivity to etoposide (ETO) exposure for 48 hours. Viable cells were measured as in (B). [LN428, open square; LN428/MPG, open circle; LN428/MPG/Polß-KD, open diamond]

(D) (*Upper panel*) Cellular cytotoxicity due to TMZ treatment in LN428 cells over-expressing either WT or a glycosylase activity null mutant of MPG (N169D) following 48 hours exposure to TMZ. Viable cells were measured as in (B). [LN428, open square; LN428/VC, filled square; LN428/MPG, open circle; LN428/MPG-mut, filled circle] (*Lower panel*) Western blots showing over-expression of mutant N169D-MPG (lane 2) as compared to LN428 cells transfected with the vehicle control (lane 1).

(E) (*Upper panel*) Cellular cytotoxicity due to TMZ treatment in LN428/MPG/Polß-KD cells complemented with Flag tagged WT Pol ß (clone 2 and 6) following 48 hours exposure to TMZ. Viable cells were measured as in (B). [LN428, open square; LN428/MPG, open circle; LN428/MPG/Polß-KD, open diamond; LN428/MPG/Flag-Polß-WT, filled triangle; LN428/ MPG/Polß-KD /Flag-Polß-WT, filled triangle] (*Lower panel*) Over-expression of Flag tagged Pol ß (WT) in the LN428/MPG/Polß-KD cell line. An immunoblot from two representative clones (clone 2 and 6; lanes 4 and 5) are shown, compared to LN428/MPG cells (lane 1), LN428/MPG/Polß-KD cells (lane 2) and LN428/MPG/Polß-KD cells transfected with the vehicle control (lane 3).

Figure S2.

(A) Hypersensitivity of Pol ß deficient cells to TMZ, MMS and MNNG. Control cells (LN428, open bars) were resistant to alkylating agents, while the Pol ß deficient cells (LN428/MPG, black bars) were significantly more sensitive. Cells were exposed to 1500μM TMZ, 1500μM MMS or 5μM MNNG for 48 hrs. Cell survival was determined by an MTS assay, while percent survival was normalized to untreated control cells, as in Figure 1B. Results are reported as the mean from three independent experiments and error bars represent SEM.

(B) TMZ induced PARP1 activation in a breast cancer cell line (MDA-MB-231) and a cell line with both elevated MPG expression and reduced Pol ß level (MDA-MB-231/MPG/Pol ß KD). Cells were exposed to 1.5 mM TMZ for 15 or 30 min and cells without treatment were used as control (0 min). PARP1 and PCNA protein expression levels are also shown.

(C) TMZ induced cytotoxicity in MDA-MB-231, MDA-MB-231/MPG and MDA-MB-231/MPG/Pol ß cells, measured as in Figure 1B. [MDA-MB-231, open square; MDA-MB-231/MPG, open circle and MDA-MB-231/MPG/Pol ß KD, open diamond]

(D) Immunoblot of PAR to determine activation of PARP1 after exposure of LN428, LN428/MPG and LN428/MPG/Pol ß KD cells to 50μM etoposide (ETO) for the time indicated.

Figure S3.

(A) TMZ induced cytotoxicity (LN428 and LN428/MPG cell lines) in the presence (solid lines) or absence (dashed lines) of the PARP1/PARP2 inhibitor DR2313. Viable cells were measured 48 hours after exposure as in Figure 1B. [LN428, open and filed square; LN428/MPG, open and filled circle]

(B) TMZ induced cytotoxicity in MDA-MB-231, MDA-MB-231/MPG and MDA-MB-231/MPG/Polß-KD cell lines in the presence (solid lines) or absence (dashed lines) of PJ34. Viable cells were measured 48 hours after exposure as in Figure 1B. [MDA-MB-231, open and filed square; MDA-MB-231/MPG, open and filled circle; MDA-MB-231/MPG/Polß-KD, open and filled diamond]

Figure S4.

(A) TMZ-induced cytotoxicity in LN428 and LN428/MPG cells with or without 50 μM of pan caspase inhibitor Z-VAD.fmk. Viable cells were measured 48 hours after exposure as in Figure 1B. [LN428, open square; LN428 + Z-VAD.fmk, filled square; LN428/MPG, open circle; LN428/MPG + Z-VAD.fmk, filled circle]

(B) TMZ or ETO induced caspase-9 activation in LN428 and LN428/MPG cells 24 hours after exposure to TMZ or ETO.

(C) TMZ-induced cytotoxicity in LN428 and LN428/MPG cells with or without pre-treatment with the autophagy inhibitor 3-MA (4 mM). Viable cells were measured 48 hours after exposure as in Figure 1B. [LN428, open square; LN428 + 3-MA, filled square; LN428/MPG, open circle; LN428/MPG + 3-MA, filled circle]

Figure S5.

Inhibition of RIP1 by necrostatin-1 does not protect cells from TMZ-induced cytotoxicity. Cells were pre-treated with necrostatin-1 or vehicle control (DMSO) for 30 minutes and were then exposed to TMZ in the presence or absence of necrostatin-1 (100 μM) for 48 hours. Viable cells were measured 48 hours after exposure as in Figure 1B. [LN428, open square; LN428 + necrostatin-1, filled square; LN428/MPG, open circle; LN428/MPG + necrostatin-1, filled circle]

Figure S6.

Absence of mitochondria to nucleus translocation of AIF due to BER failure as determined by subcellular fractionation and immunoblot analysis. Cells were treated with 1.5 mM TMZ for times indicated in the figure and subjected to subcellular fractionation and immunoblot analysis. COX IV and PCNA were used as controls to show no cross contamination between mitochondrial and nuclear fractions. COX IV and PCNA were also used as loading controls to show that equal amount of mitochondrial or nuclear samples were loaded.

Figure S7.

Inhibition of Ca^{2+} influx by BAPTA.AM does not protect cells from TMZ-induced cytotoxicity. Cells were pre-treated with BAPTA.AM or vehicle control (DMSO) for 30 minutes and were then exposed to TMZ in the presence or absence of BAPTA.AM (5 mM) for 48 hours. Viable cells were determined as in Figure 1B. Results were reported as the mean of three independent experiments ± S.E.M. [LN428, open square; LN428 + BAPTA.AM, filled square; LN428/MPG, open circle; LN428/MPG + BAPTA.AM, filled circle]

Figure S8.

FK-866 prevents BER failure induced PAR synthesis. Cells were pretreated with FK-866 (10nM) or DMSO control for 24 hours prior to exposure to MMS (1.5mM). PAR synthesis at multiple time points post exposure was measured via immunoblot. PARP1 immunoblot is provided as loading control.

Table S1: Cell lines developed and used in this study

Cell Line Name	Clone #	Cell line Description	Growth Media
LN428	-	Human glioma cell line	Alpha EMEM, heat-inactivated fetal bovine serum (10%), glutamine (2 mM), antibotic d antimycotic, gentamicin (50 µg/ml).
LN428/Pol ß KD	-	LN428 cells expressing Pol ß shRNA and cop-GFP	LN428 cell growth media
LN428//MPG	7	LN428 cells modified for over-expression of human MPG	LN428 cell growth media + 600 µg/ml neomycin
LN428//MPG/ Pol ß KD	-	LN428/MPG cells expressing Pol ß shRNA and cop-GFP	LN428 cell growth media + 600 µg/ml neomycin
LN428/MPG/GFP	-	LN428/MPG cells expressing cop-GFP	LN428 cell growth media + 600 µg/ml neomycin
LN428/VC*	1	LN428 cells transfected with vector control plasmid pIRES-neo	LN428 cell growth media + 600 µg/ml neomycin
LN428/MPG/VC*	2	LN428/MPG cells transfected with vector control plasmid pIRES-puro	LN428 cell growth media + 600 µg/ml neomycin + 0.5 µg/ml puromycin
LN428/MPG/Pol ß KD/VC*	3	LN428/MPG/Pol ß KD cells transfected with vector control plasmid pIRES-puro	LN428 cell growth media + 600 µg/ml neomycin + 0.5 µg/ml puromycin
LN428/MPG-N169D	11	LN428 cells modified to express glycosylase dead mutant (N169D) MPG	LN428 cell growth media + 600 µg/ml neomycin
LN428/MPG/Flag-Pol ß-WT*	1	LN428/MPG cells expressing Flag tagged WT Pol ß	LN428 cell growth media + 600 µg/ml neomycin + 0.5 µg/ml puromycin
	6		
LN428/MPG/Flag-Pol ß-K72A	5	LN428/MPG cells expressing Flag tagged 5'dRP lyase activity dead mutant (K72A) Pol ß	LN428 cell growth media + 600 µg/ml neomycin + 0.5 µg/ml puromycin
	16		
LN428/MPG/Pol ß KD/Flag-Pol ß-WT*	2	LN428/MPG/Pol ß KD cells expressing Flag tagged WT Pol ß	LN428 cell growth media + 600 µg/ml neomycin + 0.5 µg/ml puromycin
	6		
LN428/PARG KD	-	LN428 cells expressing PARG shRNA and cop-GFP	LN428 cell growth media + 0.5 µg/ml puromycin
LN428/MPG/PARG KD	-	LN428/MPG cells expressing PARG shRNA and cop-GFP	LN428 cell growth media + 600 µg/ml neomycin + 0.5 µg/ml puromycin

*VC: vector control.
*WT: wild type.

References

1. Trivedi RN, Wang XH, Jelezcova E, Goellner EM, Tang J, Sobol RW. Human methyl purine DNA glycosylase and DNA polymerase ß expression collectively predict sensitivity to temozolomide. Molecular Pharmacology 2008;74(2):505-16.
2. Yu J, Wang P, Ming L, Wood MA, Zhang L. SMAC/Diablo mediates the proapoptotic function of PUMA by regulating PUMA-induced mitochondrial events. Oncogene 2007;26(29):4189-98.
3. Trivedi RN, Almeida KH, Fornsaglio JL, Schamus S, Sobol RW. The Role of Base Excision Repair in the Sensitivity and Resistance to Temozolomide Mediated Cell Death. Cancer Res 2005;65(14):6394-400.

Supplementary Figure S1

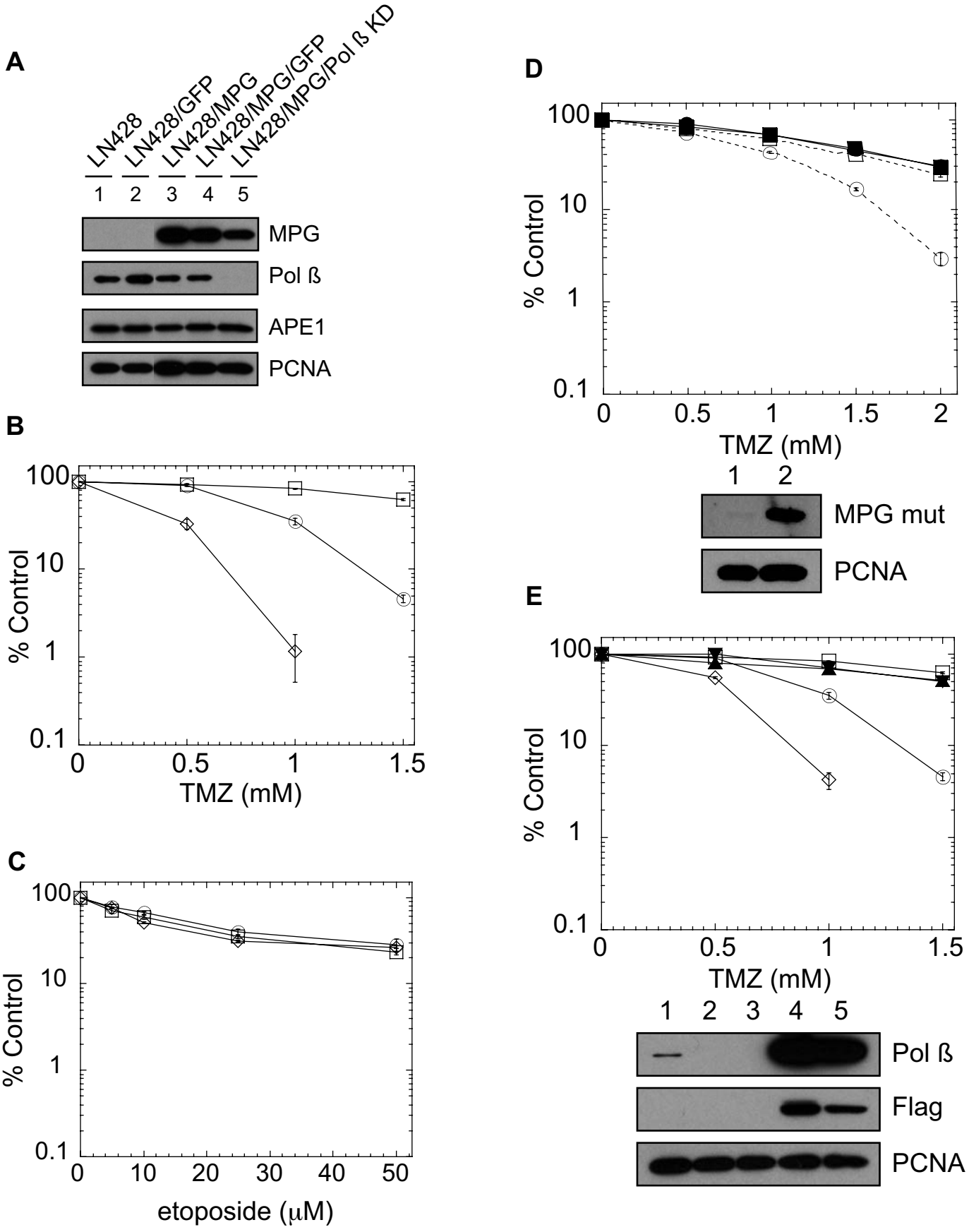

Supplementary Figure S2

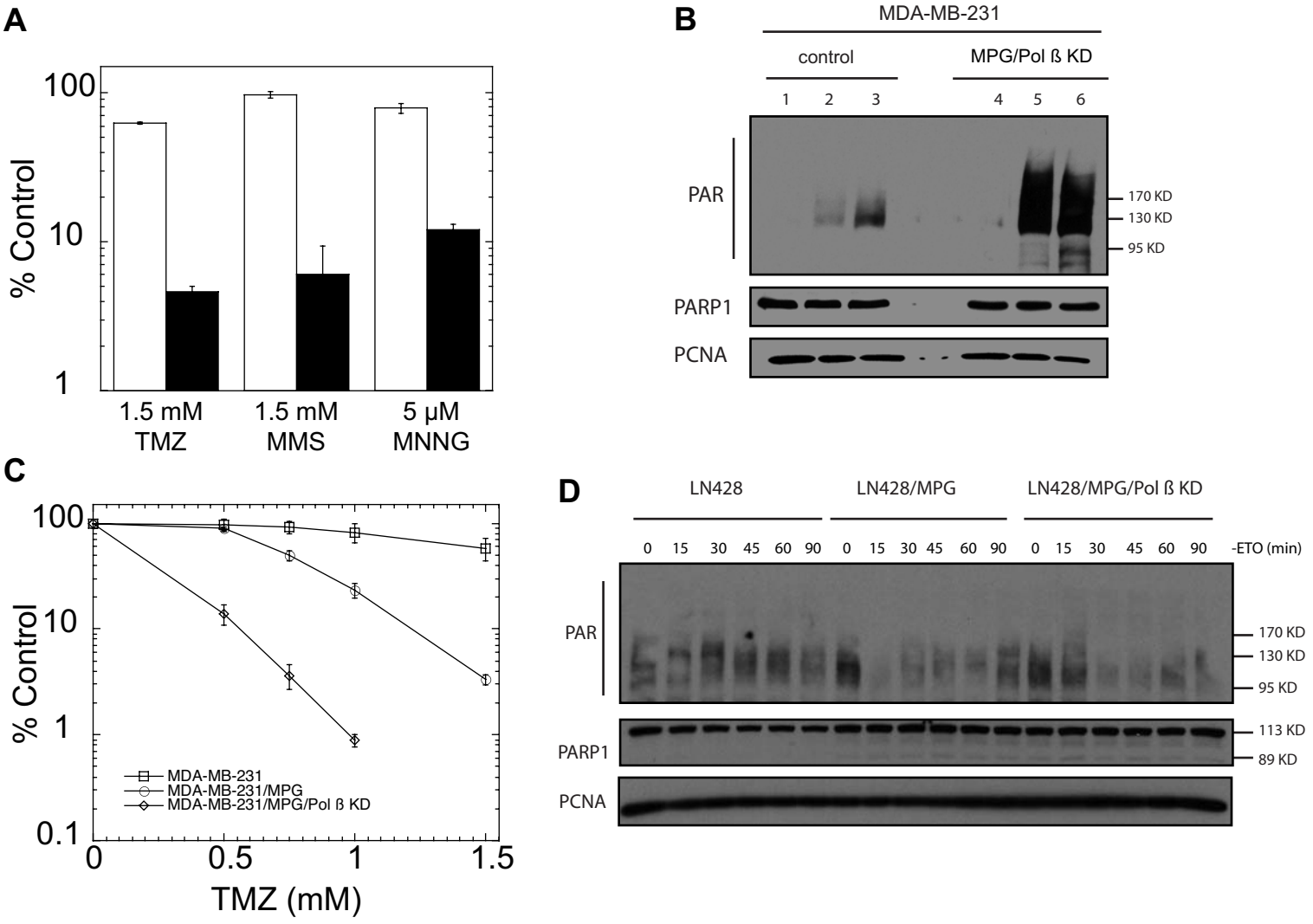

Supplementary Figure S3

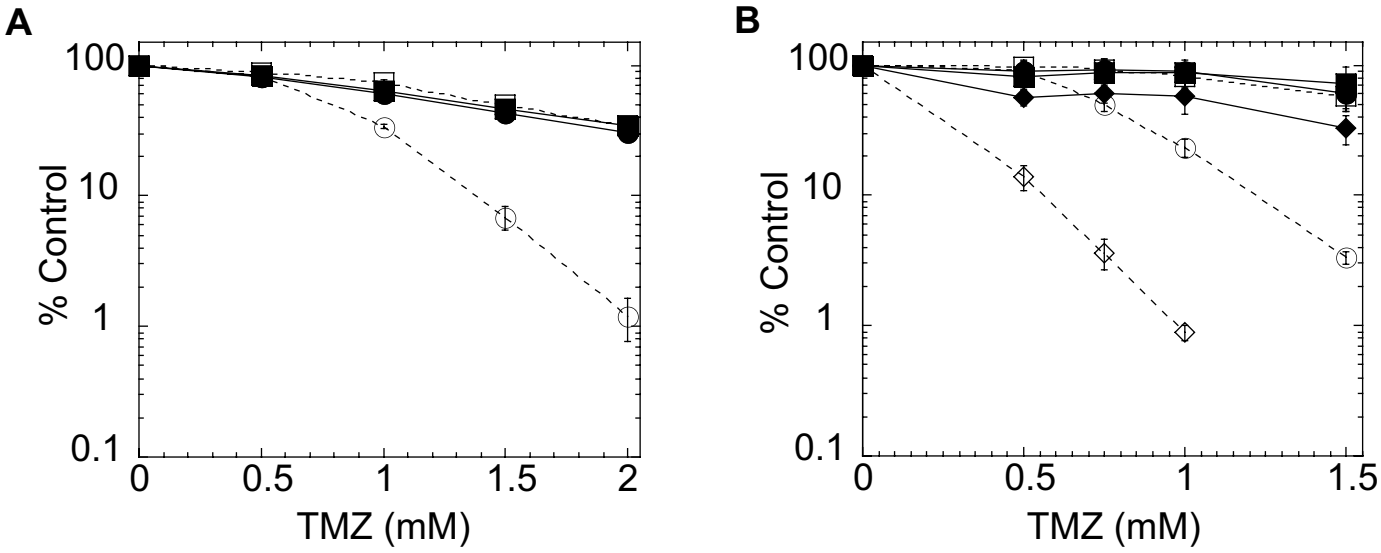

Supplementary Figure S4

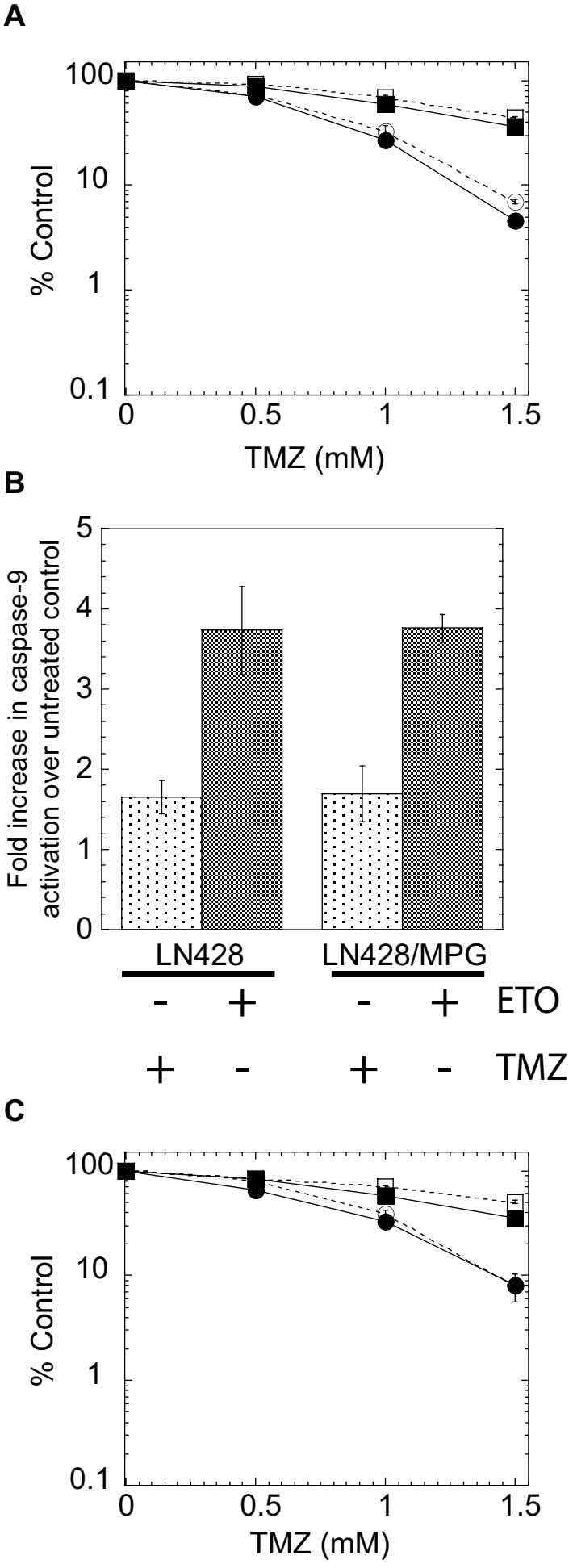

Supplementary Figure S5

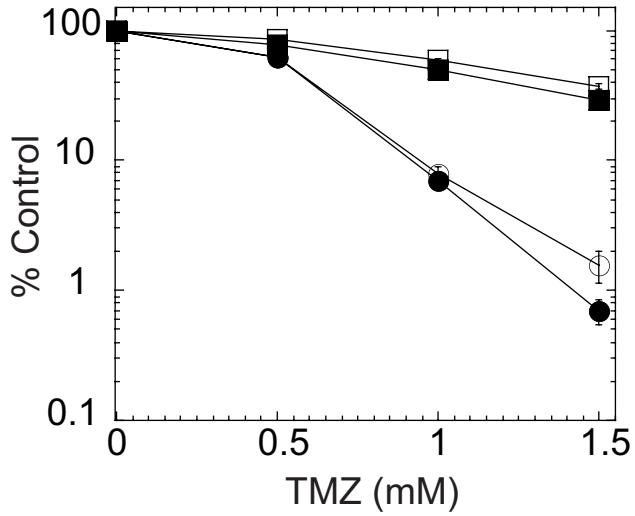

Supplementary Figure S6

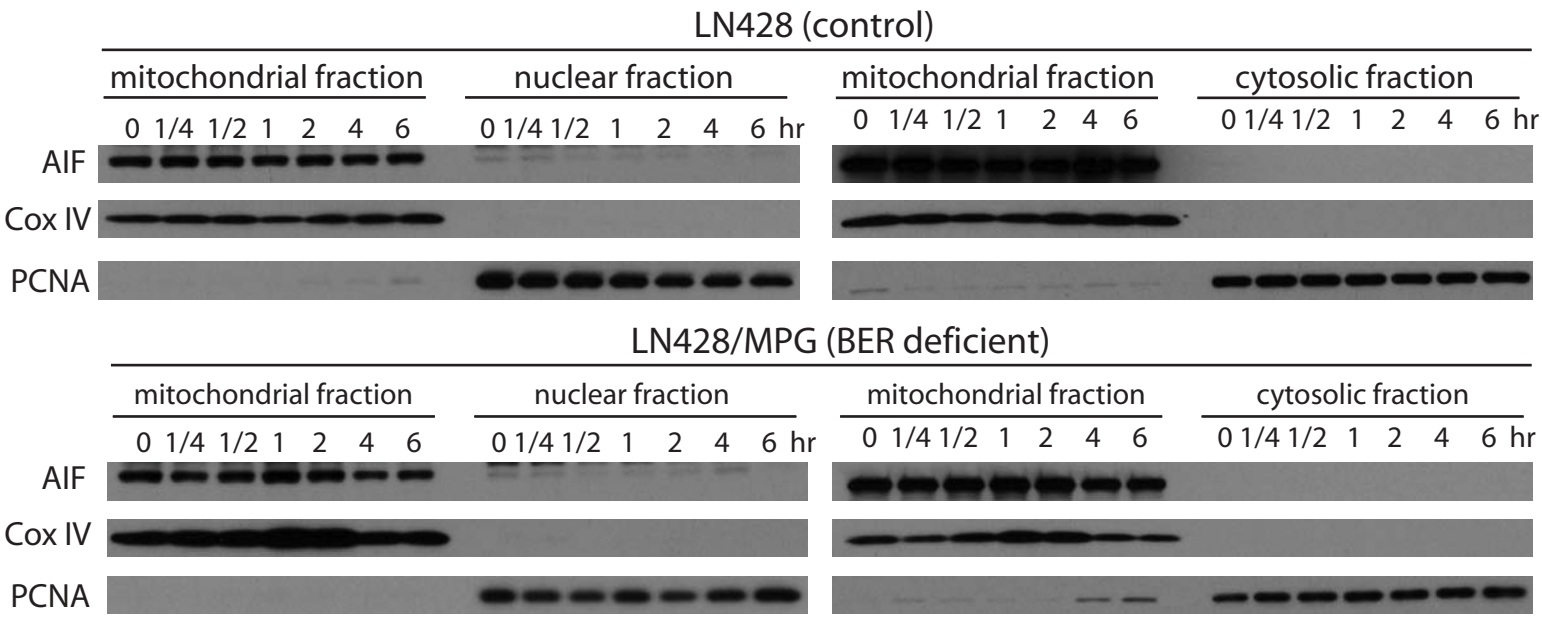

Supplementary Figure S7

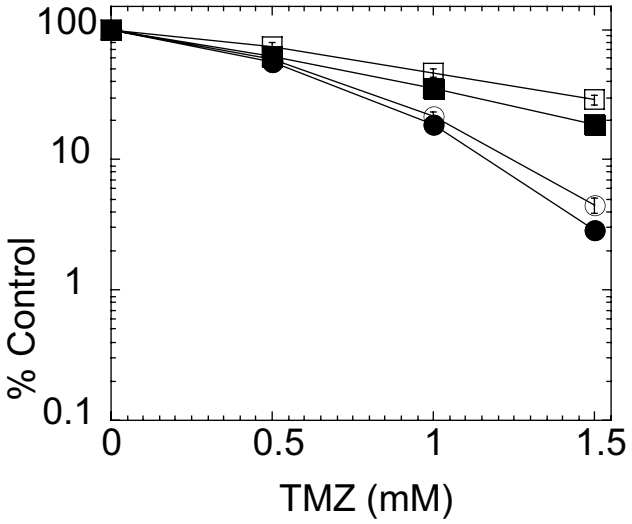

Supplementary Figure S8